HIGH SPEED ULTRASONIC PULSE-ECHO SYSTEM FOR TWO-PHASE FLOW MEASUREMENTS

HIGH-SPEED ULTRASONIC PULSE-ECHO SYSTEM FOR TWO-PHASE FLOW MEASUREMENTS

by

TATIANA MASALA

A Thesis Submitted to the School of Graduate Studies in
Partial Fulfilment of the Requierments
of the Degree
Masters of Science in Engineering Physics

McMaster University

MASTER OF APPLIED SCIENCE (2004) **McMASTER UNIVERSITY**
(Engineering Physics) Hamilton, Ontario

TITLE: High-Speed Ultrasonic Pulse-Echo System for Two-Phase Flow Measurement

AUTHOR: Tatiana Masala

SUPERVISORS: Dr. Glenn Harvel and Dr. J-S Chang

NUMBER OF PAGES: xiv, 119

ABSTRACT

Two-phase gas-liquid flow in pipes is of great practical importance in the nuclear and petroleum industries, etc. Currently, in thermalhydraulic analysis which requires modelling of a two-phase flow medium, such as boiling liquids, condensing vapors, etc., a variety of computer codes are employed to solve the time dependent mass and momentum equations in different parts of the flow system. To improve the numerical simulations, more detailed experimental knowledge of two-phase flow is required. Most instrumentation available today provides some of the required information but have various disadvantages ranging from poor sensitivity to geometrical limitations.

This work focuses on the design of a High Speed Ultrasonic Pulse-Echo system for two-phase flow parameter measurement. The ultrasonic system utilizes four ultrasonic (10 MHz frequency) transducers positioned in the axial direction on the surface of a 2.1 cm diameter cylindrical pipe, operating in pulse-echo mode. Two of the transducers are placed on the top of the pipe and the other two on the bottom of the pipe to measure the liquid level or film thickness. The liquid and gas superficial velocities studied in this work ranged from U_{ls}=0.019 m/s to U_{ls}=0.14 m/s and from U_{gs}=0.24 m/s to U_{gs}=4.33 m/s respectively, at standard conditions (1 bar, 20°C). This system was designed to acquire the data in real time 170 frames/s (A-scans/s) and the sampling rate was 2μs displaying the data at every 6msec with a spatial resolution of 0.0071 mm.

The theoretical basis for obtaining liquid level measurements, which can be used to determine the two-phase flow parameters, such as two-phase flow pattern

characterization, void fraction measurements, plug, bubble and slug velocities as well as wave amplitude and frequency for a stratified wavy and annular flow regime are discussed. The Ultrasonic System hardware and analysis software is also presented.

The High Speed Ultrasonic Pulse-Echo System can characterize accurately each different flow regime and flow regime map can be established where the flow regime map obtained in the present work is in good agreement with the previous theoretical and experimental works. The High Speed Ultrasonic Pulse-Echo System also proved to give accurate results for the determination of the liquid level within ±1.5% and the time averaged liquid level measurements performed in the present work agree within ±10% with the theoretical models. Time averaged void fraction measurements for a stratified smooth flow, stratified wavy, plug flow and annular flow qualitatively agree with the theoretical predictions. Liquid plug and bubble velocities measurements for gas superficial velocities lower than 0.48 m/s qualitatively and quantitatively agree with the correlations, while for higher gas superficial velocities it was proved that there is only qualitative agreement between the results due to the inability of the correlations to predict accurately. For slug velocity there is only qualitative agreement with the correlations, where the discrepancy is likely due to limitations in the correlations. Finally, wave height and frequency for a stratified wavy and annular flow were determined.

ACKNOWLEDGEMENTS

I would like to express my sincere thanks to my advisors Dr. G.D. Harvel and Dr. J-S Chang for the encouragement, support and guidance throughout this work. I deeply appreciate their tireless reading of my many drafts and their valuable input to this report. I thank both of them for their patience and efforts which drove me to give the best of myself.

My thanks also go to Anas Khaial, Drazena Brocilo and Greg Ksiazek with whom I had many helpful discussions in the early stage of this project, which was also the hardest time of my work. I also want to thanks to the people from UTEX Scientific Instruments who helped me to design the ultrasonic system.

Thanks to all my colleagues and friends for their help inside and outside my academic life.

Profound gratitude to my family (my Mom and Dad), and finally, this work is dedicated to my son, Andrew and my husband, Eugene, for their deep understanding and patience, and for their sacrifice in giving me the possibility to work.

Contents

LIST OF TABLES

LIST OF FIGURES

CHAPTER 1

1.1 Introduction

Two-phase flow of gas and liquids occurs in many applications in the power and process industries such as the nuclear industry, petroleum industry, etc. In a nuclear power plant, heat transport loops, two-phase flow is commonly encountered in the heat transfer from the fuel to the coolant and in the steam generators. In a CANDU fuel channel, an accurate prediction of the void fraction is essential in reactor operation and safety analyses, because it has a direct impact on the pressure drop and critical heat flux, and hence the overall mass flow rate circulating through the fuel channel. Currently, in the thermalhydraulic analysis which contains a two-phase flow medium, such as boiling liquids or condensing vapors, a variety of computer codes are employed which solve the time dependent continuity and conservation equations for flow in different parts of the system. To improve the numerical models, more detailed knowledge for physical phenomena is required. Most instrumentation available today provides some of the required information and has various disadvantages ranging from poor sensitivity to geometrical limitations. The complexity in the prediction and the design of gas-liquid systems lies in the simultaneous existence of the gas and liquid phases. The interface between the two phases can be distributed in many configurations and these are called flow patterns (also known as flow regime maps), which as was discussed earlier is a very important feature of two-phase flow. Thus, in this chapter, flow patterns and the fundamentals of two-phase flow will be discussed as a background to the work followed

by the objectives of the work.

1.2 Background of Two-Phase Flow

For the purpose of demonstrating the two-phase flow instrumentation developed in this thesis, horizontal concurrent gas-liquid two-phase flow will be studied. A pictorial representation of two-phase flow is shown in Figure 1-1 where A_l is the cross sectional area occupied by the liquid and A_g is the cross-section area occupied by the gas. The liquid holdup and gas volume fraction are defined as:

$$\alpha_l = \frac{A_l}{A} \text{ and } \alpha_g = \frac{A_g}{A}; \quad ; \quad (1\text{-}1)$$

where, A is pipe cross-sectional area. The superficial velocities of the liquid and gas phases (U_{ls} and U_{gs}) are defined as the volumetric flow rate for the phase divided by the pipe cross sectional area:

$$U_{ls} = \frac{Q_l}{A} \text{ and } U_{gs} = \frac{Q_g}{A}; \quad (1\text{-}2)$$

where Q_l and Q_g are the volumetric flow rate of liquid and gas respectively and A is the pipe cross sectional area. The defining characteristic of two-phase flow is the simultaneous flow of two phases of different densities and viscosities. In gas-liquid flow, gas moves much faster than liquid except in downward flow. The difference in the in situ average velocities between the two phases results in a very important phenomenon --- the "slip" of one phase relative to the other, or the "holdup" of one phase relative to the other [1]. This makes the in situ volume fractions different than the input volume fractions. Although "holdup" can be defined as the fraction of the pipe volume occupied by a given

phase, holdup is usually defined as the in situ liquid volume fraction, while the term "void fraction" is used for the in situ gas volume fraction as shown in Figure 1-1, After the in situ volume fraction is known, the average phase velocity can be defined for each phase as follows:

$$Ul = \frac{Ql}{Al} = \frac{Uls}{\alpha l} \text{ and } U_g = \frac{Q_g}{Ag} = \frac{U_{gs}}{\alpha g} \tag{1-3}$$

where U_l and U_g are the true average velocities of liquid and gas phases, which are normally larger than the superficial velocities.

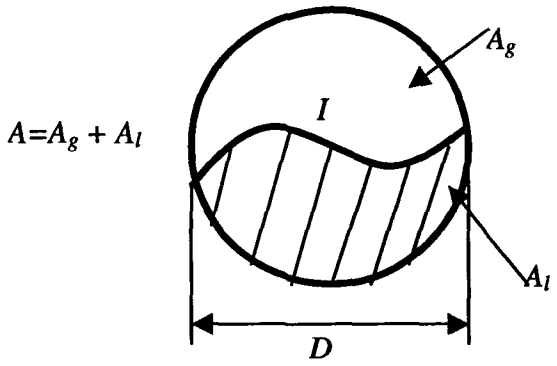

Figure 1-1: *Void fraction: A is the area of the pipe, I is the interfacial area, A_G area occupied by the gas, A_L area occupied by the liquid, and D is the diameter*

Concurrent volumetric flow of gas (Q_g) and liquid (Q_l) in horizontal channels may assume one of the patterns presented in Figure 1-2. In general, most of the flow regimes in horizontal channels show a non-homogeneous pattern, which is due to the effect of gravity on the denser fluids. This generates a tendency of stratification in the vertical direction, which means that the liquid flow has a tendency of occupying the lower part of

the flow channel forcing the gas flow to the upper part of the flow channel. However, the flow components, especially liquid, are also subject to other forces such as: surface tension, viscosity and dynamically generated body forces [2]. The two latter ones act mainly in a horizontal direction, one against and one with the flow, respectively. At high gas velocities, the frictional and dynamic forces of the gas component also become dominant. Hence in gas-liquid flow, the interface between the two phases can exist in a wide variety of forms, depending on the flow rate, fluid properties of the phases and the geometry of the system. Though authors define each flow regime somewhat differently most agree that there are six basic structures [1,2,3,4]. Figure 1-2, shows a pictorial representation of the flow patterns in horizontal pipe flow. These basic structures are called stratified smooth (SS), stratified wavy (SS), elongated bubble (plug flow-PL), slug flow (SL), annular flow (AN) and dispersed bubble flow (DB).

Stratified smooth (SS) flow is usually observed at relatively low flow rates of gas and liquid, where liquid flows at the bottom of the tube and the gas flows along the top. The surface of the liquid is smooth. Hence the two phases are well separated.

As the gas flow rate is increased the smooth interface with the liquid becomes rippled and wavy. This pattern is called stratified wavy flow (SW).

If the liquid flow rate is increased further, while the gas flow is maintained low, an intermittent flow pattern will develop in which gas pockets are entrapped in the main liquid flow due to the surface wave that touches the top surface of the tube. This is termed as plug flow (PL) or elongated bubble flow since the liquid plugs the flow channel between two gas bubbles.

If the gas flow rate is increased at high liquid flow rates, a slug flow regime will develop (SL). The major difference between plug flow and slug flow is that in plug flow there are no entrained gas bubbles in the liquid slugs and the interface is stable. In slug flow there are many entrained bubbles of various sizes and the interface is usually unstable.

At high gas flow rates, annular (also referred to as annular-mist) flow can occur. The liquid flows as a film around the pipe wall and a gas core forms in the middle. The gas core may contain some entrained liquid droplets. In this flow pattern, the gas flow rate needs to be high enough to support the gas core in the middle and prevent the liquid film from collapsing.

At high liquid flow rates dispersed bubble flow usually occurs. The liquid phase is continuous while the gas phase is distributed as discrete bubbles.

A flow pattern map, which is a two-dimensional map depicting flow regime transition boundary, is used to determine which flow pattern will occur for different gas and liquid superficial velocities. Although dimensionless variables are preferred in theory (due to ability to translate from one problem to another), the dimensional coordinates such as superficial velocities are much more generally used in practice. The generation of flow pattern maps falls into two categories. One type is the experimental flow pattern map generated directly from experimental data. Figure 1-3 shows a commonly used experimental flow pattern map, which was generated from a large amount of experimental data which included different fluid types [3]. It is completely empirical and limited to the data on which it is based. The second type of flow pattern map is the

mechanistic flow pattern map [4], such as the one shown in Figure 1-4.

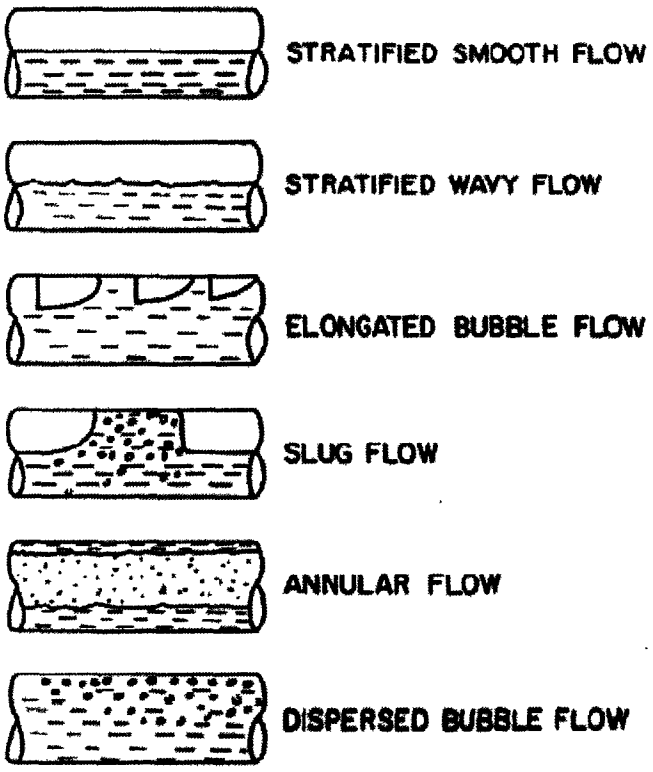

Figure 1-2: *Schematic of flow patterns in horizontal pipes; Stratified Smooth (SS), Stratified Wavy (SW), Elongated Bubble Flow or Plug Flow (PL), Slug Flow (SL), Annular Flow (AN), and Dispersed Bubble Flow (DB).*

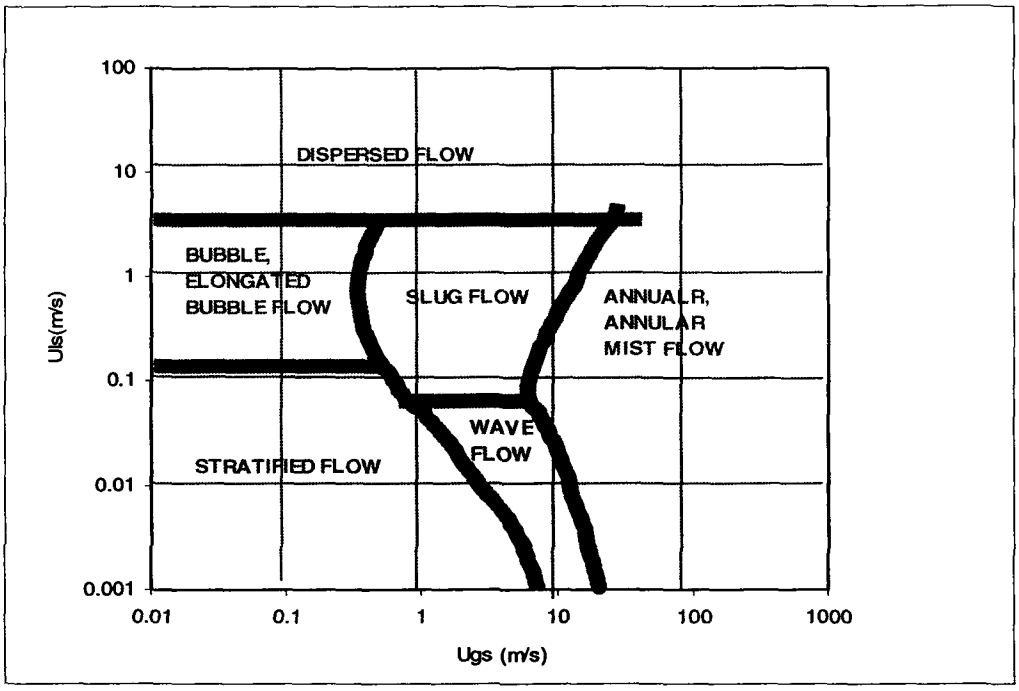

Figure 1-3: Experimental flow pattern map, Mandhane et al. [3]

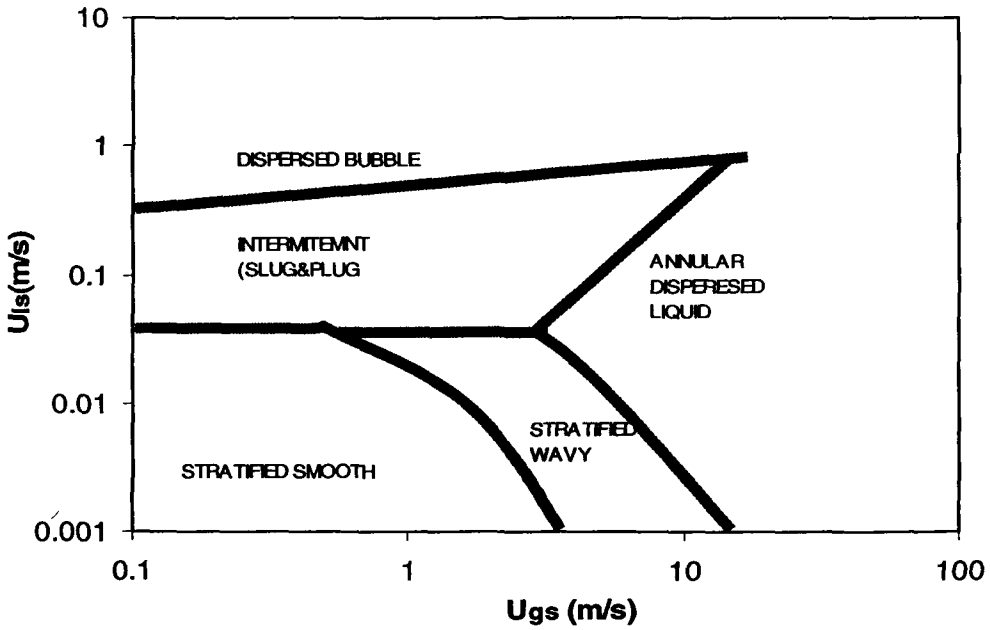

Figure 1-4: Mechanistic flow pattern map air-water horizontal tube; Taitel et al. [4]

1.3 Thesis Objectives

The main goal for this thesis is the development and construction of an Advanced High-Speed Ultrasonic Pulse-Echo system for the dynamic measurement of two-phase flow parameters. The system will be applied to horizontal gas-liquid two-phase flow to measure the following parameters: liquid level measurements, flow pattern identification, void fraction measurements, plug velocity, bubble velocity, slug velocity and wave amplitude and height. The system shall be tested for the gas and liquid superficial velocities ranging from U_{ls}=0.019 m/s to U_{ls}=0.14 m/s and from U_{gs}=0.24 m/s to U_{gs}=4.33 m/s respectively, at standard conditions (1 bar, 20°C). These conditions shall ensure that the following flow regimes are present for evaluation of the ultrasonic system: stratified smooth (SS), stratified wavy (SW), plug flow (PL), annular flow (AN).

This thesis is structured as follows: In Chapter 2 a general introduction to the existing two-phase flow measurement systems and the advantages and disadvantages of each type of system is outlined with the objective of demonstrating the need for a new advanced system. Chapter 3 discusses the basic background of ultrasonic theory pertaining to this work and describes the ultrasound measurement system to identify the fundamental capabilities of the ultrasonic system. Chapter 3 also will discuss the experimental apparatus used in this work. Chapter 4 will summarize the calibration and accuracy of the High Speed Ultrasonic Pulse-Echo System and the results of the static flow verification tests. Chapter 5 will describe the performance of the High Speed Ultrasonic Pulse-Echo System applied to horizontal two-phase gas/liquid flow. Chapter 6

provides the conclusions and Chapter 7 suggests potential for further research to improve this system.

CHAPTER 2

Review of Diagnostic Techniques for Two-Phase Flow Parameters Measurements

Some of the methods currently available for two-phase flow measurement are: impedance methods, optical methods, radiation methods and ultrasonic methods. In addition, several imaging techniques for analyzing the two-phase flow data, such as nuclear magnetic resonance imaging (NMR), x-ray computerized tomography (CT) and Ultrasonic Computerized Tomography (UCT) have been developed. These techniques can be divided into intrusive and non-intrusive technique according to whether flow fields are disturbed or not by the measuring equipment. Furthermore, in this chapter the advantages and disadvantages of these techniques for measurement of two-phase flow parameters are discussed for gas-liquid two-phase flow applications. A summary table of all techniques is shown in Table 2-1.

2.1 Impedance Methods

The impedance method is based on the fact that the liquid and gas phases have different electrical conductivities and relative permittivities [5, 6]. This impedance method can be classified into two categories, depending on the liquid material selected: the electrical conductivity method and the capacitance method. A conductivity probe makes use of the difference in conductivity of the phases [6]. Mi and Ishii et al [7, 8] used

an impedance method where eight electrodes were placed at equal distances around the circumference of a cylindrical pipe of 50.8 mm i.d. to investigate the void fraction in a slug flow regime.

Capacitance transducers measure the difference in dielectric constants between the phases. Different electrode configurations have been examined by a number of investigators [9, 10]. Alboulewafa and Kendall [11] designed a helical capacitance sensor for measuring volume fraction in air-water, oil-water and air-oil mixtures. Even though these types of capacitive sensors are quite linear, in order to allow a good sensitivity to be achieved, they are in general quite lengthy, i.e. for a 5 cm i.d. tubes the authors recommended a sensor length of 21.6 cm. Hence they are suitable for volume averaged measurements. It is apparent that this condition imposes a major limitation as the minimum size of the liquid waves that can be appropriately detected is limited by the length of the sensors. Capacitance transducers have also been used by Girard et al. [12] to determine the liquid film thickness in annular two-phase flows in reflux condensation experiments. It must be noted that for capacitance transducers that are in electrical contact with the fluid, in order to detect only the electrical permittivity of the media they must operate under a high frequency excitation mode (20-30 MHz). The use of high frequency excitation sources introduces electric instabilities making the instrument very sensitive to stray capacitances and proximity effects. In most of the current techniques, the electrodes are attached to a portion of the test section making them quite difficult to calibrate and almost impossible to move once they are installed. A more detailed review about electrical devices can be found in [6].

2.2 Optical Methods

Optical techniques are in many ways similar to acoustic techniques. In the same manner as sound attenuation can be used to measure mass fractions, light attenuation is also related to the amount of scatters in the medium. The absorption of light was used to determine the concentration of titanium dioxide particles in a suspension by Jalava et al. [13]. For opaque media it is not possible to measure the through-transmission of light. Depending on the nature of the scatters in the flow it can, however, be possible to measure Doppler shifts of reflected light. This technique is often referred to as *Laser Doppler Velocimetry* (LDV). In general, through-transmission optical methods can only be used in transparent systems, thus excluding their use in metallic pipes. De-Lasa et al. [14] used a method based on a U-shaped optic fiber. The curvature of the U is large enough for the angle incidence to be larger than the angle of total reflection for gas bubbles. At the same time the radius must be small enough for the angle of incidence to be smaller than the angle of total reflection when the fiber is in contact with water. With this setup, light will be lost in liquid (water), but conserved in gas. A mix of the two phases results in a partial absorption of the light. Andreussi et al. [15] used a fiber optic probe to measure the local void distribution in coccurent slug flow. Recently, much effort has been devoted to the development of optical techniques such as LDV (Laser Doppler Velocimetry) and PIV (Particle Image Velocimetry) [16]. However, there still remain open issues on these techniques that the probes inserted into flow fields not only disturb the flow inevitably but can gather the information only at the neighbouring regions around the probes, and optical methods give rather spatially-averaged information over

the measured flow fields.

2.3 Imaging Techniques

Until now, the methods described above have been more or less direct sensing methods, which measure the properties of the flow directly. Another approach can be to generate some type of image of the flow, and to use information extracted from this image to determine the properties of interest. The following two subsections give examples of two such techniques.

2.3.1 Nuclear Magnetic Resonance Imaging

Nuclear Magnetic Resonance imaging (NMR) [17] is a non-invasive method based on the magnetic properties of the nuclei of certain atoms. Each nucleus has a spin quantum number characterizing the stable ground state of the nucleus. Associated with the spin of the nucleus, there is an angular momentum, **p** and a proportional magnetic dipole moment, $\mu = \gamma \mathbf{p}$, where the scalar γ is the gyromagnetic ratio. In an NMR experiment, the atoms interact with a static magnetic field. The nuclear spins orient themselves in this field, and hence the nuclear magnetic moments orient in this static field, so that the nuclear spins are either parallel or anti-parallel to the field. The magnetic moments precess at a certain frequency (Larmor-frequency), characteristic of the nucleus and proportional to the strength of the applied magnetic field. A broadband *Radio-Frequency* pulse (RF) is then transmitted orthogonally to the static field, and the magnetic components of the RF-field interact with the nuclear magnetic moments. When the frequency of the RF-signal is equal to the Larmor-frequency an energy transfer

occurs, which results in a flip of the nuclear spin, *i.e.* a resonance phenomenon. This energy absorption is recorded and can be used to determine concentrations and other properties. NMR has received a lot of attention due to the advances made in medical imaging. NMR is also useful in many non-medical applications, for example in measuring flow velocity in paper fiber suspensions [18]. However, if some of the objects to be measured in a multiphase flow are magnetic materials, NMR will not work.

2.3.2 Radiation Techniques

Although techniques based on small probes are accurate and give good time-resolution, they only measure local properties of the flow. In order to obtain information of the entire flow profile, a setup with several probes or a scanning configuration has to be used. With *Computerized Tomography* (CT) an image of a cross section of the flow is obtained. This technique has recently been used to obtain parameters such as void fraction and void distribution in two-phase flow systems [20]. Tomography based on penetrating radiation (i.e X-rays or γ-rays) has been used in medical applications since the mid-50's [20] to locate or examine a specific organ without the need of surgery. By the early 70's, the methods for inverse had been developed which allow strongly to be usable in practice. In medical imaging, techniques involving penetrating radiation are placed in two categories: attenuation techniques and emission techniques. Some of these techniques have recently been adapted to engineering applications, such as multiphase flow measurements. Attenuation techniques involve an external source of radiation, usually X-rays or γ-rays, but sometimes also ultrasound. The ultrasonic CT is described

in more detail in Section 2.4. X-rays and γ-rays are often used in a through-transmission mode. This means that a signal is transmitted through the flow, from all different angles, while sensors at the opposite side of the object record the signal. The procedure is repeated for all angles as shown in Figure 2-1. These projections can then be used to reconstruct an image of the sample object [20]. A method using high speed X-ray tomography for measuring void fraction distribution was presented in [21]. Absorption or scattering of radioactive emissions (γ, X, β and neutrons) has been widely used [22]. Even though the absorption of γ rays has been successfully used in determining the void fraction in steam-water flow, their applicability for large moving flow structures, i.e. slugs, requires the use of very strong source. The difference in the absorption of β particles by the water and the gas makes this technique applicable for the measurement of void fraction. This technique has the same drawback as the absorption of γ rays and is mostly useful when the liquid is dispersed in a gas core (dispersed annular flow). Furthermore, the use of β particles becomes almost impossible when the test section is made of a thick absorbent material.

More sophisticated non-intrusive methods, such as real time neutron radiography (RTNR) or X-ray computed tomography (X-CT), allow for the measurement of the distribution of void fraction. Notably, the results obtained by Harvel et al. [21] show reconstruction of two-dimensional cross-sectional images taken at frequencies up to 250 Hz. For instance, Harvel et al.'s work also used an RTNR technique to determine lateral void fraction with respect to time. A key drawback of these techniques is that they require quite heavy shielding structures.

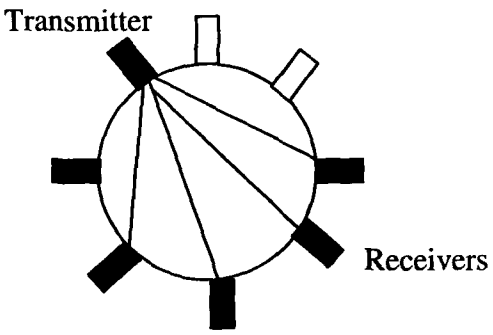

Figure 2-1: X-ray Sensor configurations for tomographic flow measurements through transmission setup. The sensors take turn transmitting a signal through the flow while the others are used as receivers

2.4 Ultrasonic Applications to Two-Phase Flow Measurements

Knowing the limitation of the techniques that were described earlier to two-phase flow measurements it is clear that there is still need for more development in the instrumentation for two-phase flow analysis. However, from past studies [23,25,46] it was proved that the ultrasonic methods may offer more practical applications and can be used when other alternative are not possible. Therefore in the next section a review of the ultrasonic techniques to two-phase flow is presented.

Ultrasonic measurement is based on time-varying deformations or vibrations in media, which is generally referred to as acoustics. A given medium substance is comprised of atoms, which may be forced into vibration motion about their equilibrium positions. Many different patterns of vibration motion exist at the atomic level; however, most are irrelevant to acoustics and ultrasonic measurements. Acoustics is focused on particles that contain many atoms that move in unison to produce a mechanical wave. A detailed discussion about the basic ultrasonic theory and the High Speed Ultrasonic

Pulse-Echo System used in this work is given in the next chapter. This section reviews some of the ultrasonic techniques currently used by other researchers for two-phase flow measurements.

There are three ultrasonic methods for two-phase flow diagnostics, namely the pulse-echo, transmission, and the Doppler shift methods. A summary of all techniques is shown in Table 2.1. at the end of this chapter.

The Doppler shift method has relative advantage as applied in low void fraction liquid flow velocity measurements and gas bubble velocity measurements. Morriss and Hill [24] developed a Doppler velocity method for two-phase pipe flow. With this method, representative images can be obtained in air-water flow for large values of water holdup, however sharper focusing is needed to resolve millimetre scale bubbles accurately.

The pulse-echo method was intensely studied by numerous authors for two-phase flow measurement. Chang et al. [23, 25] developed an ultrasonic system to measure the instantaneous liquid levels; time averaged void fraction and interfacial area in a gas-liquid two-phase system by using the pulse-echo and transmission methods. The two techniques are non-interfering and can be applied to metal pipes. With special transducers or temperature delay devices can withstand high temperatures of up to 400^{o} C. By this technique, it is possible to measure moderately transient bubbly flow of the order of 1s time intervals, and with a spatial resolution of 0.075 mm. Using a polynomial regression method, it is possible to recognize flow patterns such as stratified smooth, stratified wavy, plug flow and slug flow for an interval of 10s, and it was observed that as the flow

entrainment increases, the accuracy of the results decreases. Chang and Morala's system can measure the bubble velocity up to 0.7 cm/s. However, it is clear that this method cannot be directly applied to bubble flow or to any flow that contains a high degree of entrainment, and more transducers are necessary for more accurate results. Gai and Beck [26] presented a method for flow imaging by using multiple receivers per transmitted signal, which can be an advantage regarding to the data acquisition system and flow imaging. Further studies for the liquid level measurements were performed by Serizawa and Nagane [27] and suggested that the problem associated with the pulse-echo method are its large sensing area and its incapability of detecting a sharp edge of the interfacial waves. The beam of the transducer is an important trend in measuring the liquid level. A narrower beam has poor detection capability due to smaller scattering angles at the reflection interface. The measured film thickness is a decreasing trend with an increase in the inclination angle.

Another important aspect for two phase flow measurement is to reconstruct a cross sectional image of the flow by using ultrasonic computerized tomography. In this mode, one can determine important parameters for two-phase flow measurements such as local void fraction, averaged void fraction, and distribution of phases in a two-phase flow system. Therefore, Xu and Han [28, 29] developed an ultrasonic transmission system for tomographic imaging of gas-liquid two-phase flow based upon a fast binary back-projection image reconstruction algorithm. They used 42 transducers in parallel scanning and fan-shaped beam scanning geometry. Yet, the experiments are presented only for simulated phantoms or static. Dynamic flow phenomena were not demonstrated. Multiple

continuous tomographic images are needed which can be achieved by the time history of cross sectional variations. With this system it is not possible to distinguish two or three bubbles that are close together (they are visualized only as a single bubble) but it can separate two bubbles if the distance between them is larger than 14 mm. The measurable speed for a bubble is less than 1.7 m/s with this system and the image reconstruction 41.7 frames/sec. However, in this case the image reconstruction algorithm needs to be improved rather than increasing the number of the transducers. As the number of transducers is higher, it takes more time to reconstruct the image and also the number of the transducers is restricted by the pipe diameter. Yang and Schlaberg [30] developed a method that employs 36 transducers having a fan shaped beam profile to effectively cover the cross-section. With this configuration, 100 frames/sec were achieved using a parallel image processing technique. It was also demonstrated that a better reconstruction quality is achievable by widening the beam angle to 70^{o} of the ultrasound transducers without increasing the number of the transducers. Improvements of the quality are also achieved by the use of multiple receiver data acquisition modes in combination with the transmission mode. Warsito et al. [31, 32] developed an ultrasonic transmission technique for three phase flow imaging. By this method it is possible to investigate only time averaged cross section distributions and the method also may be applied to a real time three component imaging of three phase system by developing a better transducer array of data acquisition, and development of a better reconstruction algorithm. Wiegand et al. and Hoyle [33, 34] developed a pulse-echo ultrasound tomography technique that generates cross-sectional image of the flow, which forms the basis for the deduction of

flow parameters, such as the void fraction, etc. By computer simulation, different sensor arrangements were studied and it was proved that by using a multi-segment sensor there is a significant improvement in the signal to noise ratio and image quality. Yet, this method was not tested on real targets, and because a larger number of transducers and equipment are necessary for achieving such configuration, this method may be difficult to implement in industrial applications.

Table 2.1 - Diagnostic Techniques for two-phase flow measurement

Technique	Interfering	Steady State	Slow transient	Fast Transient	Flow Regime	Local Void fraction	Averaged Void fraction	Void fraction distribution	Phase Velocity
Conductance	Yes	Yes	Yes	Yes	No	Yes	No	Limited	Yes
Capacitance	No	Yes	Yes	Yes	Yes	No	Yes	Limited	Yes
Optical techniques	Yes	Yes	Yes	Yes	Yes	Yes	Yes	Limited	Yes
Gamma ray	No	Yes	Yes	Need Strong Source	Yes	No	Yes	Limited	Yes
X-ray	No	Yes	Yes	Yes	Yes	No	Yes	Yes	Yes
Neutron Radiography	No	Yes	Yes	No	Yes	No	Yes	Yes	Yes
Ultrasonic	No	Yes	Yes	Yes	Yes	Limited	Yes	Yes	Yes

Table 2.2 - Ultrasonic Techniques for Two-Phase Flow Measurements

Author	Diagnostic Method	No of Transd-ucers	Flow System	Flow Pattern Recognition	Bubble Localisation	Phase Velocity	Slug&Plug Flow Velocity	Averaged Void fraction	Local Void Fraction
Morala &Chang	Pulse-Echo	1	Horiz. P.	SS,SW,PL,SL	1	No	No	Yes	No
Morala &Chang	Pulse-Echo	2	Horiz. P.	SS,SW,PL,SL	1	Yes	No	Yes	No
Chang & Morala	TM	2	Vertical P.	No	1	Limited $\varepsilon<20\%$	No	Yes	No
Serizawa &Nagane et al	Pulse-Echo	1	Horizontal Plate	Liquid Level and inclination angle	-	No	No	No	No
Xu &Han et al	TM-UCT	42	Phantoms (H)	SS,SW,PL,SL, AN	-	No	No	No	Yes
Young & Schelberg at al	TM -UCT	36 ($\alpha=70^{o}$)	Phantom (H)	Bubble Flow	3-4	Yes (1.61m/s)	No	-	Yes
Wiegang & Hoyle et al	Pulse-Echo UCT	30	Phantom	Bubbly Flow	3	Yes (0.5m/s)	-	-	Yes

CHAPTER 3

Two-Phase Ultrasonic Measurement System and Experimental Setup

An application of the high-speed ultrasonic pulse-echo system to two-phase flow diagnostics is explored in this chapter. In section 3.1, the basic theory of ultrasonic measurements to two-phase flow application is presented; then in section 3.2 the measurements system is presented in detail. Finally, in section 3.3 the experimental setup for the verification of the measurement system is described.

3.1 Ultrasonic Propagation Theory

Ultrasonic measurement is based on time-varying deformations or vibrations in materials, which is generally referred to as acoustics. All material substances are comprised of atoms, which may be forced into vibrational motion about their equilibrium positions. Many different patterns of vibrational motion exist at the atomic level; however, most are irrelevant to acoustics and ultrasonic measurement. Acoustics is focused on particles that contain many atoms that move in unison to produce a mechanical wave. When a material is not stressed in tension or compression beyond its elastic limit, its individual particles perform elastic oscillations. When the particles of a medium are displaced from their equilibrium positions, internal (electrostatic) restoration forces arise. It is these elastic restoring forces between particles, combined with inertia of the particles that leads to oscillatory motion of the medium.

Ultrasonic vibrations travel in the form of a sound wave, with a frequency (f) and a wavelength (λ). Also, ultrasound requires an elastic medium such as a liquid or a solid. Shown in Figure 3-1 are the basic parameters of a continuous wave (cw). These parameters include the wavelength (λ) and the period (T) of a complete cycle.

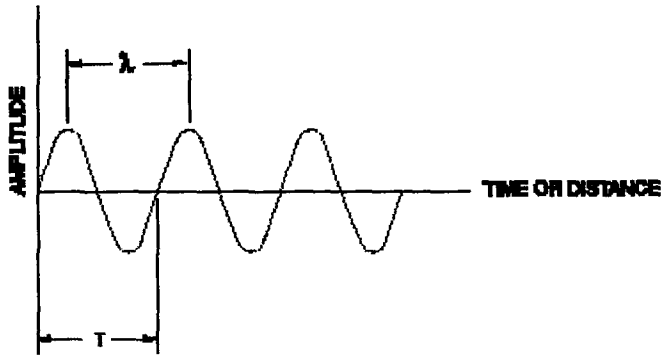

Figure 3-1: *Wave propagation – the wavelength λ and the period T of a complete cycle*

In a perfect elastic medium at a given temperature and pressure, the velocity of ultrasound, c, is constant. The relationships between c, f, λ and T is given by:

$$\lambda = c/f \quad or \quad \lambda = cT; \tag{3-1}$$

where, c is the sound velocity from the given material and f is the frequency of the sound wave which represents the number of the waves which passes a particular point per second. Ultrasonic waves can be propagated either longitudinally or transversely in a medium. The particle movement responsible for the propagation of longitudinal and shear waves is shown in Figure 3-2.

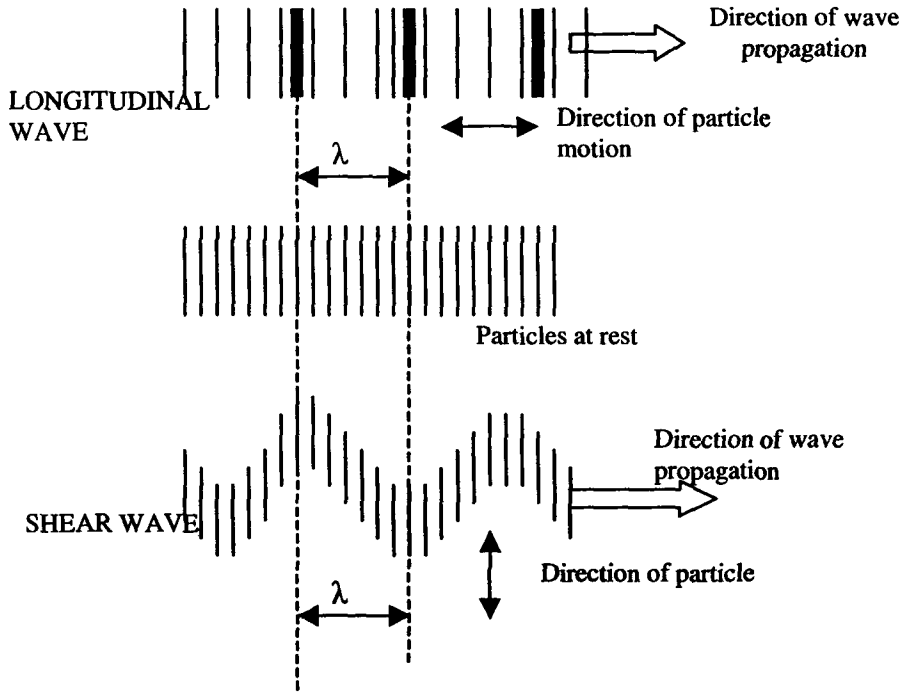

Figure 3-2: Wave propagation – longitudinal wave; shear wave

As can be seen from the Figure 3-2 in longitudinal waves, the particle oscillations occur in the longitudinal direction or the direction of wave propagation. Since compressional and dilatational forces are active in these waves, they are also called pressure or compressional waves. Compressional waves can be generated in liquids, as well as solids because the energy travels through the atomic structure by a series of compression and expansion (rarefaction) movements. In the transverse or shear waves, the particles oscillate at a right angle or transverse to the direction of propagation. Shear waves require an acoustically solid material for effective propagation and, therefore, are not effectively propagated in materials such as liquids or gases. Shear waves are relatively weak when compared to longitudinal waves. In fact; shear waves are usually generated in materials

using some of the energy from longitudinal waves.

3.1.1 Propagation at an interface between media

In the majority of the situations presented in this work, the boundaries encountered by a travelling ultrasonic wave is considered to be normal to the propagation vector of the wave as shown in Figure 3-3. When a wave travelling in the $+x$ direction interacts with a boundary between two different materials, a portion of the incident wave will be reflected back in the $-x$ direction and another portion will be transmitted into the second material and continue travelling in the second medium in the $+x$ direction. The amplitudes of both the transmitted and reflected waves, as well as the phase of the reflected wave, are determined by the reflection and transmission coefficients both of which are functions of the acoustic impedances of both materials. In the case of air/water system, 99% of the signal is reflected back. The acoustic impedance of a material, Z, is defined as the density of the material (ρ) multiplied by the speed of sound in that material (c). Z_1 is the acoustic impedance of the first material in which the incident wave is travelling and Z_2 is the acoustic impedance of the second material. When interacting with a simple interface at normal incidence, both reflection and transmission coefficients are entirely real and as such are multiplied with the incident wave to calculate the reflected and transmitted waves. The transmission (T) and reflection (R) coefficients for a wave encountering an interface at normal incidence as described above are given as (3-2) and (3-3), respectively.

$$T = \frac{I_t}{I_i} = \frac{4Z_1Z_2}{(Z_1+Z_2)^2} \qquad (3\text{-}2)$$

$$R = \frac{I_r}{I_i} = \left[\frac{Z_2 - Z_1}{Z_2 + Z_1}\right]^2 \qquad (3\text{-}3)$$

In the transmission case, since $Z_1 > 0$, T is entirely real and must always be greater than zero, hence no phase shift occurs when a wave is transmitted through a boundary.

As can be seen from equation (3-3), if R is likewise entirely real, it lies in the range [-1,1]. This implies that the reflected wave is a scaled and negated version of the incident wave when $R < 0$. It can easily be seen from equation (3-3) that this inversion occurs when Z1 > Z_2. In the case of two-phase flow experiment, Z1 > Z2 for the liquid/air interfaces, but not when travelling from the liquid into the plexiglas at the liquid/wall tube interface. Based on these properties of the wave propagation it is possible to detect different mediums such as a plexiglas/liquid interface or a liquid/air interface as encountered in the present work and even measure them if the sound velocity through that medium is known. Therefore based on the ultrasonic properties, very useful information can be obtained by the time-of-flight of the wave, which is based on the propagation velocity of the ultrasound through media. Having known the propagation velocity through a medium and measuring the time-of-flight of a wave, the distance that the wave travels through the media can be determined very accurately by:

$$h = c \cdot t_s / 2 \quad , \qquad (3\text{-}4)$$

where h is the material thickness, c is the material sound velocity and t_s is the time of flight.

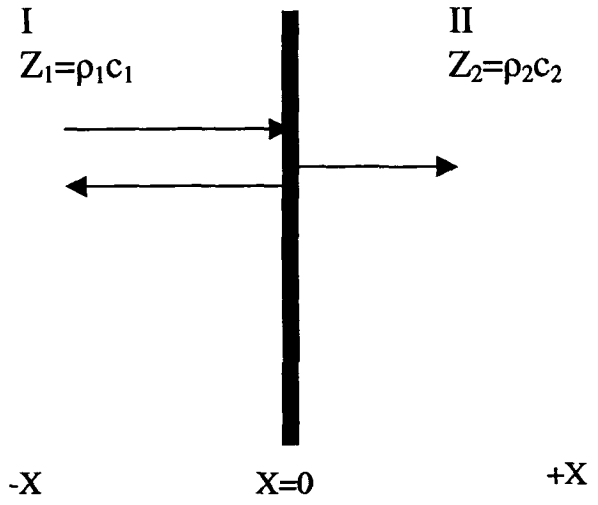

***Figure 3-3:** Wave propagation at a boundary between two different media; Z_1 acoustic impedance of medium I; Z_2 acoustic impedance of medium II*

3.1.2 Ultrasonic Transducer and Excitation Theory

The transducers used in this work are 6 mm diameter 10 MHz center-frequency wideband transducers. A schematic representation of the ultrasonic transducer is represented in Figure 3-4. An ultrasonic transducer converts electrical energy to mechanical energy, in the form of sound, and vice versa. The waves they produce can be approximated as plane waves in the "near field". The "near field" is defined by the region for which the path length from the transmitter to the receiver satisfies equation (3-5):

$$r < \frac{d^2}{\lambda} \quad , \tag{3-5}$$

where r is the path length from the transmitter to the receiver, λ is the wavelength, and d is the diameter of the transducer. Since the transducers used are 6 mm diameter, i.e., their radius is roughly 3 mm, thus d^2/λ can be calculated for the center frequency of 10 MHz

to be approximately 60 mm in water. This implies that as long as the liquid level is less than 6.1 cm in thickness, the liquid level can be measured within the near field, hence less error due to the divergence effects. The cross-section of the ultrasound beam is roughly constant and the same area as the footprint of the transducer element over the near field. Beyond the near field, the beam diverges as per equation (3-6):

$$\sin 2\alpha = 0.5\frac{\lambda}{r}; \qquad (3\text{-}6)$$

where r is the radius of the transducer. In the present work, the divergence angle beyond the near filed translates to $\alpha = 1.69^{o}$ (in water) and thus the cross-section becomes larger and attenuates faster resulting in less accurate results. As indicated by Filipczynsky et al [35] the best directional characteristics of longitudinal waves are achieved when $\lambda << 2r$.

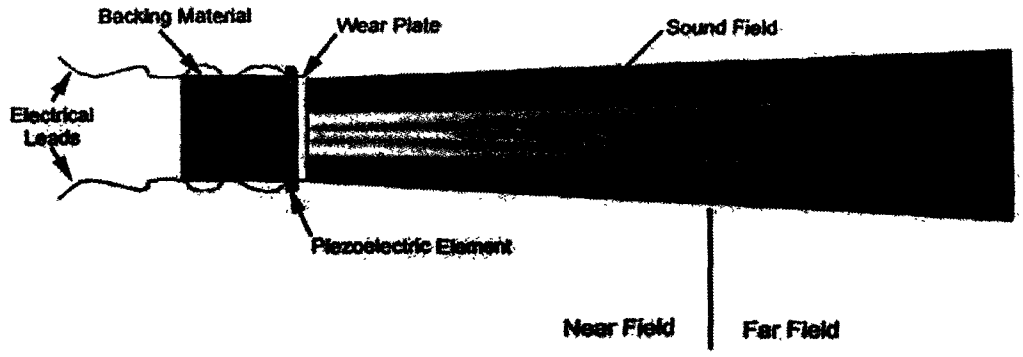

Figure 3-4: Schematic representation of an ultrasonic transducer; near field and far field.

3.1.3 A-scan and C–scan Algorithms

An A-scan algorithm displays the amount of received ultrasonic energy as a function of time as shown in Figure 3-5. The relative amount of received energy is plotted along the vertical axis and elapsed time (which may be related to the sound energy travel time within an object) is displayed along the horizontal axis. Also the signal displayed by the A-scan is a radio frequency signal (RF), more specifically a fully rectified RF signal. In the A-scan presentation, the attenuation of an ultrasonic signal can be determinate as well as the liquid level by the position of the signal on the horizontal axis. A more detailed description of an A-scan is presented in Chapter 4 (Section 4.1). The key items of interest in the A-scan are the initial pulse (labelled (a) in Figure 3-5) and the reflected pulse from the gas/liquid interface (labelled (c) in Figure 3-5).

Ultrasonic C-scan algorithm is one of the methods used in non-destructive examinations to analyze cracks or certain defects through a material. A C-Scan algorithm is the plotting of a collection of gated amplitudes of ultrasonic A-Scan signals. The C-scan presentation provides a plan-type view of the location and size of the object to be tested as shown in Figure 3-6. The plane of the image is parallel to the scan pattern of the transducer. C-scan presentations are produced usually with an automated data acquisition system, such as a computer controlled scanning system. Typically, a data collection gate is established on the A-scan and the amplitude or the time-of-flight of the signal is recorded at regular intervals as the transducer is scanned over the test piece. The relative signal amplitude or the time-of-flight is displayed as a shade of grey or a colour for each

of the positions where data was recorded. The C-scan presentation provides an image of the features that reflect and scatter the sound within and on the surfaces of the test.

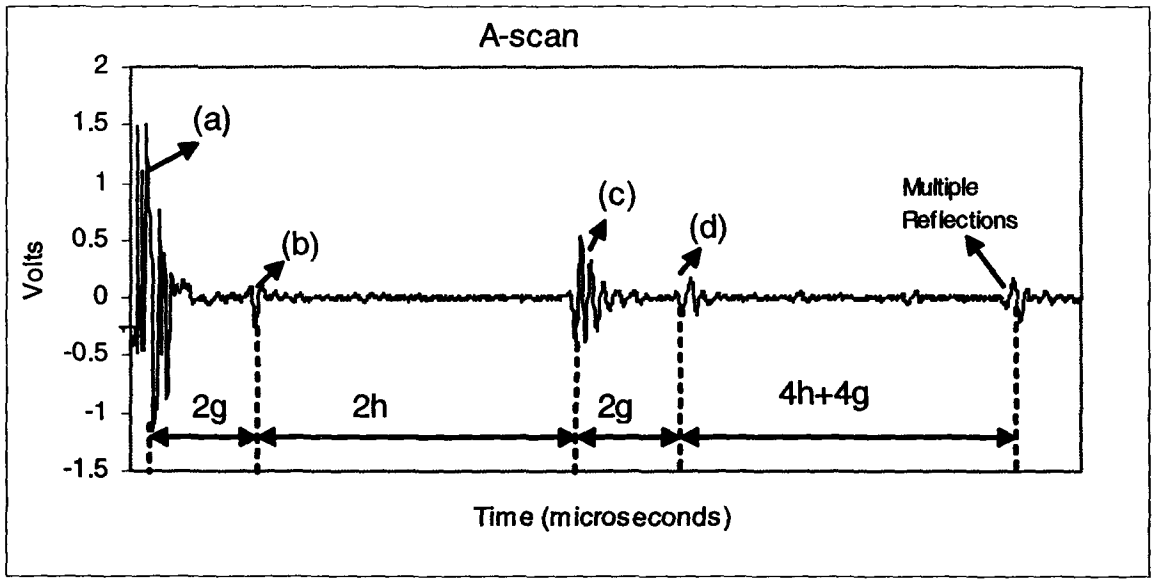

Figure 3-5: *Typical representation of the wave from an A-scan where (a) is the initial pulse, (b) is the wave reflected from the tube-wall/liquid interface, (c) is the wave reflected from the liquid/gas interface, multiple reflection from the tube/liquid interface, (d) is reflected from liquid/gas interface and tube wall/liquid interface.*

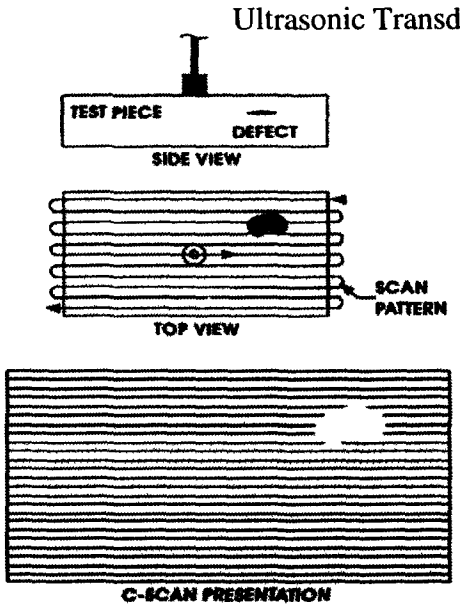

Figure 3-6: *C-scan algorithm; typical representation of a side view and top view of a scanning object.*

3.2 Overall Description of the Measurement System

The measurement system developed in this work to monitor the two-phase flow phenomena is comprised of three physical parts: a Computer (PC), a Multiplexer and four Ultrasonic Transducers as shown in Figure 3-7. The Computer (PC) is equipped with: a Data Acquisition Card (Digitizer – Compuscope12100 model-100MHz), a Motion Controller Card (DMC1800) and the Winspect Data Acquisition Software. The Winspect software initiates a data acquisition cycle by first setting the multiplexer to the correct channel via a DMC 1800 parallel connector unit and then by sending a software trigger to the digitizer. The digitizer has the capability to send a synchronous external trigger pulse when it receives a software trigger, and so begins the acquisition at the same time it

sends the external trigger pulse and at the instant an echo is received. This pulse is used to trigger the Pulser/Receiver unit from the multiplexer to generate a pulse to send to the four transducers. The echoes received by the transducers produce the RF signal, which travels back to the Pulser/Receiver unit from the multiplexer, and is amplified and passed on to the digitizer which then acquires and digitizes the data. The Staveley Sonic 260 multiplexer reports its current channel number as a binary value on four-output channel address lines. These lines are available on the parallel connector of the unit. The Winspect software then processes this RF data, and a liquid level estimate is generated and displayed on both C-scan or on an A-scan processors.

The multiplexer is set to RUN automatically, which means that all four transducers receive an electrical pulse and at the interval of 6 msec the second pulse occurs and so on until the scanning time is completed. For the present experiments, the scanning time was chosen to be between 3 seconds and 10 seconds respectively.

3.2.1 PC based Ultrasonic Signal Control and Analysis System

The computer (PC) used for this research is a Pentium® 4 CPU series computer with 1.60 GHz processor frequency and 1.00 GB of RAM, running Microsoft Windows XP. This computer was chosen to ensure adequate processor speed and RAM to support the needs of the analysis required in the present work. The program performs several computationally intensive tasks such as communicating between the compuscope digitizer and the motion controller collecting 16 MB of data from up to eight ultrasonic transducers, and performing a C-scan to allow for real-time data analysis (30 frames/s)

instead of storing the data and then post-processing it after the experimental run.

a. Operational System

Microsoft Windows was chosen as the operating system for the computer to allow easy interoperability with other lab computers. Specifically, the Microsoft Windows XP version was used since the Winspect Software only works on this system without any modification.

b. Winspect Data Acquisition and Processing Software

Winspect Data Acquisition Software is an advanced commercial software package used for building inspection and material characterization systems [36]. This software was chosen for its multitasking capability, as it allows communication between the data acquisition card and motion controller card, and it analysis the amplitude and time of flight data, in real time. Also, it processes fast enough on A-scan data, live gated data and as a post-processing engine on saved data. The Winspect processor that was used in the present system was a C-scan algorithm that collects continuously the data in real time. This processor has the capability to set the scanning time (ex. 3 sec, 10 sec) that is needed to acquire the data as well as the timestep that is needed in order to acquire the data in real time (30frames/s and anything greater is high speed) such as 170 frames/sec and it saves the data directly into the memory.

c. Digitizer- Compuscope 12100

The digitizer card (Gage Compuscope 12100) is used to process the digital signals using its own fast processor. It has on-board memory, running in parallel with the PC-

processor and is a multi-card master/slave system which can provide 2 channels of simultaneous A/D conversion, therefore allowing for a very fast data acquisition time, where a trigger occur every 2μs. Data transfer rates from digitizer memory to PC memory is 50 MB/s. This digitizer operates normally without using any IRQ line, but it has the capability of generating an interrupt on one or more of several events, including the following: trigger, end of capture and memory full which is a real advantage for the present system since the multiplexer can be externally triggered.

d. Motion Controller card- DMC 1800

The DMC 1800 is directly installed in the PC slot. This controller has a non-volatile program memory, fast encoder speed and provides two channels for high-speed communication FIFO for sending and receiving commands. In the present system, a program was loaded into and run on the DMC 1800 motion controller. This continuously looping program reads the four discrete inputs representing the multiplexer channel address, and converts these inputs to a program variable within the DMC 1800 controller. Winspect software can then interrogate the controller for the value of this variable, thus obtaining the current multiplexer channel address.

f. Multiplexer, Staveley Sonic 260

This multiplexer is an eight-channel multiplexer that works as a broadband ultrasonic analyzer, and includes a pulser/receiver, and a stepless gate. The pulser/receiver section has operator controls with discrete, calibrated settings as well as

continuous adjustment capability. The pulser section generates short, large amplitude electric pulses of controlled energy which, when applied to an ultrasonic transducer, are converted into short ultrasonic pulses. The receiver section amplifies the voltage signals produced by the transducer, which represent the received ultrasonic pulses.

g. Panametrics Transducers

Four Panametric Ultrasonic Transducers (Model # A112S 10MHz ¼" 6mm diameter) contact were used for this work. The transducers were attached to a coaxial cable via an SMB jack on the side of each transducer near the rear end connected to the multiplexer unit via coaxial cable. The transducers were mounted on the pipe by pressing them using a spring system. This method was chose upon due to good acoustic coupling efficiency, simplicity, and ease of mounting. A common silicone lubricant (high vacuum grease) was used which acted as an acoustic coupling layer. During testing, it was observed that it was important to ensure the cleanliness of the transducers surface and the tube prior to mounting since any foreign object present between the transducer and tube surface give false echoes or attenuated the signal introducing errors in the measurement.

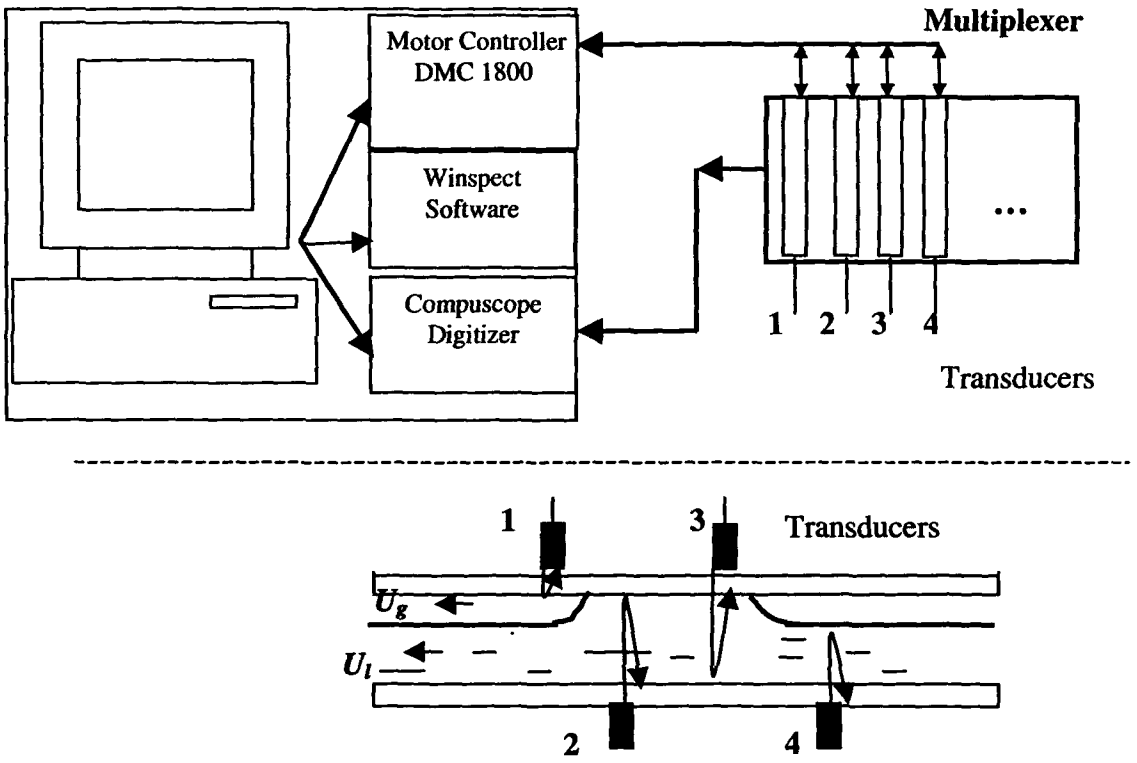

Figure 3-7: Schematic representation of the equipment used for ultrasonic pulse-echo measurements

3.3 Experimental Setup

Figure 3-8 shows a schematic diagram of the experimental setup for horizontal two-phase flow in a cylindrical pipe. The pipe has an inner diameter of 2.1 cm and was made of glass to allow visualization of the flow patterns. Water and air at atmospheric conditions are injected into the end of the pipe and single phase flow rates have been measured by two Brooks rotameters (models 1110-08H2A1D, 1110-10H3A1D), before the mixing section. All reported superficial gas velocities are at standard conditions (1

bar, 20°C). The superficial velocity of the liquid was varied between 0.019 m/s and 0.14 m/s and the superficial velocity of the gas ranged from 0.24 m/s to 4.33 m/s. The superficial velocities were calculated as the ratio between the volumetric flow rate of the phase and the cross-sectional area of the pipe. The errors in the determination of the superficial velocities were therefore due to the error associated with the rotameters in providing the volumetric flow rates, and the error in the determination of the pipe diameter. The pipe diameter was determined ultrasonically, so that its error is a combined measure of the imprecision in the determination of the speed of sound in water, the transducer resolution and the imprecision in locating the transducer at the bottom of the pipe while performing the pipe diameter measurements. Based on these considerations, the relative error of the superficial velocities was estimated to 2%.

At the entrance of the liquid into the pipe there is a mixing section that is used to enhance the onset of fully developed two-phase flow. The measurement transducers are located downstream from the mixer section with a maximum L/d = 119.8 cm (251.5 divided by 2.1 I.D. tube diameter) to allow the flow to be developed as much as practical for the experimental system. Transducer 1 and transducer 3 were mounted on the top surface of the pipe at a distance approximately L=263cm (transducer 1) and L=251.5cm (transducer 3) respectively a distance between them is 11.5 cm. Transducers, 2 and 4 were mounted on the bottom surface of the pipe at roughly a distance of L=266cm (transducer 2) and L=254cm (transducer 4) respectively with a separation distance of 12cm. The separation distance is chosen to obtain reasonable time of flight results and ensure transducers were not located next to a mechanical joint of the piping system. The

difference in location between a top and bottom transducer was chosen to avoid the interference of the signals received by the transducers.

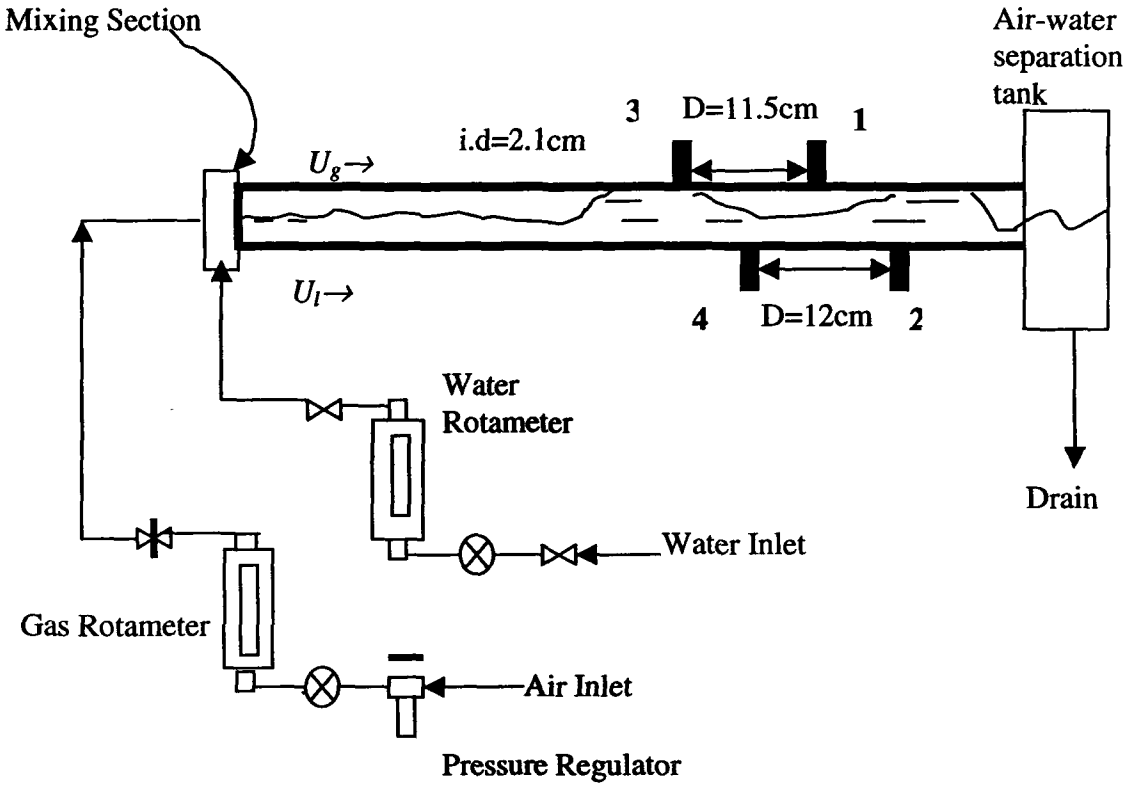

***Figure 3-8:** Experimental apparatus for air-water two-phase flow measurement*

CHAPTER 4

High Speed Ultrasonic Pulse-Echo System Characterisation

This chapter presents an overview of the calibration results, C-scan results and signal processing involved for the dynamic measurements of two-phase flow parameters.

4.1 Determination of Measurements Accuracy

The experimental system used for the calibration was a horizontal cylindrical pipe partially filled with a known amount of water (static). The liquid level was measured using one ultrasonic contact transducer, model # A112S 10MHz ¼" (6mm) diameter working in a pulse-echo mode. A typical result from the A-scan is shown in Figure 4-1, where the first signal (a) represents the initial pulse, the second signal (b) is the echo that comes from the tube wall/liquid interface, the third signal (c) is the signal from the liquid/air interface and all the echoes that come after (c) represents multiple echoes from the tube wall/liquid interface or liquid/air interface. In order to proceed for any liquid level measurements or any other measurements the sound velocity through the water should be known. Therefore the sound velocity for the present experiment was measured when the tube was full with liquid. By knowing the diameter of the tube (50 mm) and the time (Δt) that the sound travelled through the liquid the sound velocity was calculated to be 1480±1.5 m/sec, where the theoretical value is 1500m/s at T= 22° C [37]. The errors in the measured sound velocity could be due to a difference in the water temperature where was T=20°C. The time delay for sound reflections is converted into thickness by simply

applying equation (4-1) as follows:

$$h = c \times \frac{\Delta t}{2} \quad , \tag{4-1}$$

where c is the speed of sound in the liquid phase, Δt is the time interval between reflected signal from the tube-wall/liquid interface (b), and liquid/gas interface (c) as shown in Figure 4-1. The liquid thickness can be also obtained from the geometrical representation of the apparatus using the following relation:

$$h_{Geometry} = r(1 - \cos\frac{\theta}{2}), \tag{4-2}$$

where $h_{Geometry}$ is the liquid thickness in the tube, r is the tube radius and θ is the angle as is shown in Figure 4-2. The void fraction is simply defined by equation (4-3):

$$\alpha = \frac{\left(V_{total} - V_{liquid}\right)}{V_{total}} = 1 - V_{liquid} / V_{total}, \tag{4-3}$$

where $V_{total} = \pi \cdot r^2 \cdot L$ and L is the tube length. In all the present tests, measured quantities are L = 350 mm; r = 25 mm; $V_{liquid} = \frac{L}{2} r^2(\theta - \sin\theta)$ where θ is calculated from the transcendent equation (4-4):

$$\theta - \sin\theta = 2\pi(1 - \alpha), \tag{4-4}$$

where α is the void fraction and is simply defined by equation (4-3).

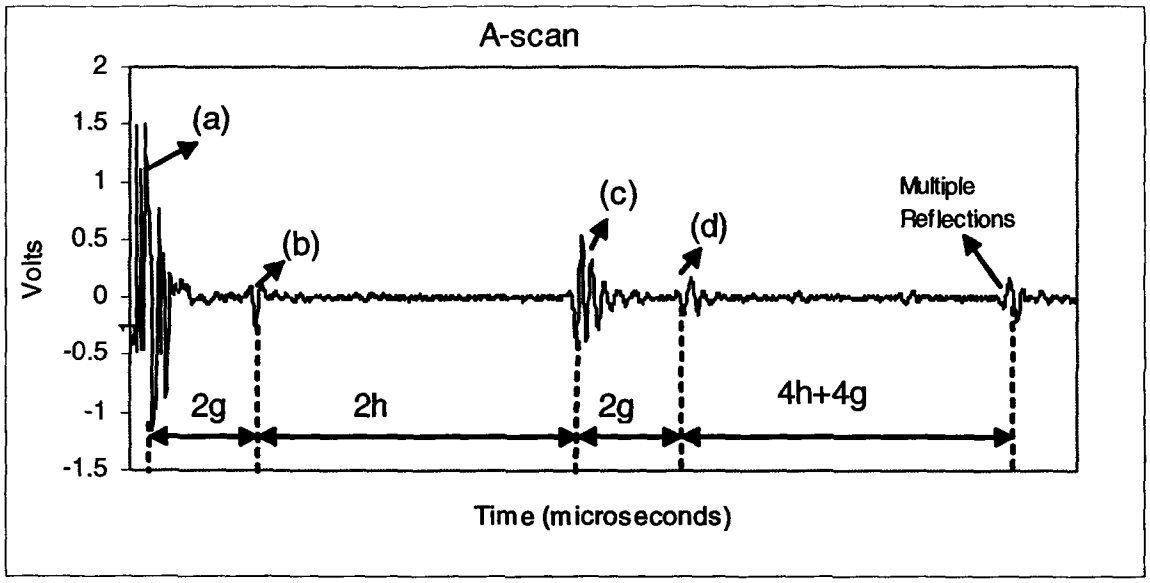

Figure 4-1: *Typical representation of the wave from an A-scan where (a) is the initial pulse, (b) is the wave reflected from the tube-wall/liquid interface, (c) is the wave reflected from the liquid/gas interface, multiple reflection from the tube/liquid interface*

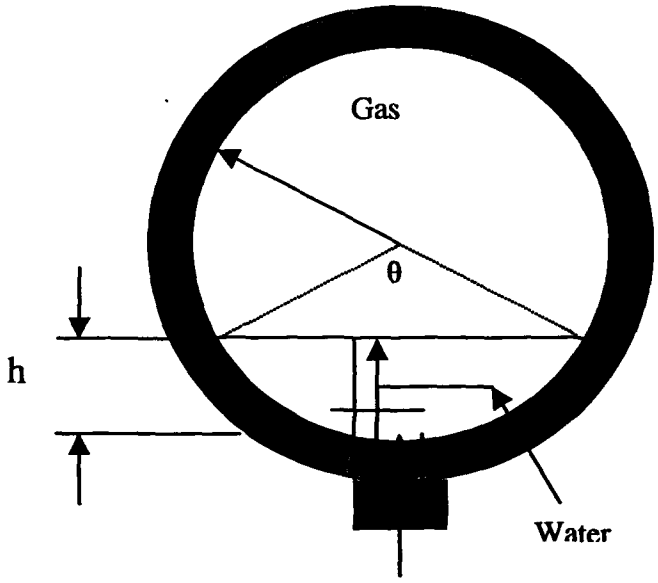

Figure 4-2: *Liquid level measurements; geometrical representation in a horizontal tube*

Figure 4-3 represents the liquid levels calculated based on the liquid volume in the tube (h-geometry) as a function of liquid levels measured by the ultrasonic pulse-echo technique (h-ultrasonic). A least squares fit analysis is applied to show the accuracy of the measurements. The points fit very well on a line through the origin, with a coefficient of determination $R_2 = 0.9996$ and an accuracy of measurements less than 1.5% absolute error. The measurement error is due to a combination of the following factors: the transducer resolution, the imprecision in the determination of the speed of sound in water, the imprecision in locating the transducer exactly at the bottom of the pipe. In addition, although not due to an error of the measurements, a difference in the results between the geometrically calculated levels and the measured ones in Figure 4-3 may come from the capillarity effects at the interface between the water surface and the pipe walls, where the water surface curbs towards the walls, thus affecting the overall water level.

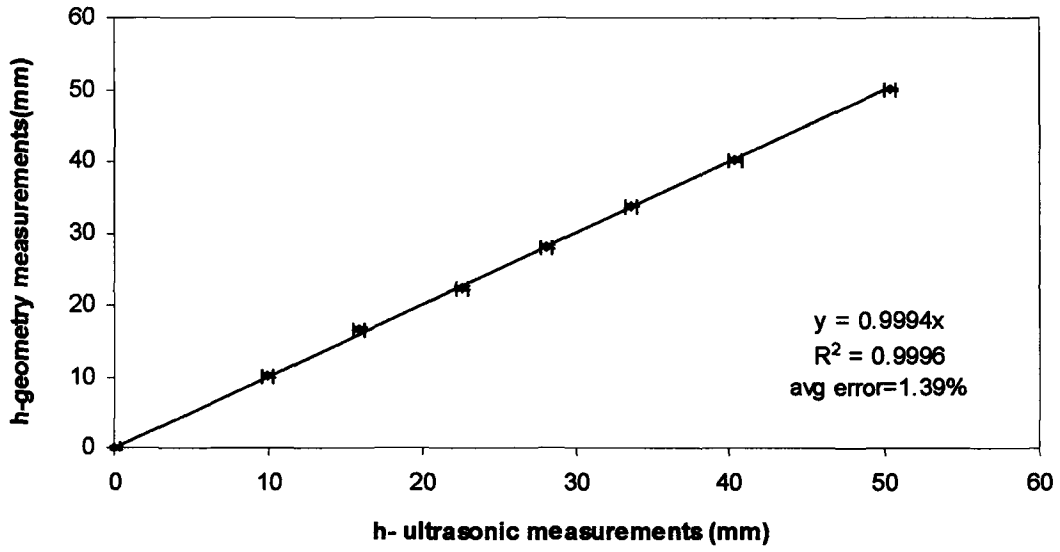

Figure 4-3: *Measurement accuracy results for a 50 mm i.d. tube*

4.2 C-scan Experimental Results by High Speed Ultrasonic Pulse-Echo System

For a better understanding of the signal processing involving a liquid level that corresponds to a plug flow regime is chosen as it is shown in Figure 4-4. In the present configuration each transducer sends a signal and when a liquid/air boundary is encountered each transducer receives its own echo back. This data is acquired in real time using a C-scan algorithm as was explained in Chapter 3. An example of the real time data acquisition obtained by C-scan, with transducer # 2 placed on the bottom surface of the tube, is shown in Figure 4-5. As the figure shows, C-scan plots show the proper liquid level as a function of time (several A-scans) in the case of plug flow. It is hard to interpret a C-scan, because some of the unidentified points represent noise due to the sudden change of level and high frequency noise. Therefore before a liquid level estimate can be made, some signal processing must be done for a successful repeatable measurement to be obtained.

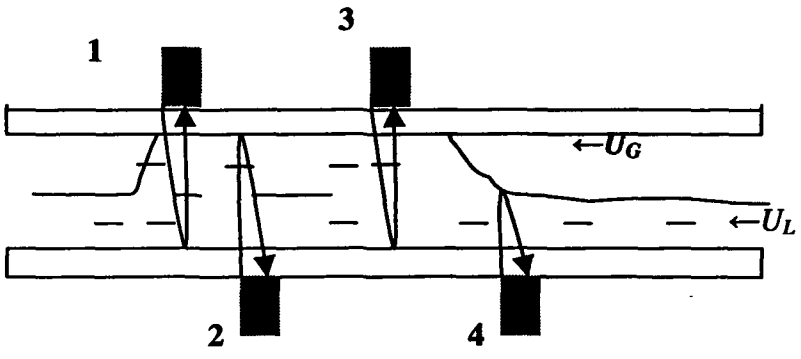

Figure 4-4: Plug flow regime representation and signal detection

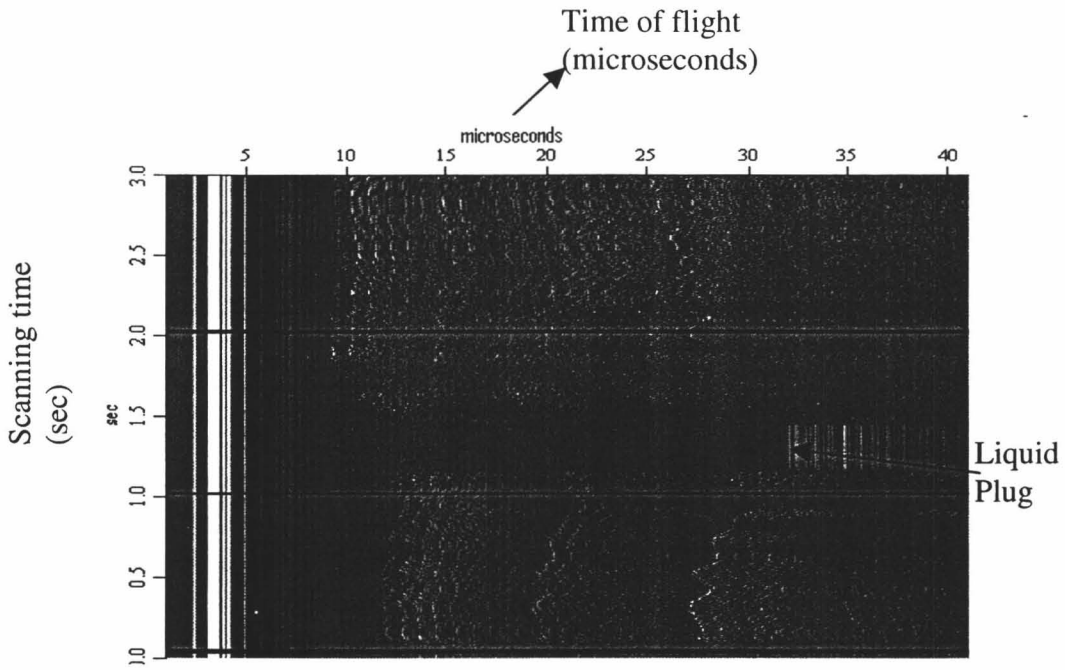

Figure 4-5: *C-scan image using transducer # 2 from the bottom of the pipe with no filter applied*

4.2.1 Signal Processing

The RF signal received by the digitizer from the transducer via the multiplexer consists of the desired signal, which contains information about liquid level, void fraction, plug velocity, etc. However not all the RF data received is useful, such as multiple repetitions, therefore a gate was used that allows only the acquisition of the signal that travels a distance equal to the diameter of the tube and all other repetition echoes are ignored. As was mentioned in the earlier discussion some signal processing is required to improve the waveforms and implicit the C-scan for a more clear interpretation of the results. The pre-subtraction and post-subtraction signals are shown in Figure 4-6 (a, b, c), by using data for the liquid level from a plug flow regime. The first step in the

process is to filter the signal to remove the unidentified points. The second process is to rectify the waveform and finally apply an enveloping function. This has the effect of tapering the ends of the data array without affecting the center portion significantly. The filtering is done via point-by point multiplication with the center half of the signal being multiplied by unity while both the beginning and end quarters are multiplied by coefficients which taper from unity at the center of the segments to zero at the ends. The filter is used to cut down on noise in the next step of processing due to sudden changes at the ends of the data segment. Once the waveform signal processing is completed, the C-scan images shown in Figures 4-7 to 4-10 can be very easily interpreted. These C-scan images can be interpreted by extracting the A-scan waveforms that were described earlier which give the time of flight and implicitly the liquid level. Figure 4-7 represents a typical result by the C-scan and A-scan method as it was detected by transducer # 1 placed on the top surface of the tube in the case of a plug flow regime. During a 3 seconds data acquisition time, transducer # 1 was able to record the instantaneous location of the tube wall/gas interface and liquid/tube-wall interface. More specifically from Figure 4-7 it is observed that between 0s and 1.3s acquisition time the transducer recorded the instantaneous location of the tube wall/gas interface where between 1.3s and 1.6s it shows that a liquid/ tube wall interface is present and again after 1.6s acquisition time a tube-wall/gas interface exists.

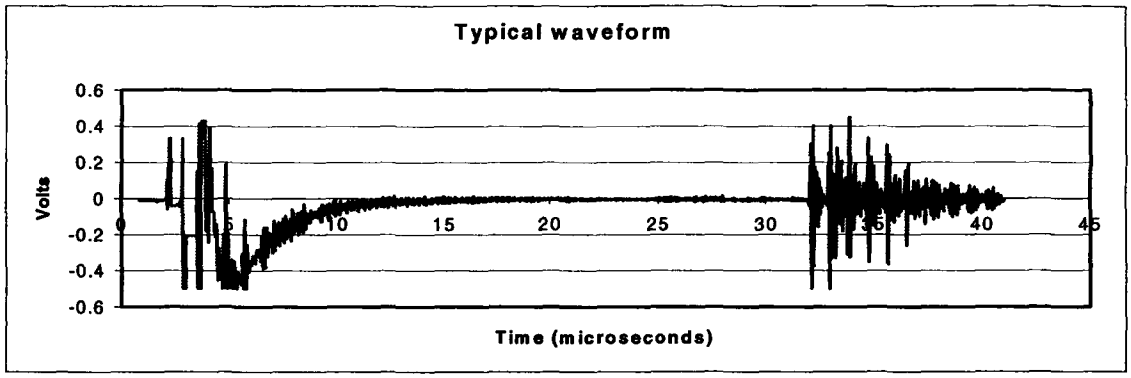

(a)

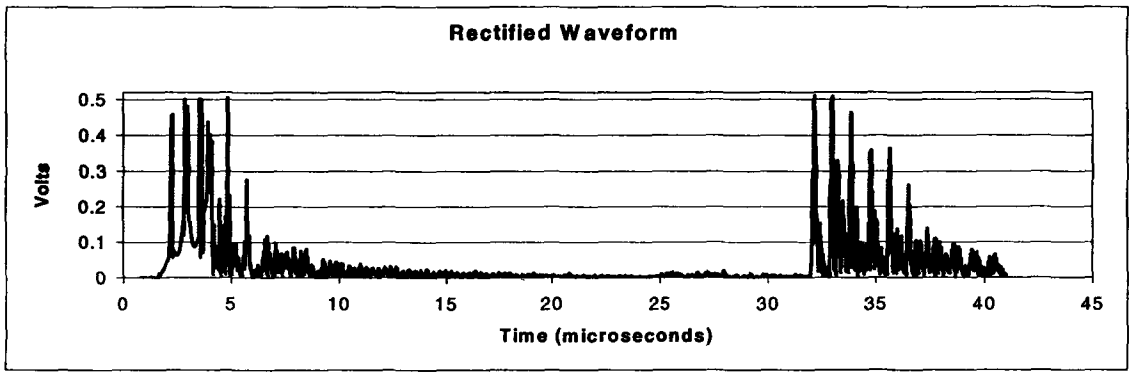

(b)

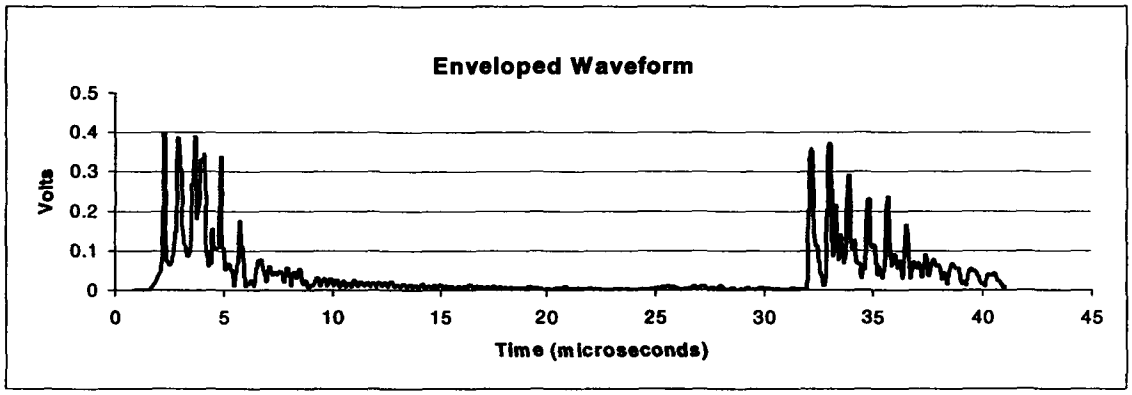

(c)

***Figure 4-6:** Wave processing – Typical waveform (a), Rectified waveform (b), Enveloped waveform (c)*

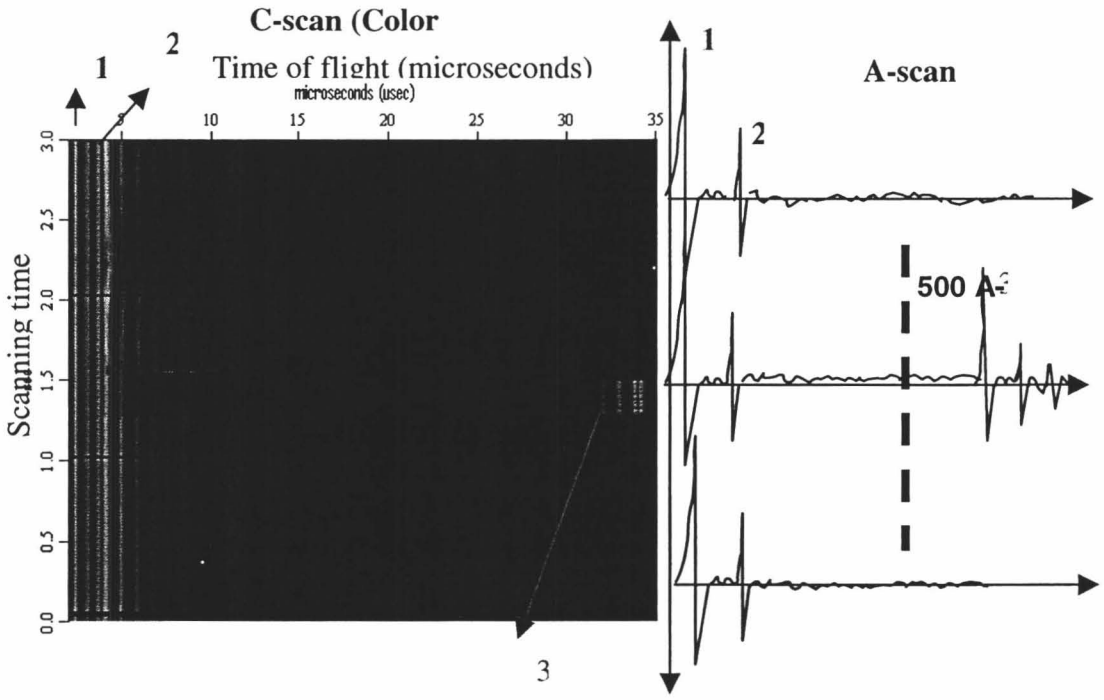

Figure 4-7: *C-scan and A-scan representation of the ultrasonic signals detected by transducer # 1, 1- initial pulse, 2- tube wall/liquid interface, 3- liquid/air interface*

Figure 4-8 represents the C-scan plot as was detected by transducer # 2 placed on the bottom surface of the tube at roughly 4 cm distance from transducer #1. As can be seen from the figure, this transducer recorded the instantaneous location of the liquid/gas interface and liquid/tube-wall interface. The liquid/tube-wall interface is encountered in the region between 1 and 1.7s acquisition time and it is recognized by the fact that the sound travelled a distance through the water equal to the diameter of the pipe.

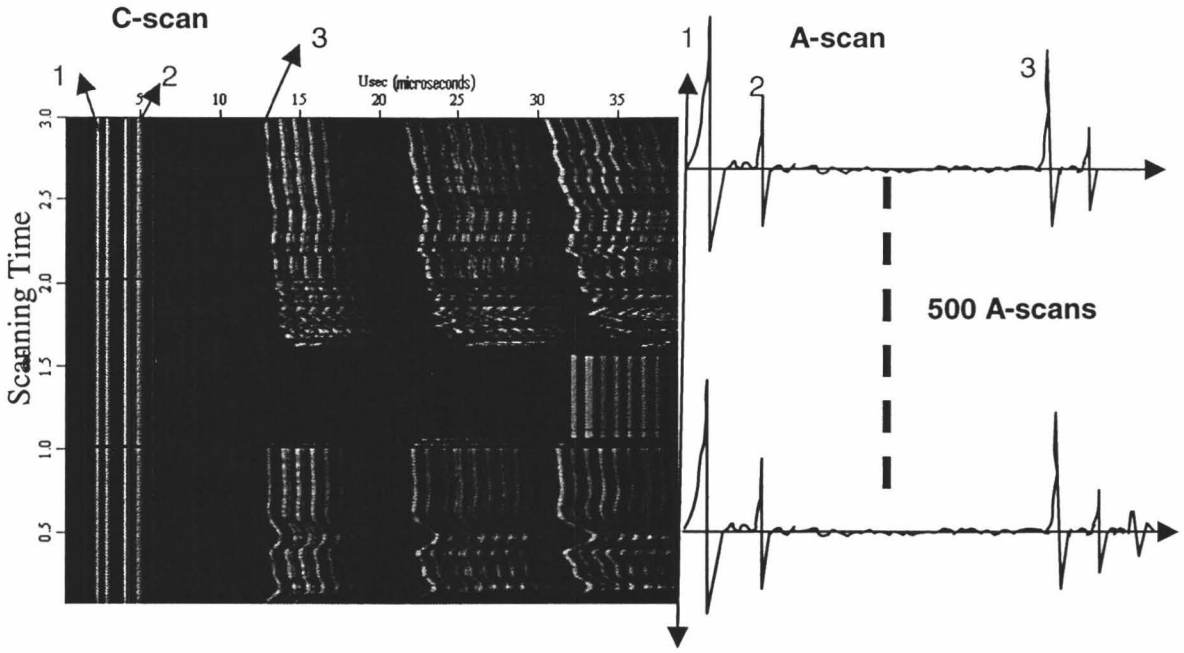

***Figure 4-8**: C-scan and A-scan representation of the ultrasonic signals received from transducer2, 1- initial pulse, 2- tube wall/liquid interface, 3- liquid/air interface*

Figure 4-9 shows the C-scan plot obtained by transducer # 3 that is placed at 11.5cm distance from transducer # 1. By comparing Figure 4-7 and 4-9, it can be observed that the only difference between them is that the transducer # 3 shows the instantaneous location of the liquid/ tube-wall interface between 1.2s and 1.55s acquisition time, which corresponds to a moment earlier than can be detected by transducer # 1. This is expected due to the distance between the two transducers. The same result can be observed by comparing Figure 4-8 and Figure 4-10 where, transducer #4 records the liquid plug earlier than transducer # 2.

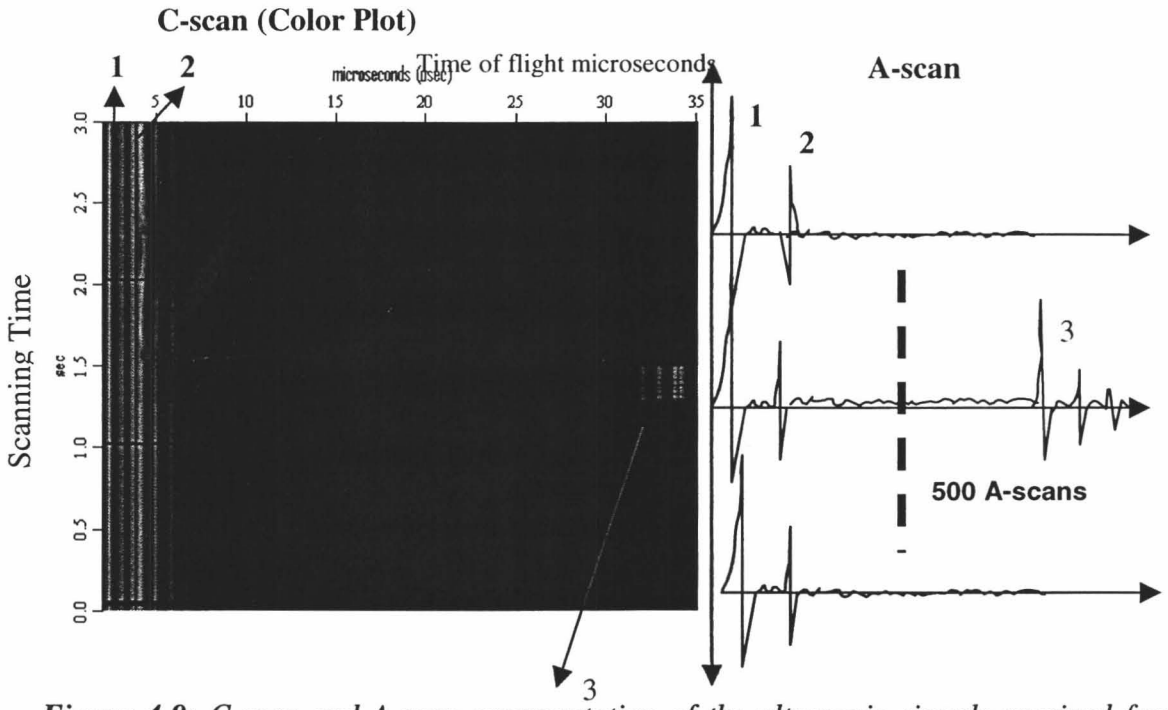

***Figure 4-9**: C-scan and A-scan representation of the ultrasonic signals received from transducer 3, 1- initial pulse, 2- tube wall/liquid interface, 3- liquid/air interface*

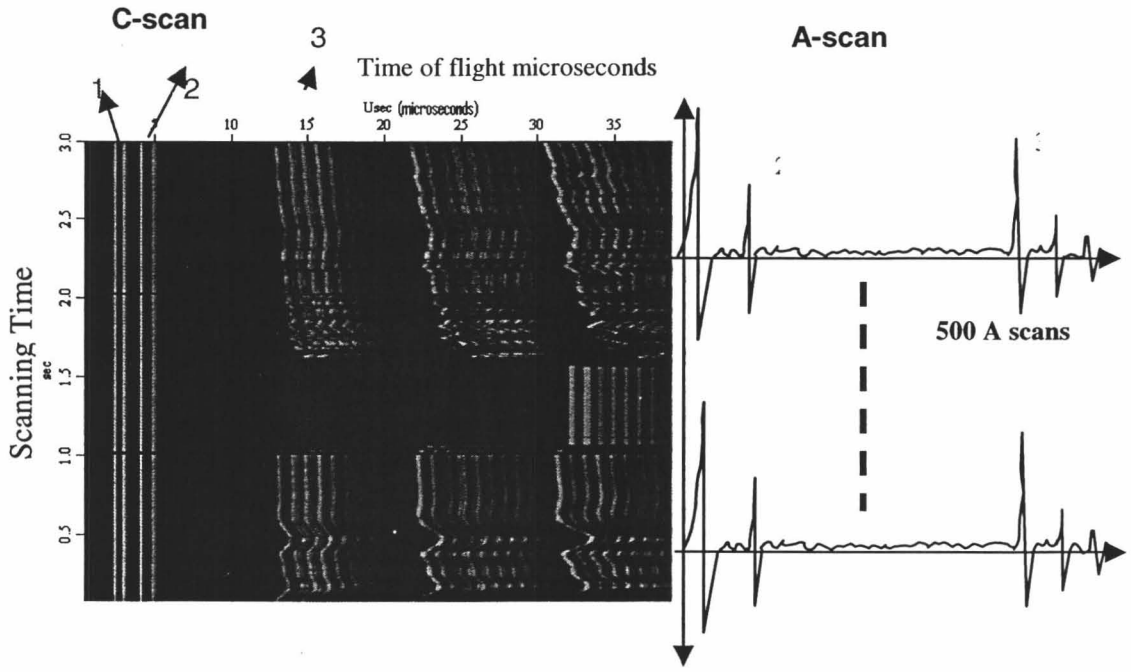

***Figure 4-10:** C-scan and A-scan representation of the ultrasonic signals received from transducer 4, 1- initial pulse, 2- tube wall/liquid interface, 3- liquid/air interface*

4.2.2 Detection of Δt and Liquid Level Calculation

The waveform resulting from the above method is analyzed with a peak-detection algorithm to identify the amplitude peaks. The algorithm is part of a program written in Visual Basic and its purpose is to automatically provide liquid level information inside the tube from the C-scan processor. The algorithm first reads the time-of-flight data from the C-scan files and stores them into variables. A logic diagram for this algorithm is presented in Appendix A. It then converts all the data into A-scans for each sample. The user has the option to set the algorithm to read the data starting with the signal that corresponds to the tube-wall/liquid interface or tube-wall/gas interface. The algorithm then detects all the other peaks from the A-scan that are greater than a set percentage of the amplitude of the highest peak by finding the highest remaining peak, therefore it can identify the signal coming from the reflection at the liquid/gas interface, or tube-wall/liquid interface, reads the time-of-flight of that signal and calculates the liquid level using equation (4-1). More information about the peak detection algorithm is presented in Appendix A.

CHAPTER 5

Experimental Results for Horizontal Two-Phase Flow System

In this chapter, two-phase flow parameter measurements obtained by the high-speed ultrasonic pulse-echo system are discussed. The two-phase flow pattern characterisation for stratified smooth (SS), stratified wavy (SW), plug flow (PL), slug flow (SL) and annular flow (AN) is performed.

5.1 Liquid Level Measurements

The instantaneous location of the liquid/gas interface was accomplished by using the C-scan method described in Chapter 3. Then a peak-detection algorithm is used to convert the raw ultrasonic C-scan (20,000 A-scans) data provided by the four transducers during a 3s acquisition period into liquid level measurements. Figure 5-1 and 5-2 shows the liquid level measurements performed for various gas and liquid superficial velocities. As can be seen from Figure 5-1, for a constant gas superficial velocity (U_{gs}=0.24m/s) and increasing liquid superficial velocity from 0.019m/s to 0.072m/s, the liquid level increases almost linearly with liquid flow velocity as expected. Therefore it can be implied that the gas/liquid interface is smooth. Figure 5-2 shows the variation of the averaged liquid level as a function of gas superficial velocity. Initially the system is setup in stratified smooth flow with a gas superficial velocity of U_{gs}=0.48m/s, and a liquid superficial velocity of 0.048m/s. For increasing gas superficial velocity from 0.48m/s to

1.92m/s, the time average liquid level decreases with increasing gas flow velocity as shown in Figure 5-2. At the same time the liquid level oscillates between a minimum "Min" and a maximum "Max" value which corresponds to region number (1) in the figure, therefore the gas/liquid interface is no longer smooth and a transition from stratified smooth to stratified wavy (SS/SW) has occurred. Note the oscillations are small and in the range of 2mm which correspond to a wave amplitude consistent with stratified wavy flow. However increasing the gas superficial velocity it is observed that the average liquid level continues to decrease but the oscillations between the minimum liquid level "Min" and maximum liquid level 'Max" continue to increase. When the minimum liquid level is about 3.8mm (which represents approximately 20% of the diameter of the pipe) and the maximum liquid level is approximately 15mm which is almost 75 % of the diameter of the pipe a transition from stratified wavy to slug flow (SW/SL) occurs. This is shown in region number (2) of Figure 5-2. Essentially the system has demonstrated that it can measure the liquid level and identify different phenomena that occur.

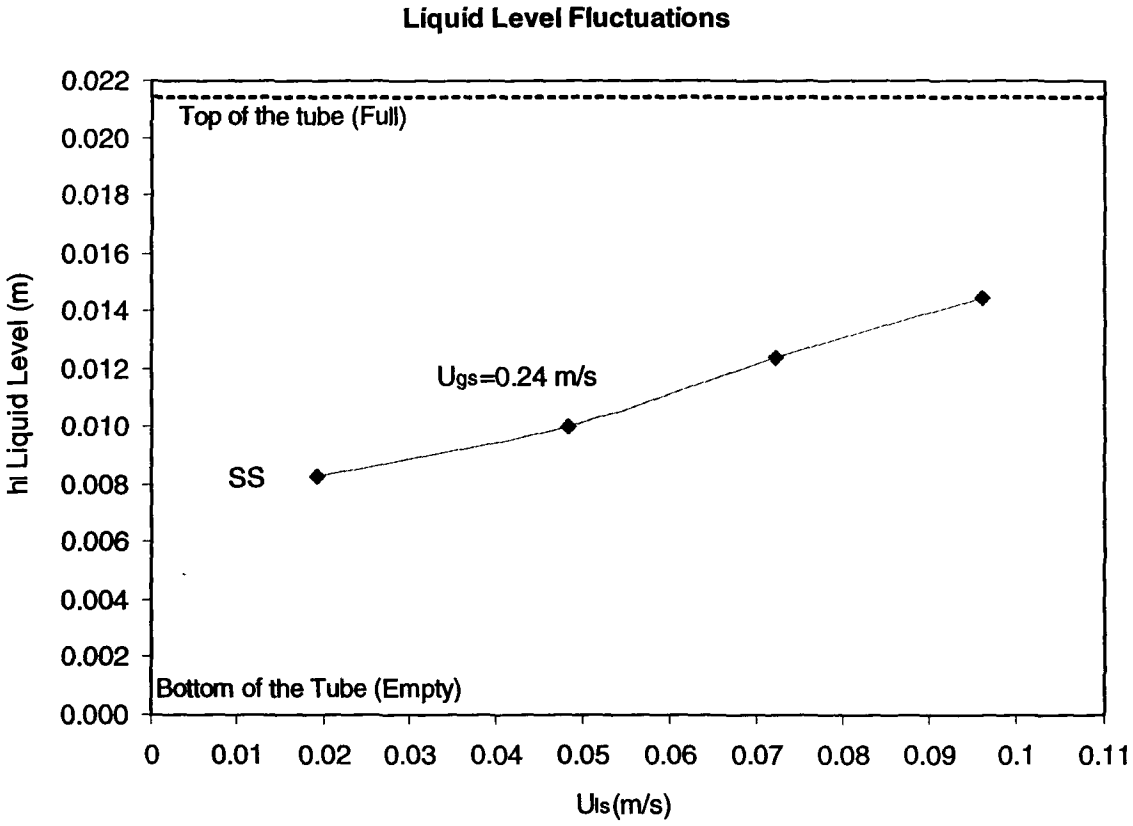

Figure 5-1: Time averaged liquid obtained by the high-speed ultrasonic pulse-echo system in a horizontal two-phase flow system for U_{gs}=0.24m/s.

flows at the bottom of the pipe and the gas at the top and the interface between them is smooth. While transducer #1 from the top of the tube shows that there is no liquid level in the tube which means that no liquid touched the top surface of the tube. Hence this flow pattern corresponds to a stratified smooth (SS) flow regime as represented in Figure 5-3c. Optical visualisation (by eye) through the glass tube confirmed that the flow pattern was stratified smooth.

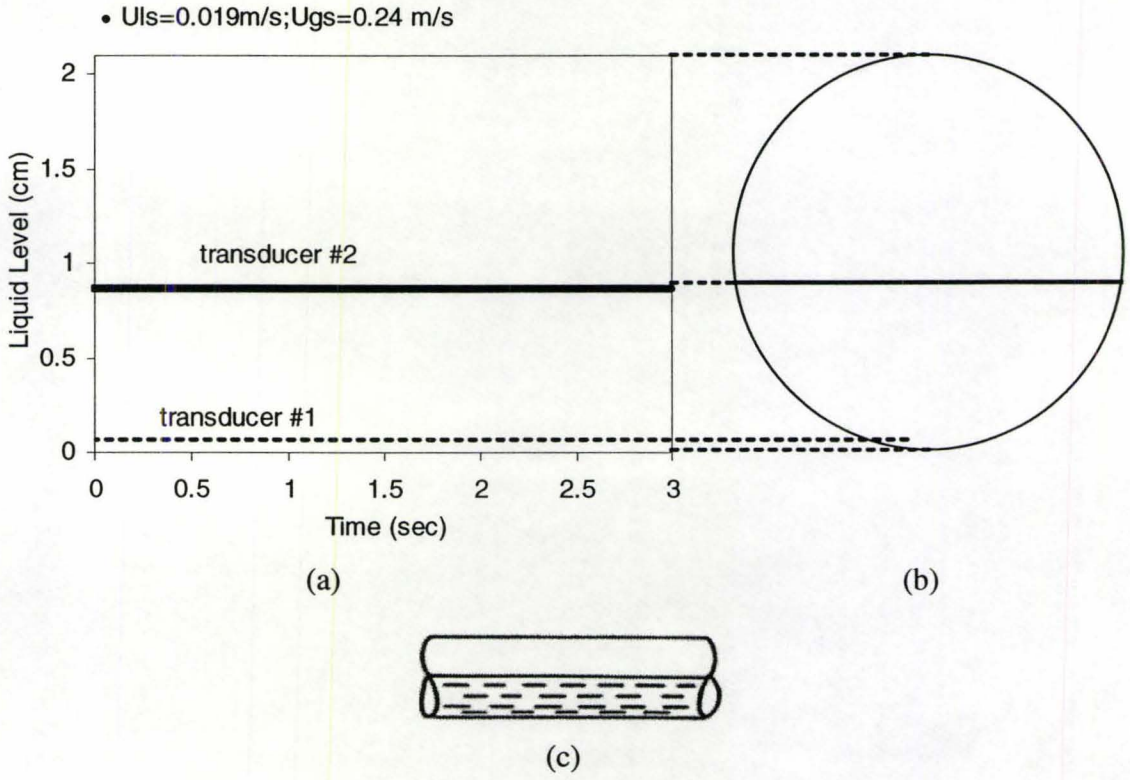

Figure 5-3: *Typical liquid level transient waveform for stratified smooth flow detected by transducers #1 and #2. (a) – liquid level as a function of time; (b) – liquid level in cross-section of the pipe, (c) –stratified smooth flow pattern*

For a gas superficial velocity of 0.96 m/s and a liquid superficial velocity of 0.019m/s, a time dependent variation in the liquid level between maximum and minimum value is observed. Typical liquid level transition detected by transducer #2 for this

combination of superficial velocities is shown in Figure 5-4, and it is observed that the gas/liquid interface is disturbed with a rippled surface which appears to give the stratified wavy flow pattern (SW) as shown in Figure 5-4c. Note transducer #1 indicated that no liquid touched the top of the tube (the liquid level is zero). Optical visualisation through the glass tube confirmed the flow pattern as stratified wavy flow (SW).

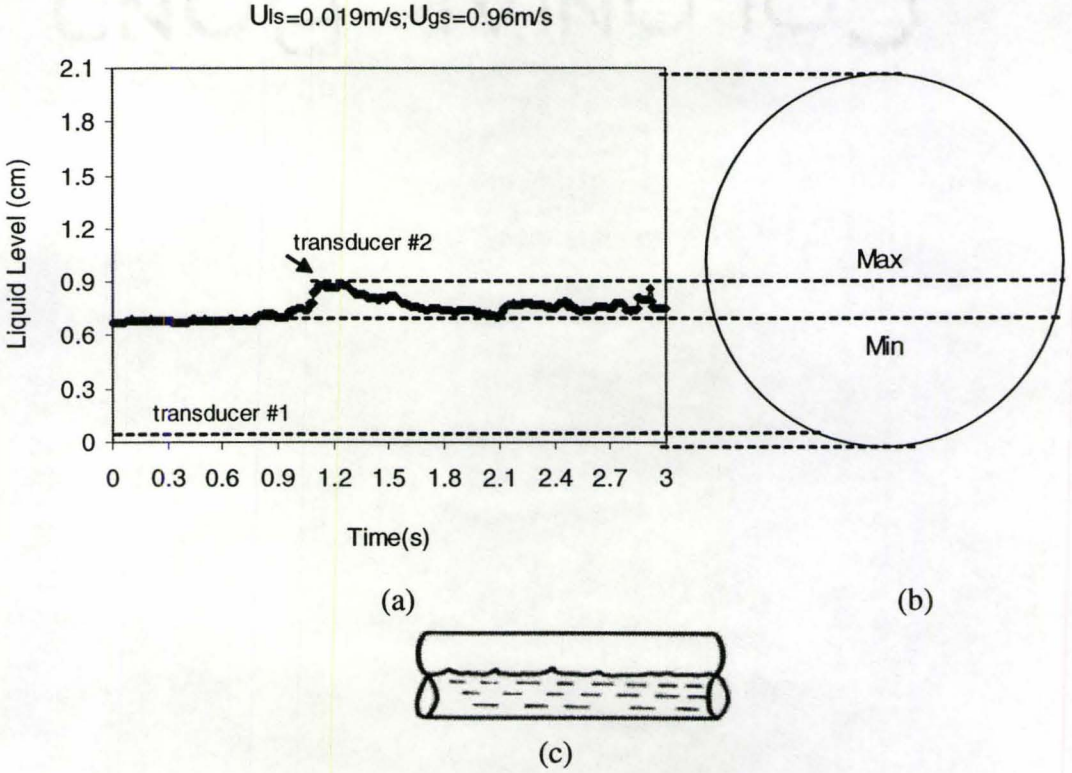

Figure 5-4: *Typical liquid level transient waveform for stratified wavy flow detected by transducer #2 and #4; (a)- liquid level as a function of time; (b) – liquid level in cross-section of the pipe, (c) –stratified wavy flow pattern.*

For a gas superficial velocity of 1.92m/s and a liquid superficial velocity of 0.072m/s slug flow is observed. Figure 5-5 shows a typical liquid level transient for this combination of superficial velocities detected by transducer #4 from the bottom and transducer #3 from the top. Transducer #4 shows that the liquid level oscillates between a

minimum liquid level of 0.31cm and maximum liquid level of 1.16cm. Transducer #3 from the top records some liquid level in the region of 0.7s and 1.3s at a moment later than transducer #4 recorded and this is expected because of the distance between the transducers. Therefore from these indications it can be implied that the gas/liquid interface is not smooth and this flow pattern is known as the slug flow regime.

For gas superficial velocity of U_{gs}=0.96m/s and liquid superficial velocity of U_{ls}=0.097m/s plug flow can be observed. The difference between slug flow and plug flow is that the liquid level associated with the liquid plug does not oscillate between a minimum and maximum value and the gas/liquid interface is smooth as shown in Figure 5-6 and 5-7. As can be seen from the figures, this combination of velocities results in a long swell wave developed which completely blocks the pipe, forming a liquid plug, hence a plug flow regime was formed. Additional information that the liquid touches the top surface of the pipe is confirmed also by the results obtained using the top transducers # 1 and # 3 respectively as shown in Figure 5-7.

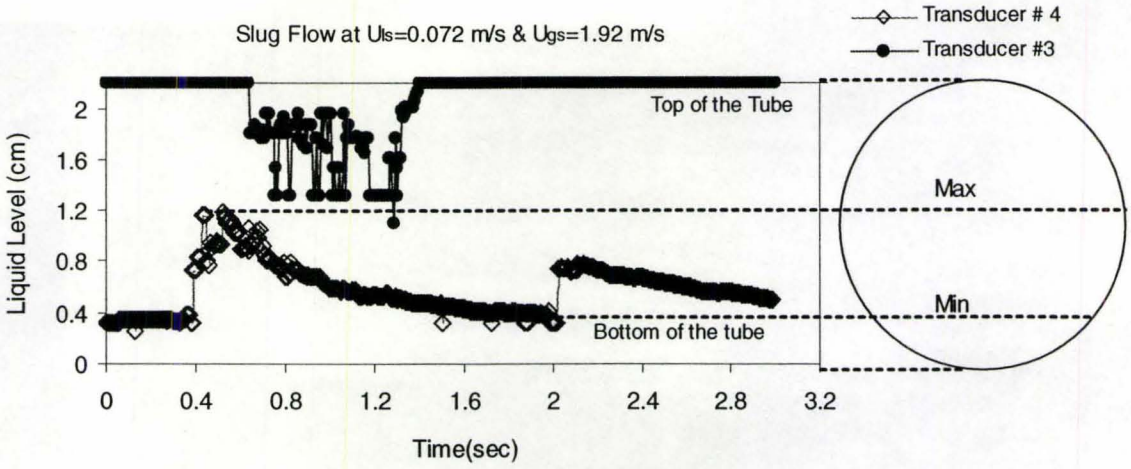

(a)

(b)

Figure 5-5: *(a) Typical liquid level transient for slug flow detected by transducer #4 from the bottom and transducer #3from the top; (b)- Slug flow regime representation.*

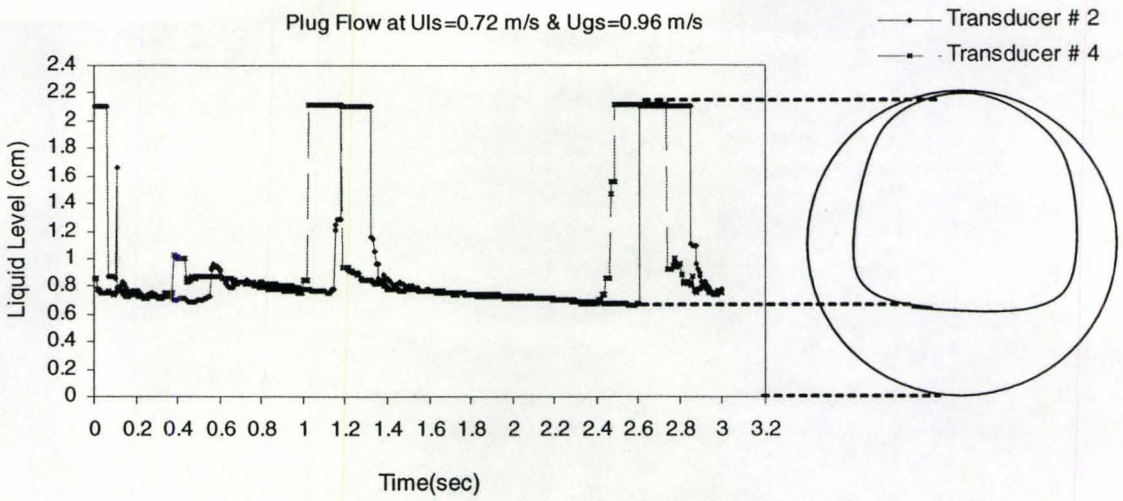

(a) (b)

Figure 5-6: *(a) Typical liquid level transient for plug flow detected by two bottom transducers; (b)-cross-sectional representation.*

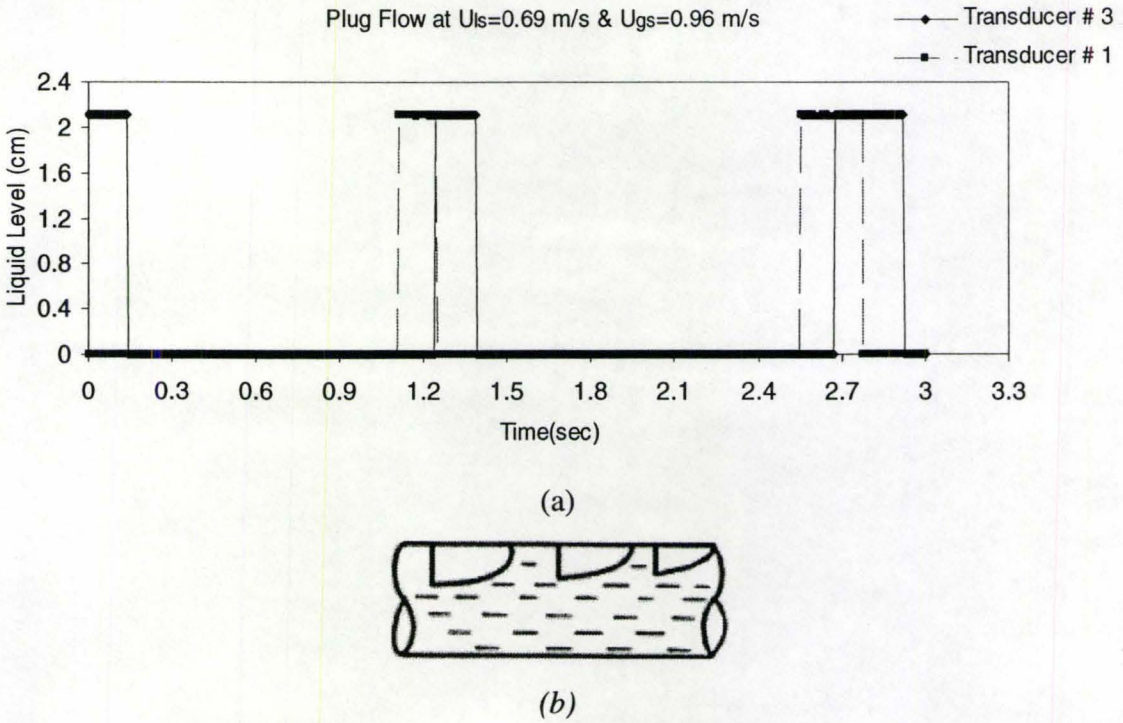

(a)

(b)

Figure 5-7: *(a) Typical liquid level transient for plug flow detected by two top transducers; (b) Plug flow regime representation.*

Figure 5-8 shows an example of the liquid level evolution obtained for gas superficial velocity of 4.33m/s and liquid superficial velocity of 0.072m/s. The liquid film formed at the top of the pipe is thinner than that formed at the bottom of the pipe as it was expected, due to gravity effects. Also it should be noted that the liquid film presents a maximum and minimum liquid level, hence it can be implied that there are some waves formed at the gas/liquid interface. These characteristics correspond to an annular flow regime where the liquid is swept up and around the pipe to form an annulus.

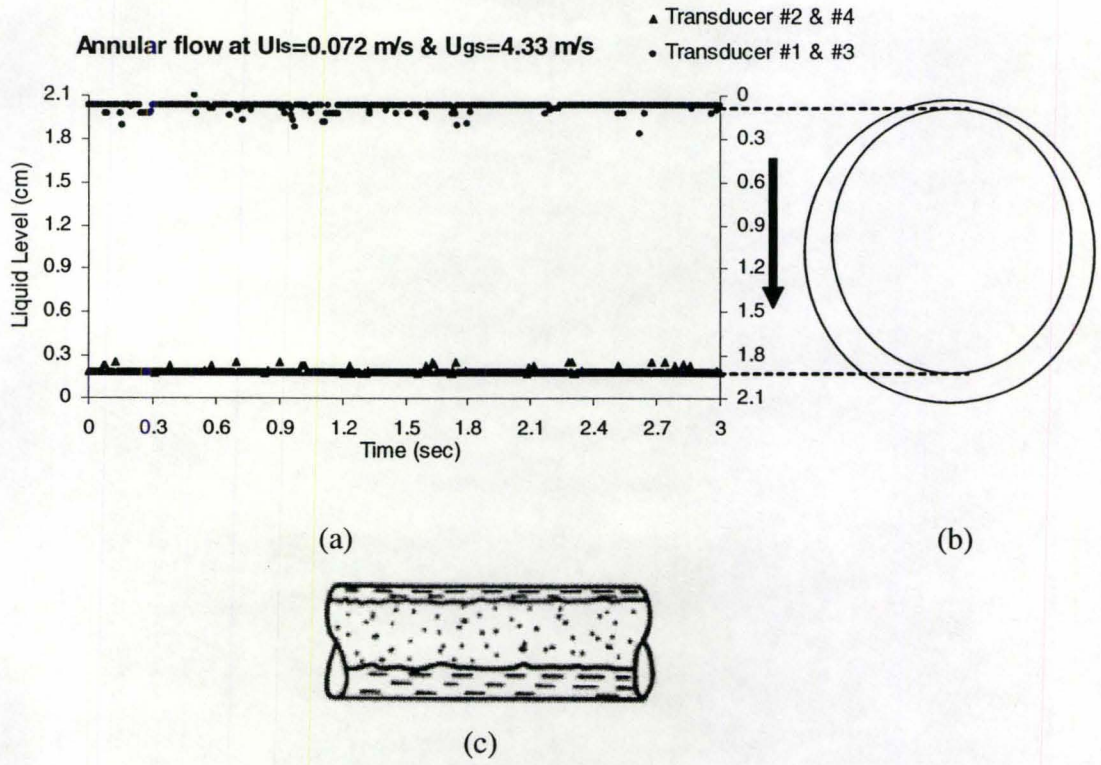

Figure 5-8: *Typical liquid level transient waveform for annular flow detected by four transducers; (a)- liquid film as a function of time; (b) – liquid film in cross-section of the pipe*

5.3 Two-Phase Flow Regime Map

For a quantitative description of the conditions which lead to the transition of flow regimes from one pattern to another, a flow regime map is created based on the superficial velocities of the liquid and gas. Over 70 data points were used to define the flow map for this experimental work that is shown in Figure 5-9. The flow regime map obtained by the high speed ultrasonic pulse-echo system is compared (Figure 5-9) with Lightstone et al. [38] experimental results by capacitance method. As seen from Figure 5-9, good agreement between the present experiment and Lightstone et al. [38] experiment is obtained. The present results are also compared with Mandhane et al. [3] experimental results. Figure 5-10 shows that the results are in good agreement.

Figure 5-11 shows a comparison of the present results with the theoretical model of Taitel and Dukler [4]. As Figure 5-11 shows there is good agreement between the experimental and theoretical results. The small discrepancies between predicted and observed transitions for stratified smooth to stratified wavy and slug to annular flow are quite acceptable to within error. However there is disagreement between Taitel and Dukler's [4] model and the current experimental results for the transition from stratified smooth to stratified wavy (SS/SW) to plug or slug flow. This discrepancy likely arises from the simple assumptions made in Taitel and Dukler's model [4], where the gas phase velocity (u_g) for the transition from stratified smooth to stratified wavy was assumed to be as follows:

$$u_g \geq \left[\frac{4g\nu_l(\rho_l - \rho_g)}{s\rho_g u_l}\right]^{1/2} \quad ; \qquad (5\text{-}1)$$

where, g is the gravitational acceleration, ρ_l is the density of the liquid, ρ_g is the density of the gas, u_l is the liquid velocity and s is the sheltering coefficient. For a transition from stratified smooth to intermittent flow, Taitel and Dukler [4] considered the gas velocity as per equation (5-2) as the transition criteria.

$$u_g > B\left[\frac{g(\rho_l - \rho_g)A_g}{\rho_g \frac{dA_l}{dh_l}}\right]^{1/2} \quad ; \qquad (5\text{-}2)$$

where B=0.5, g is the gravitational acceleration, ρ_l is the density of the liquid, ρ_g is the density of the gas, h_l is the liquid height and A_g, A_l are the gas and liquid cross sectional area. From equation (5-1), it can be observed that the transition from stratified smooth to stratified wavy is predicted without knowledge of the characteristic of the interfacial waves. Furthermore there is no account for the change in liquid velocity or any consideration of the liquid velocity at all, as the slug forms as seen from equation (5-2).

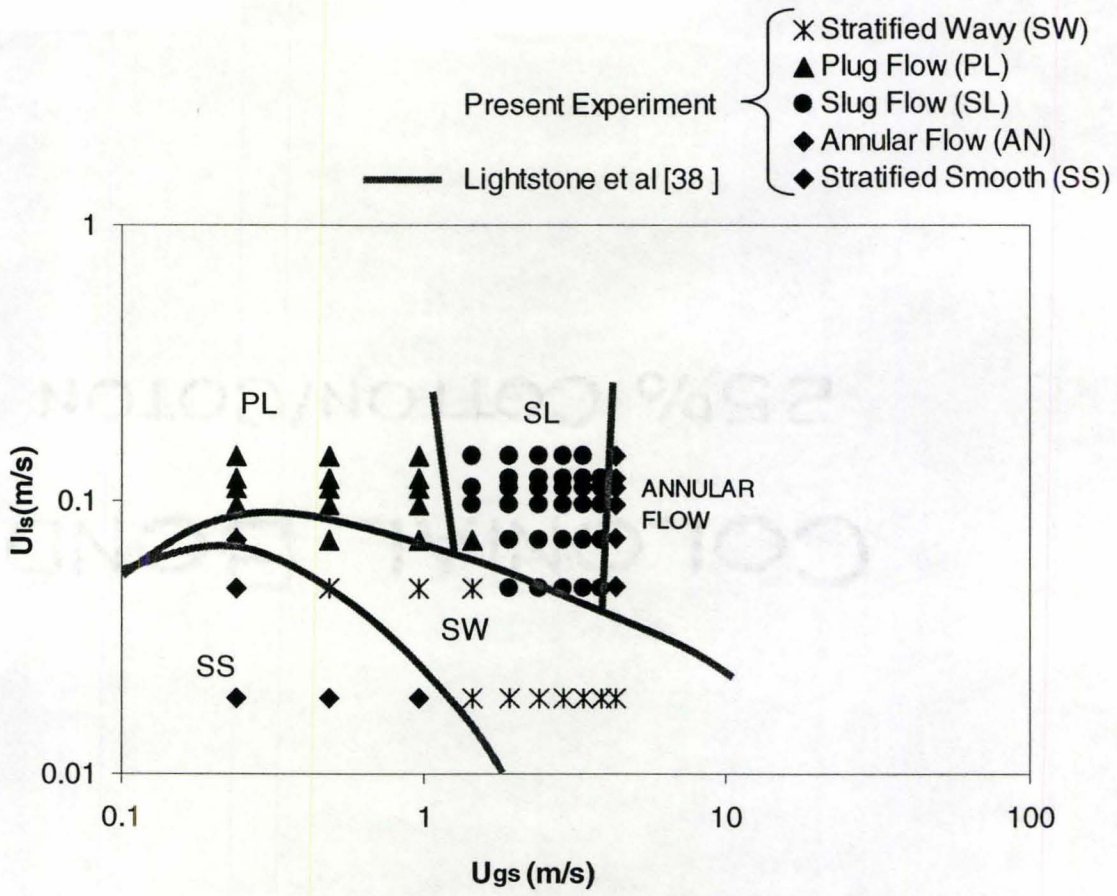

Figure 5-9: *Two-Phase flow regime map; comparison of the present results with Lightstone et al experimental results [38].*

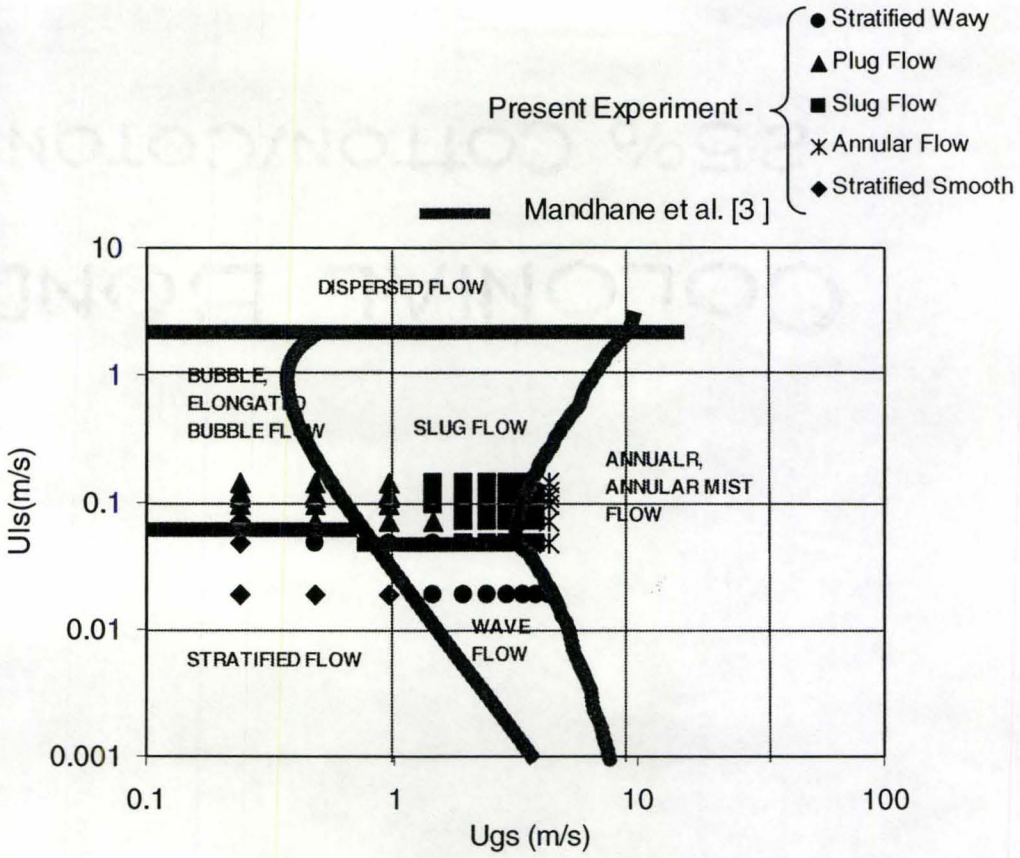

Figure 5-10: *Two-Phase flow regime map; comparison of the present results with Mandhane et al experimental results [3].*

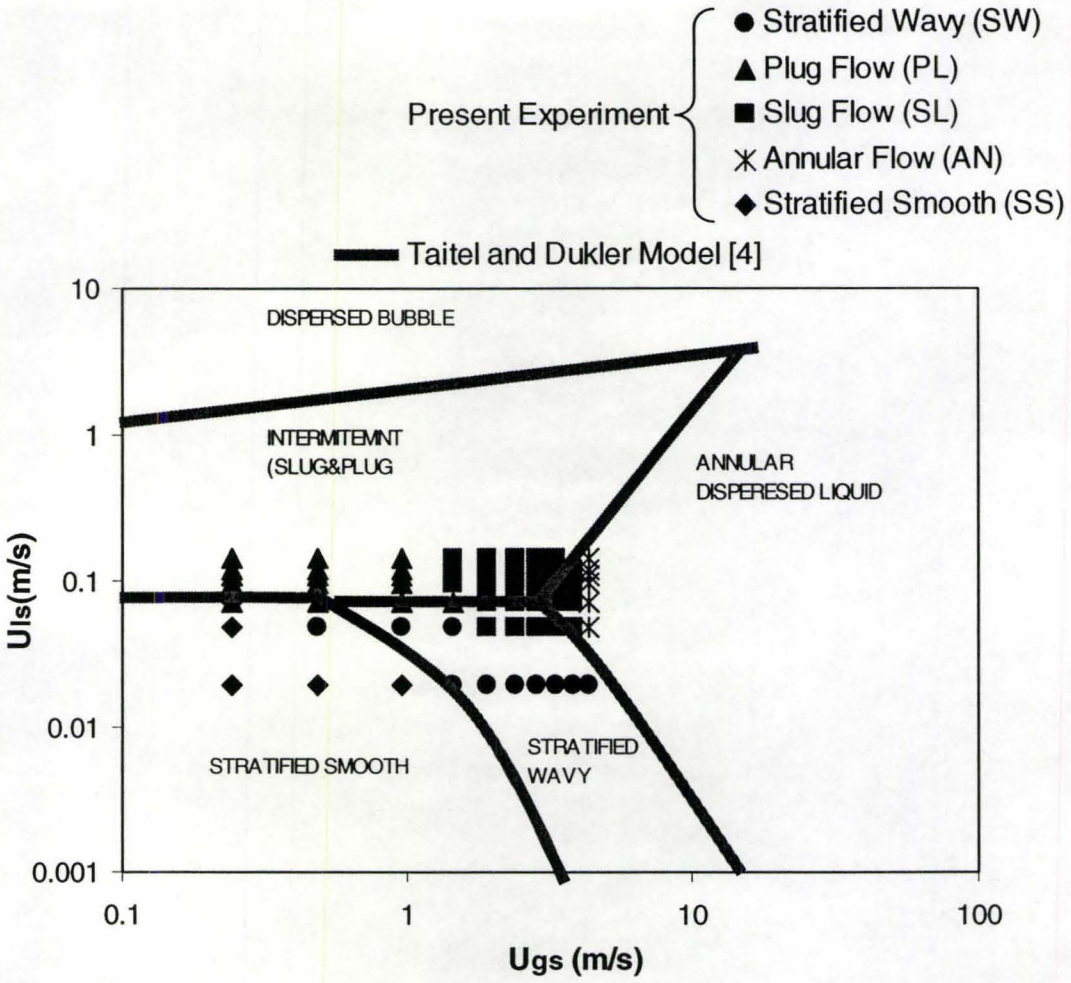

Figure 5-11: *Two-Phase flow regime map; comparison of the present results with Taitel and Dukler Model [4].*

5. 4 Void Fraction

5.4.1 Liquid Level and Void Fraction for Stratified Smooth Flow (SS)

The liquid level as a function of liquid superficial velocity (U_{ls}) and at a constant gas superficial velocity (U_{gs} =0.24m/s) is shown in Figure 5-12 and shows that the liquid level increases almost linearly with increasing liquid superficial velocity as expected. A comparison with the theoretical prediction of Taitel & Duckler [4] shown in Figure 5-12 shows that the liquid level for a stratified smooth flow (SS) results are in good agreement with theoretical predictions. Thus the theoretical prediction of Taitel and Dukler [4] for stratified smooth flow as per equation (5-3) predicts accurately this type of flow regime.

$$X^2 = \frac{\frac{4C_L}{D}\left(\frac{u_L{}^s D}{\nu_L}\right)^{-n} \frac{\rho_L (u_L{}^s)^2}{2}}{\frac{4C_G}{D}\left(\frac{u_G{}^s D}{\nu_G}\right)^{-m} \frac{\rho_G (u_G{}^s)^2}{2}} \quad ; \quad \text{n=m=1} \qquad (5\text{-}3)$$

where, C_G=C_L=16 for a laminar flow, u_L^S, u_L^S are the liquid and gas superficial velocities, D is the pipe diameter; ν_L, ν_G are the kinematics viscosity of liquid and gas; ρ_L, ρ_G are the liquid and gas density and X is the Martinelli parameter.

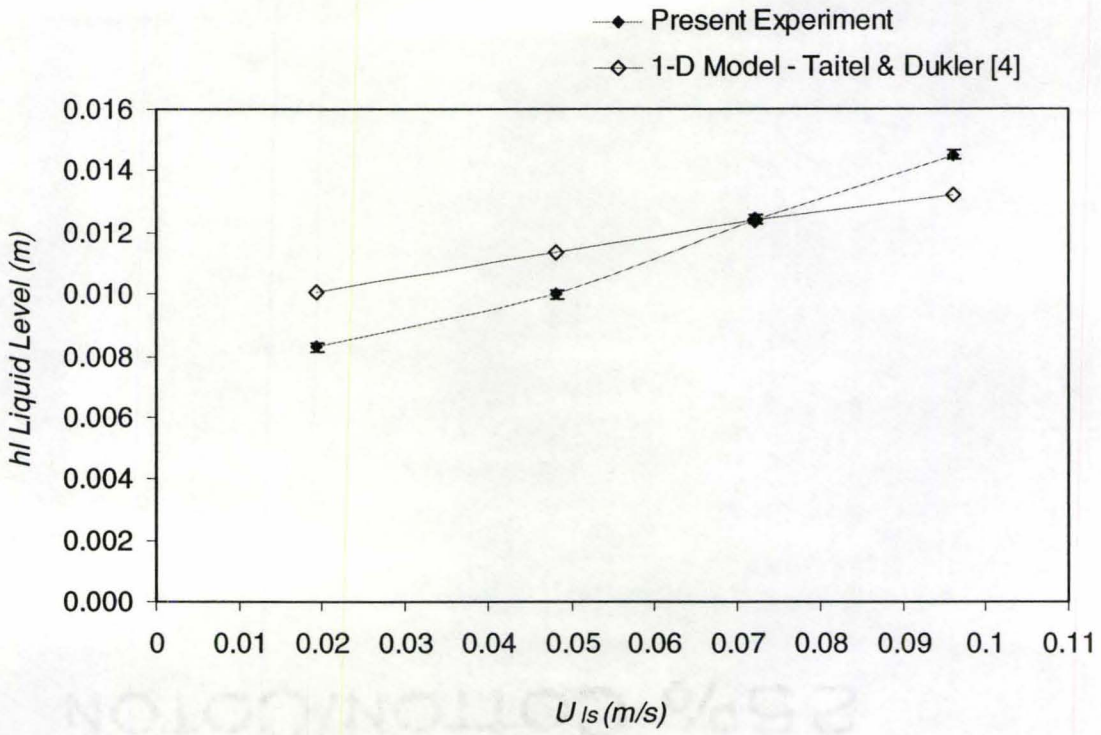

Figure 5-12: *Liquid level for stratified smooth flow regime as a function of liquid superficial velocities at constant gas superficial velocity U_{gs}=0.24 m/s; comparison with Taitel& Dukler's 1-D Model[4].*

Once the liquid level for a stratified flow regime is known the void fraction can be determined. For stratified smooth flow, a smooth gas/liquid interface in the x-axis (cross-section) is considered. The void fraction was calculated by dividing the cross-sectional area filled with gas to the total cross-sectional area of the pipe shown in Figure 5-13:

$$\alpha = \frac{1}{N}\sum_{i=1}^{N}\left(1-\frac{A_{li}}{A}\right) \quad , \qquad (5\text{-}4)$$

where, N is the number of measurements, A_{li} is the cross-sectional liquid area and A is the total cross-sectional area of the pipe. The cross-sectional area of the pipe filled with liquid is given by:

$$A_{li} = R^2 \cdot \left[\frac{\pi}{2} - \sin^{-1}\left(1 - \frac{h_{li}}{R}\right)\right] - (R - h_{li})\left(2Rh_{li} - h_{li}^{\ 2}\right)^{1/2}, \qquad (5\text{-}5)$$

where R is the radius of the pipe and h_{li} is the instantaneous liquid level.

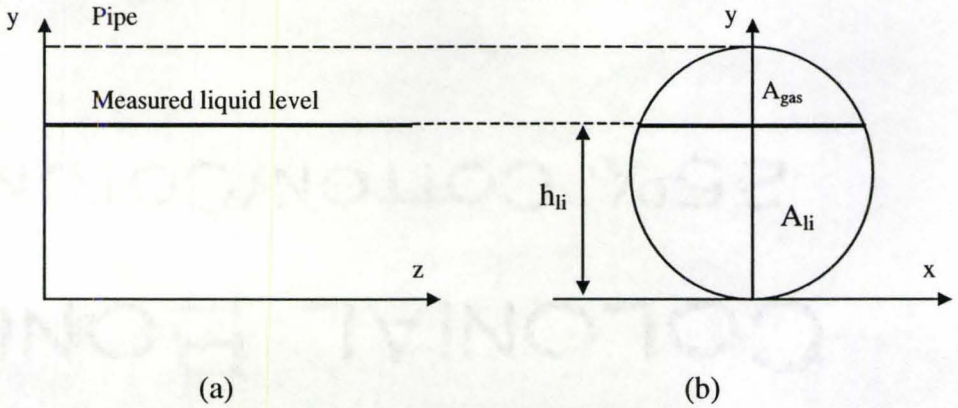

Figure 5-13: *Longitudinal representation of stratified smooth flow, based on liquid level data read by the instrumentation (a) and cross-sectional representation (b).*

By measuring the instantaneous liquid level during 3s acquisition period, void fraction can be simply determined using equations (5-4) and (5-5). Typical experimentally observed time and cross sectional averaged void fraction for the stratified flow regime is shown in Figure 5-14 as a function of liquid superficial velocities. As Figure 5-14 shows, with increasing liquid superficial velocity, the void fraction decreases in almost linear fashion. Lightstone et al. [38] used a capacitance method to measure the instantaneous and time averaged void fraction and developed 1-D [38] and 3-D theoretical models [39]. The results obtained for the void fraction by the high speed ultrasonic pulse echo system are in good agreement with those obtained by Linghtstone and Chang [39] for the capacitance method as Figure 5-14 shows. For lower liquid

superficial velocities than the experimental data the 3-D model predicts a higher void fraction. At a higher liquid superficial velocity (U_{ls}>0.04 m/s), the present experiment agrees well within ±10% of the 3-D Model. The fact that one dimensional model shows a lower value is could be due to the assumption that there is equal pressure drop in each phase and no pressure differential across the fluid-fluid interface as per equation (5-6) and (5-7).

$$-\frac{dP}{dz}-\tau_l\frac{S_l}{A_l}+\tau_i\frac{S_i}{A_l}=0 \quad ; \quad (5\text{-}6)$$

$$-\frac{dP}{dz}-\tau_g\frac{S_g}{A_g}+\tau_i\frac{S_i}{A_g}=0 \quad ; \quad (5\text{-}7)$$

where, A_g is the gas cross sectional area, A_l is the liquid cross sectional area, S_g, S_l are the gas and liquid wetted pipe perimeter, S_i is the interfacial perimeter, τ_g, τ_l are the gas wall and liquid-wall shear stress, τ_i is the interfacial shear stress

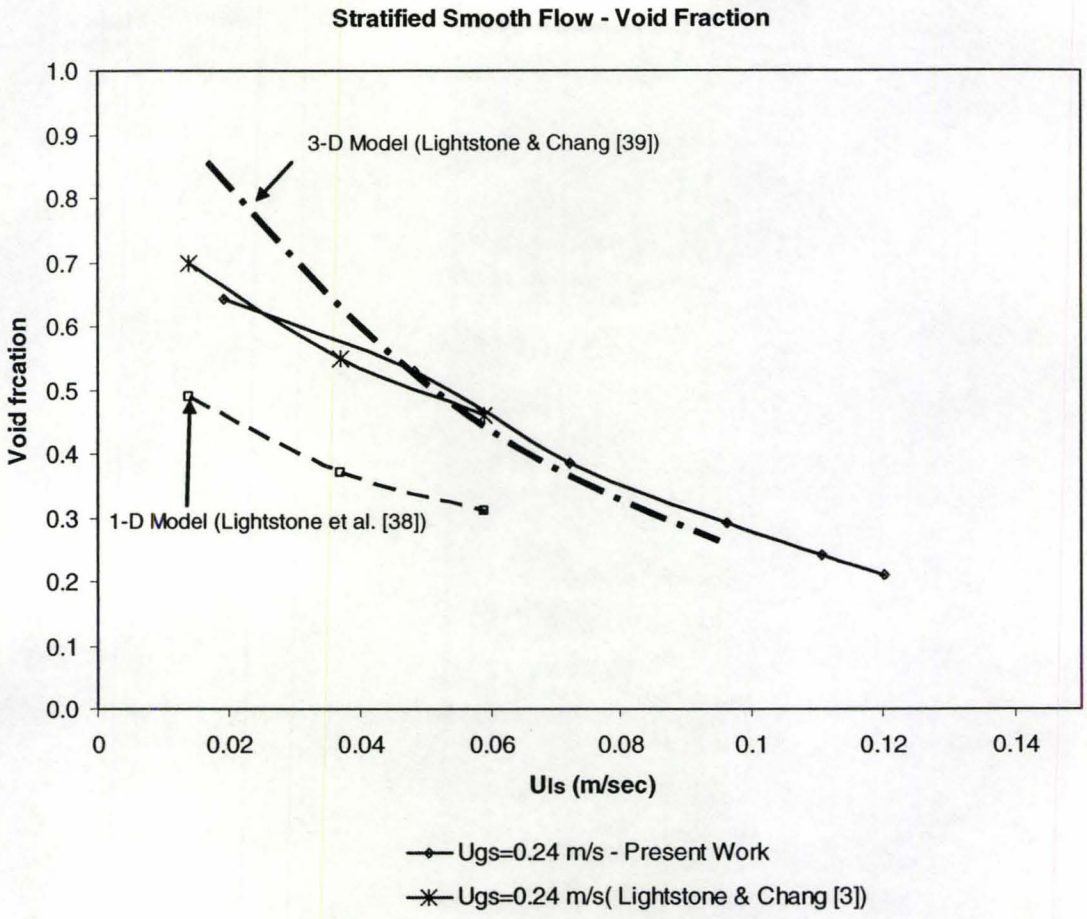

Figure 5-14: *Cross-section averaged void fraction under stratified smooth flow regime as a function of superficial liquid velocity (U_{ls}) at constant gas superficial velocity (U_{gs}=0.24m/s); Comparison with 1-D and 3-D Models [38,39]*

5.4.2 Liquid level and void fraction for a stratified wavy flow

The time averaged liquid level as a function of gas superficial velocity for two different liquid superficial velocities is shown in Figure 5-15. As expected, the liquid level decreases with increasing gas superficial velocity and the liquid level is higher for a higher liquid superficial velocity. The present results for stratified wavy flow (SW) are

compared with Taitel and Dukler's 1-D Model [4]. Taitel and Dukler [4] used the following assumptions:

$$X^2 = \frac{\frac{4C_L}{D}\left(\frac{u_L^s D}{\nu_L}\right)^{-n}\frac{\rho_L (u_L^s)^2}{2}}{\frac{4C_G}{D}\left(\frac{u_G^s}{\nu_G}\right)^{-m}\frac{\rho_G (u_G^s)^2}{2}} \quad ; \text{n=m=1;} \qquad (5\text{-}8)$$

where, C_G=C_L=16 for a laminar flow, u_L^S, u_L^S are the liquid and gas superficial velocities, D is the pipe diameter; ν_L, ν_G are the kinematics viscosity of liquid and gas; ρ_L, ρ_G are the liquid and gas density and X is the Martinelli parameter.

As Figure 5-15 shows, the present results qualitatively agree with 1-D Model. For a higher gas superficial velocity of 0.049 m/s there is also quantitative agreement between the present results and Taitel and Dukler's 1-D Model [4], but for lower gas superficial velocity of 0.019m/s there is a discrepancy between the two results. The discrepancies between the experimental and predicted results at low gas and liquid superficial velocities could be due to the assumption of equal pressure drops in each phase for laminar-laminar flow and not considering any surface wave at all as per equation (5-9) and (5-10).

$$-A_L\left(\frac{dP}{dx}\right)-\tau_{wL}S_L+\tau_i S_i+\rho_L A_L g=0 \qquad (5\text{-}9)$$

$$-A_G\left(\frac{dP}{dx}\right)-\tau_{wG}S_G+\tau_i S_i+\rho_G A_G g=0 \qquad (5\text{-}10)$$

However with increasing flow rates the validity of the assumption improves, hence, the analyses of Taitel & Dukler [4] apply except for low flow rates.

The void fraction for a stratified wavy flow was calculated using the same equations that were used for stratified smooth flow and the results are shown in Figure 5-16. Void fraction for a stratified wavy flow is increasing with increasing gas superficial velocity as is shown in Figure 5-16 and for an increase in the liquid superficial velocity is decreasing as was expected. Comparing the present results with those obtained by Lightstone et al. [38] 1-D Model it is observed that there is qualitative agreement between the two results to within ±20%.

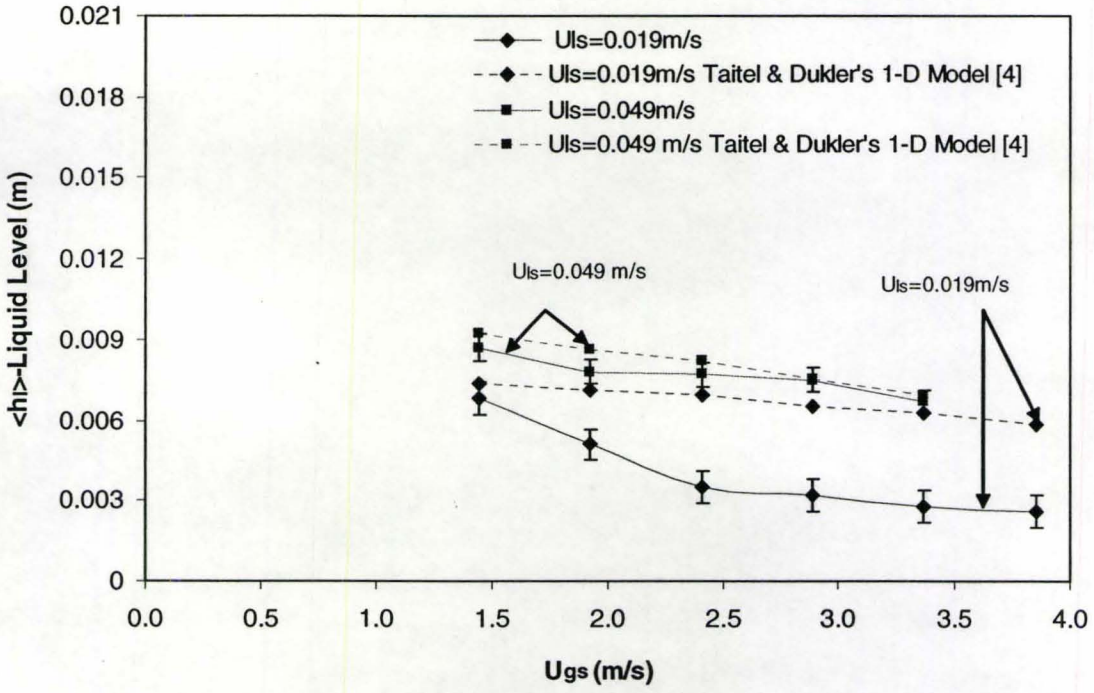

Figure 5-15: *Time averaged liquid level for a stratified wavy flow as a function of gas superficial velocity at liquid superficial velocities of U_{ls}=0.019 m/s and 0.048 m/s; comparison with Taitel & Dukler's 1-D Model [4].*

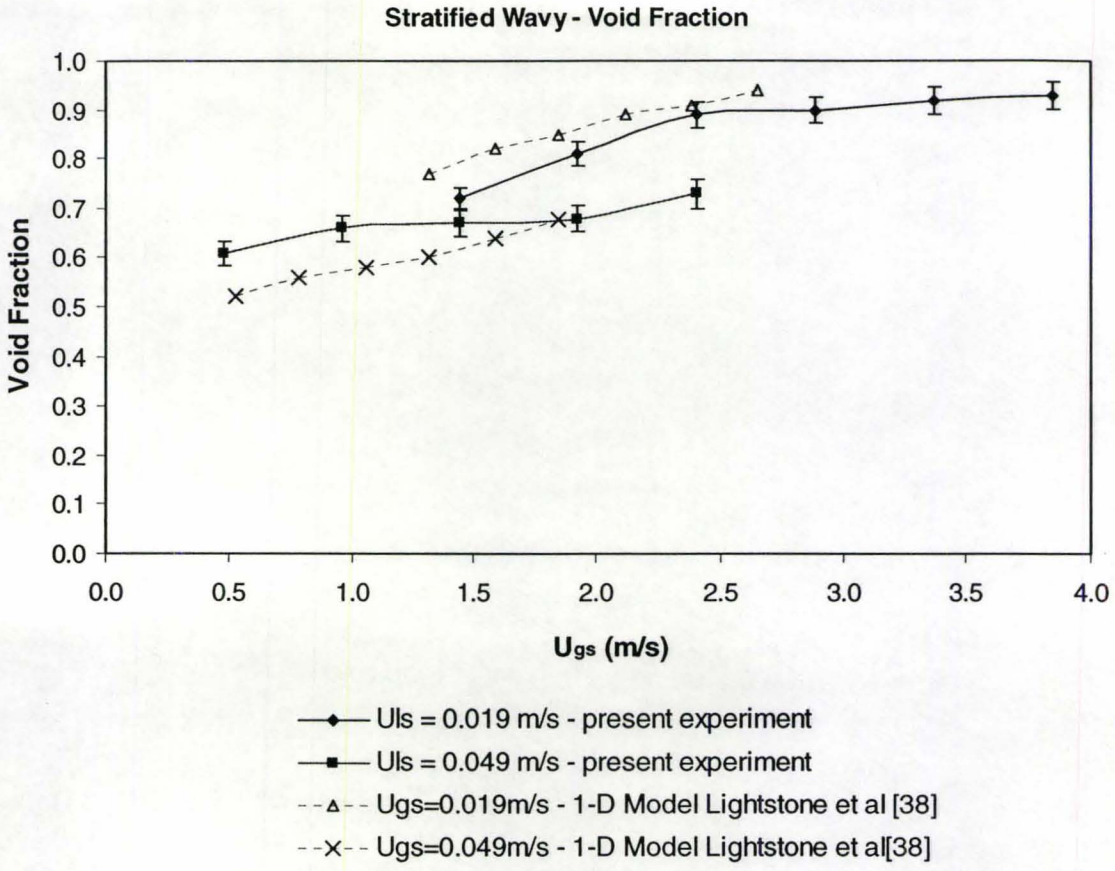

Figure 5-16: *Cross-section averaged void fraction under stratified wavy flow regime as a function of gas superficial velocity (U_{ls}) at liquid superficial velocities of U_{ls}=0.019m/s and U_{ls}=0.049m/s; comparison with Lightstone et al 1-D Model[38].*

5.4.3 Void Fraction in a Plug Flow Regime

In order to calculate the void fraction for a plug flow regime by present technique, the cross-sectional shape of the elongated bubble was assumed to be elliptical. The area of the ellipse is $A = \pi \cdot r_1 \cdot r_2$, where r_1 is the semi-major axis of the ellipse (the horizontal axis, as per Figure 5-17) and r_2 is the semi-minor axis. Then, the cross-sectional area of

the gas/liquid interface in a pipe filled with water in a plug flow regime is given by subtracting the cross-sectional area of the gas (ellipse, r_1, r_2) from the cross-sectional area of the pipe (circle, R):

$$A_{li} = \pi(R^2 - r_1 r_2) \tag{5-11}$$

The semi-minor axis of the ellipse is calculated as $r_2 = R - h_{li}/2$, where h_{li} is the instantaneous liquid level as measured by instruments and the semi-major axis can be calculated with an approximation as: $r_1 \cong \sqrt{R^2 - (h/2)^2}$. Considering the liquid cross-sectional area given by equation (5-11) the void fraction for plug flow can be calculated. The ellipse approximation works well for small diameter pipes. The ellipse-like shape of the elongated bubble in the cross-section is due to the surface tension of the liquid, which tends to push the liquid up on the pipe walls. For larger tube diameter, this approximation does not hold anymore because the curvature of the gas/liquid interface at the contact with the walls is too large. Therefore, in these situations, the shape will be a combination of an arc of a circle in the upper side of the elongated bubble, following the pipe wall shape, and a linear shape at the bottom, at the liquid surface, with curvatures in the areas where the free surface of the liquid wets the pipe walls. For a better estimation of the cross-sectional shape of the elongated bubble, additional experimental work and analysis is necessary.

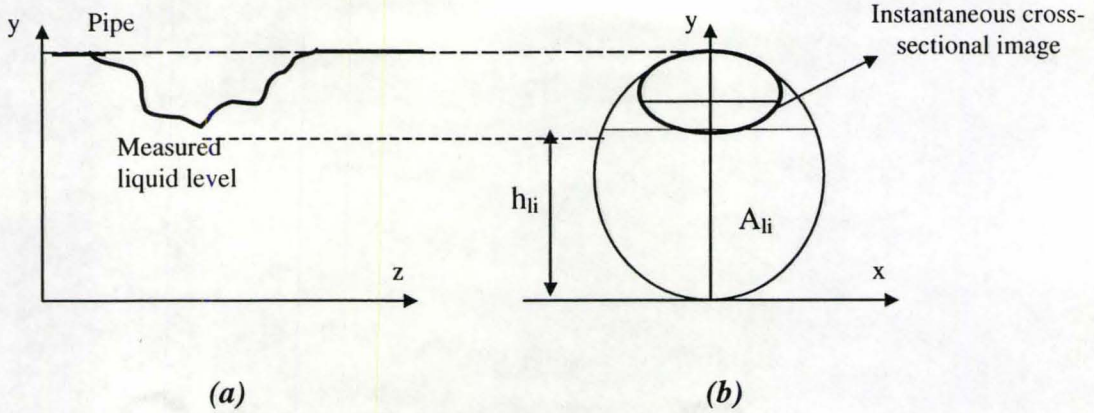

Figure 5-17: *Longitudinal representation of plug flow, based on level data read by the instrumentation (a) and instantaneous corresponding cross-sectional representation (b)*

The time averaged void fraction as a function of liquid superficial velocity for different gas superficial velocities for plug flow regime is shown in Figure 5-18. Figure 5-18 shows that for an increase in gas superficial velocity form 0.48 m/s to 0.96 m/s the void fraction increases which is in agreement with the 1-D Model results obtained by Lightstone et al. [38]. This could be explained from the simple fact that for higher gas flow rates, the formation of the water bridge becomes a very effective method for pushing the liquid out of the pipe resulting in the observed increase in void fraction. Comparing the present results with the 1-D model of Lightstone et al. [38] there is good agreement within ±40%, as is shown in Figure 5-18. The discrepancy between the present results and 1-D model arises from the fact that in the present results the void fraction is higher than the in the case of 1-D Model. This could be due to the changes in the plug shape and frequency which Lightsone's 1-D Model [38] does not take into account as per equation (5-6) and (5-7).

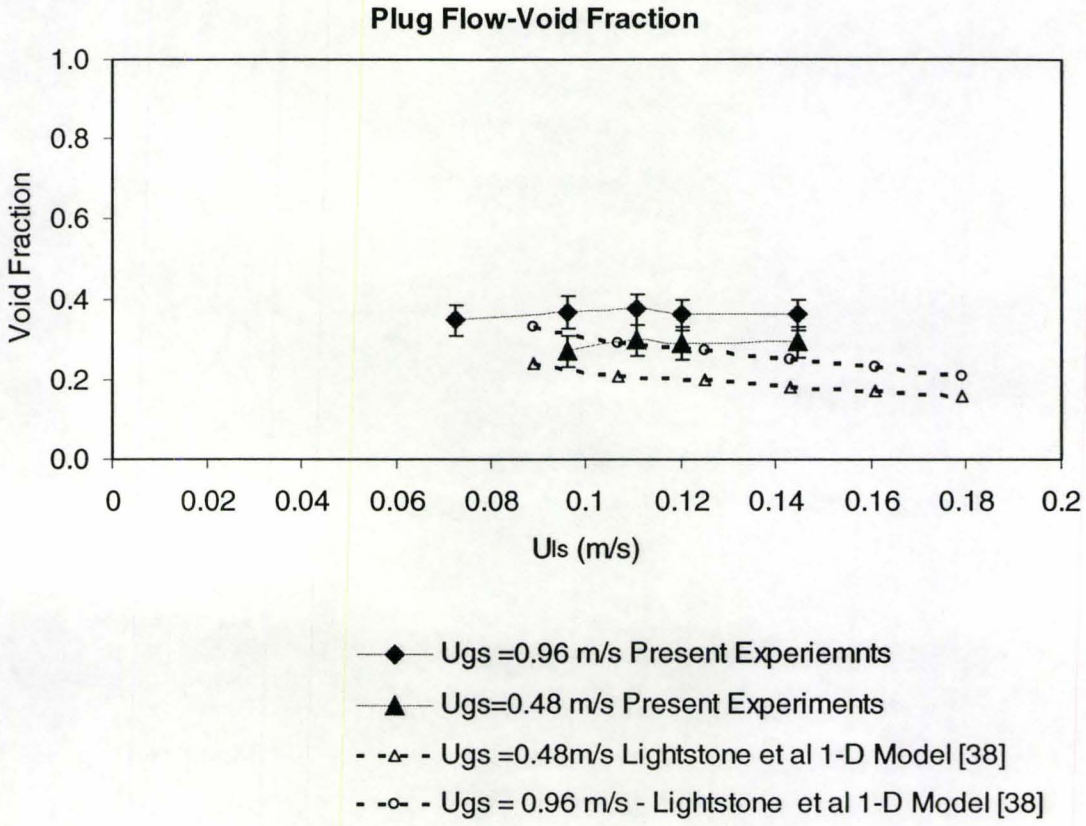

Figure 5-18: *Time and cross-sectional averaged void fraction measurements for different liquid superficial velocities under plug flow regime for U_{gs}=0.96m/s and U_{gs}=0.48m/s. Comparison with Lightstone's et al. 1-D Model[38].*

5.4.4 Film Thickness and Void Fraction in an Annular Flow Regime

Liquid film thickness at the top and bottom of the tube as a function of the liquid superficial velocity at U_{gs}=4.33m/s for an annular flow regime is given in Figure 5-19.

As Figure 5-19 shows, the liquid film thickness is dependent on the liquid superficial velocity, increasing the liquid superficial velocity the liquid film thickness increases. At the same time, the liquid film thickness from the bottom is thicker than that

from the top as expected, due to gravity effects. Figure 5-19 shows a comparison of the present results for the averaged film thickness in an annular flow regime with the theoretical predictions by Laurinat and Hanrantty [40]. It is observed that there is quantitative agreement between the two results but the theoretical model shows lower values for the film thickness than the present experiment. This can be explained by the fact that Laurinat and Hanrantty's model [40] does not take into account the fact that the film thickness from the bottom is thicker than that from the top as per equations (5-12 to 5-15)

$$\frac{m}{d_t} = \frac{6.59 F_H}{\left[2.3^5 + (90 F_H)^5\right]^{0.2}} \tag{5-12}$$

$$F_H = \frac{\gamma_H(\mathrm{Re}_{LF})}{\mathrm{Re}_G^{0.90}} \left(\frac{\nu_L}{\nu_G}\right) \sqrt{\frac{\rho_L}{\rho_G}} \tag{5-13}$$

$$\gamma_H(\mathrm{Re}_{LF}) = \left[\left(0.566\,\mathrm{Re}_{LF}^{0.5}\right)^{2.5} + \left(0.0303\,\mathrm{Re}_{LF}^{0.9}\right)^{2.5}\right]^{0.4} \tag{5-14}$$

$$\mathrm{Re}_G = \frac{(d_t - m) U_G}{\nu_G} \quad \mathrm{Re}_{LF} = \frac{4Q}{P\nu_L} \quad Q = U_L \cdot A \tag{5-15}$$

where m is the average height around a pipe circumference, d_t is the pipe diameter, F_H is the flow factor for horizontal pipes, $\gamma_H(Re_{LF})$ is the dependency of dimensionless liquid level gamma on liquid film Reynolds number for horizontal pipes, Re_{LF}, Re_G are the Reynolds number of gas phase and liquid film respectively, ν_L, ν_G are the kinematic viscosity of gas and liquid respectively, ρ_L, ρ_G are the liquid and gas density, U_G, U_L are the liquid and gas velocities, Q is the volumetric flow of the liquid in the film, and P is

the pipe diameter.

The cross-sectional liquid/gas interface for an annular flow is considered to be circular as shown in Figure 5-20. If h_{lb} and h_{lt} are the instantaneous liquid films as measured by the system, then the diameter of the circular gas area is $d = D - h_{lb} - h_{lt}$. Therefore, the cross-sectional area of the pipe filled with liquid is given by subtracting the cross-sectional area of the gas (circle, d) from the cross-sectional area of the pipe (circle, D):

$$A_{li} = \pi(D^2 - (D - h_{lb} - h_{lt})^2)/4 \qquad (5\text{-}16)$$

Then the void fraction for annular flow is calculated using equation (5-11) by considering the liquid cross-sectional area given by equation (5-16).

The time averaged void fraction as a function of liquid superficial velocities at a constant gas superficial velocity U_{gs} =4.33m/s is shown in Figure 5-21. From the Figure it is observed that as the liquid superficial velocity increase the void fraction decrease. It is evident; the results are also confirmed from the liquid level measurements that were discussed before, where it was shown that as the liquid superficial velocity increases the liquid level also increases. The present results are compared with Lightstone et al. 1-D Model [38], theoretical prediction. Figure 5-21 show that the results agree both qualitatively quantitatively and within ±5%.

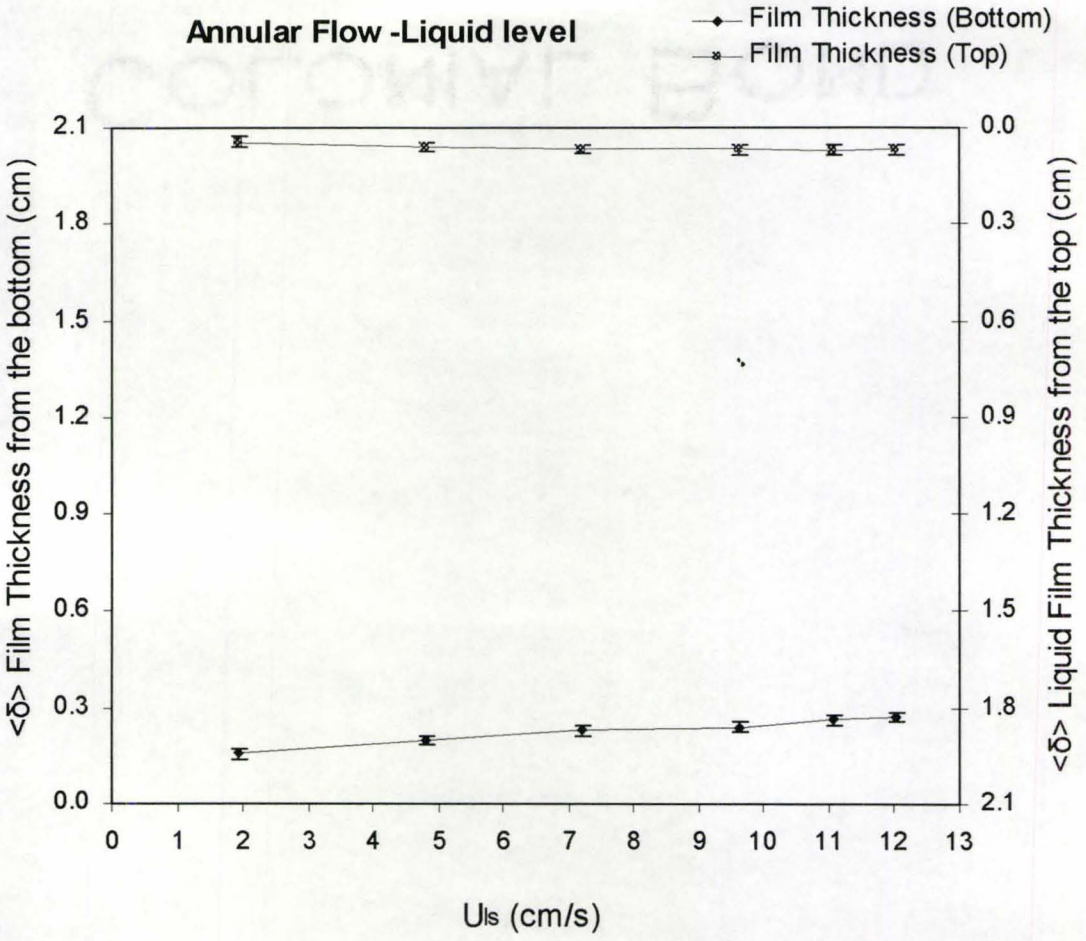

Figure 5-19: *Liquid film thickness at the top and bottom of the tube as a function of the liquid superficial velocity at U_{gs}=4.33m/s for an annular flow regime.*

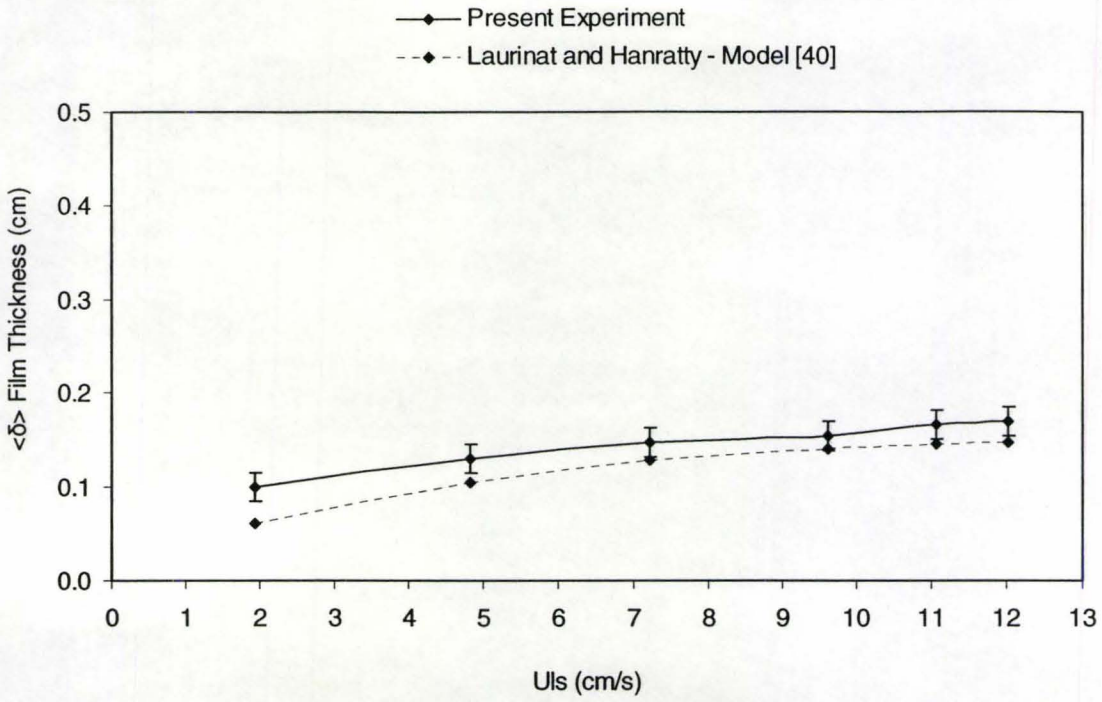

Figure 5-20: *Cross-sectional averaged film thickness for an annular flow regime, comparison with averaged film thickness obtained by Lauriant and Hanratty's model [40].*

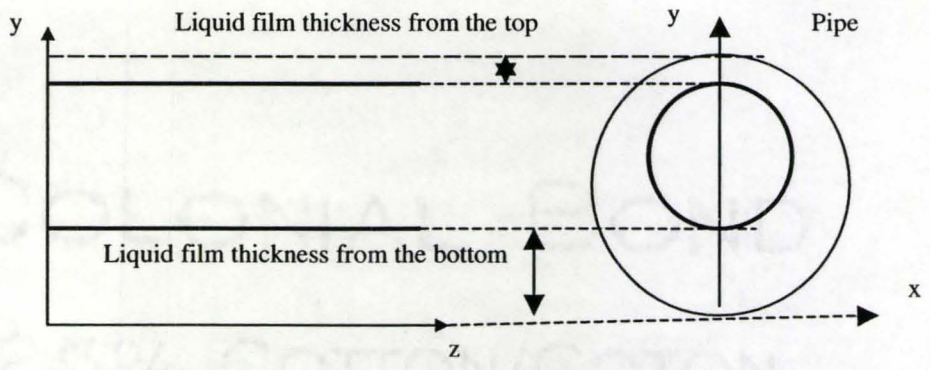

(a) ***(b)***

Figure 5-21: *Longitudinal representation of annular flow, based on level data read by the instrumentation (a) and instantaneous corresponding cross-sectional representation (b)*

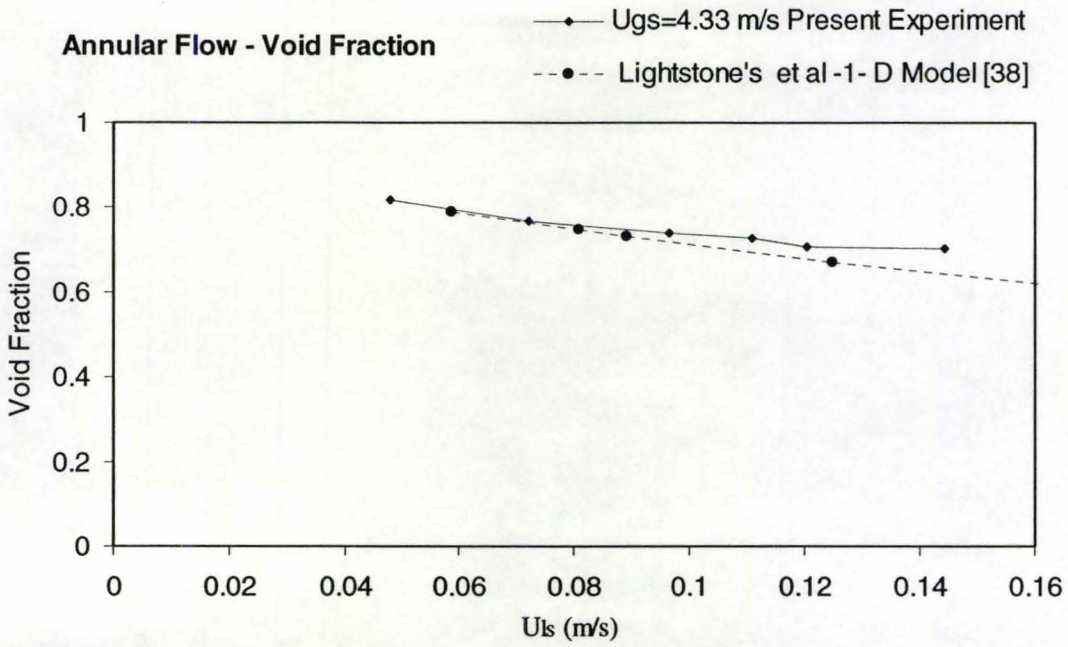

Figure 5-22: *Cross-sectional averaged void fraction as a function of liquid superficial velocity at Ugs=4.33m/s.; Comparison with Lightstone et al 1-D Model [38].*

5. 5 Other Two-Phase Flow Parameters

5.5.1 Wave amplitude and frequency in stratified wavy flow

In this section the amplitude and frequency of the waves in a stratified wavy regime are discussed. The high speed ultrasonic pulse echo system was capable of measuring the amplitude of the waves for the liquid superficial velocities of 0.048 m/s and 0.019m/s respectively. The dependency of the wave amplitude on the gas superficial velocity is presented in Figure 5-22 and shows that there is an increase in the wave amplitude with increasing gas superficial velocity, which was expected since the waves are driven by the gas flowing above the liquid surface. For the lower liquid superficial velocity of 0.019 m/s however, the wave amplitudes were too small to infer a dependency on the gas superficial velocity. Figure 5-24a and 5-24b shows a comparison of the liquid level evolution in time for different liquid superficial velocities of U_{ls}=0.049 m/s and U_{ls}=0.019 m/s respectively, at a constant gas superficial velocity, U_{gs} = 1.92 m/s. For a liquid superficial velocity of 0.049m/s the liquid level was approximately 0.7 cm while for a liquid superficial velocity of 0.019 m/s, the liquid level was 0.35 cm. Therefore the gas superficial velocity above the liquid level was higher for the higher level since the cross-sectional area occupied by the gas becomes smaller, and that caused the higher amplitudes of the waves, on the order of 0.4 mm, as opposed to less than 0.1 mm in the case of the lower liquid superficial velocity. Actually, in the latter case, the regime was at the transition point between stratified smooth and stratified wavy and the amplitudes of less than 0.1 mm were measured near the resolution limit of the ultrasonic system. Figure

5-23 shows the evolution of wave frequency with increasing the gas superficial velocity and as it is observed that the wave frequency is increasing with increasing the gas superficial velocity as was expected.

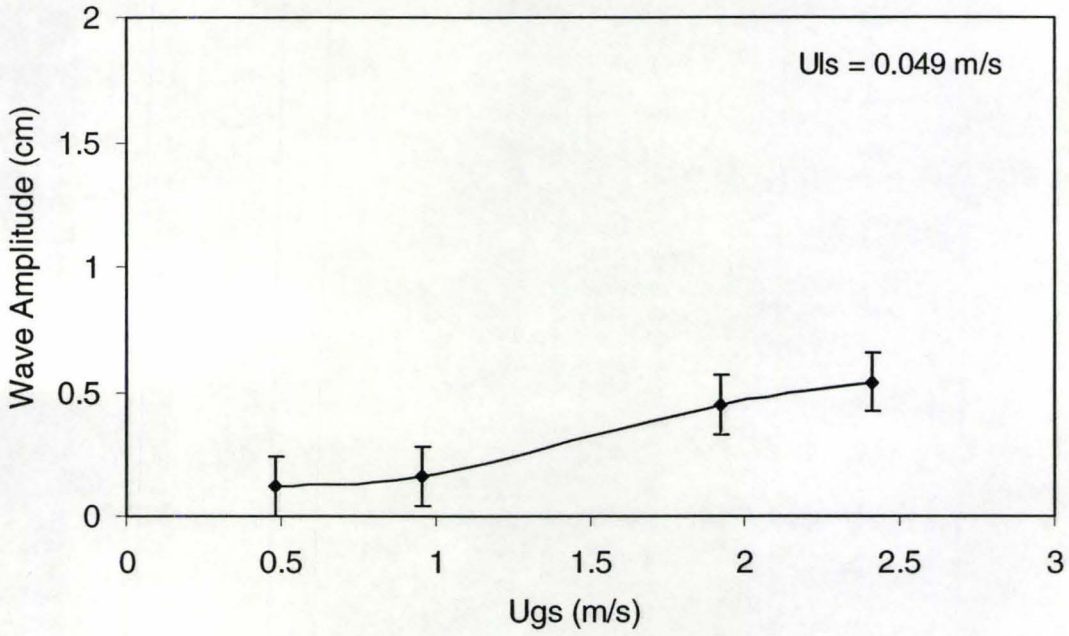

Figure 5-23: *Wave amplitude as a function of gas superficial velocity in stratified wavy flow for* U_{ls}*=0.049m/s*

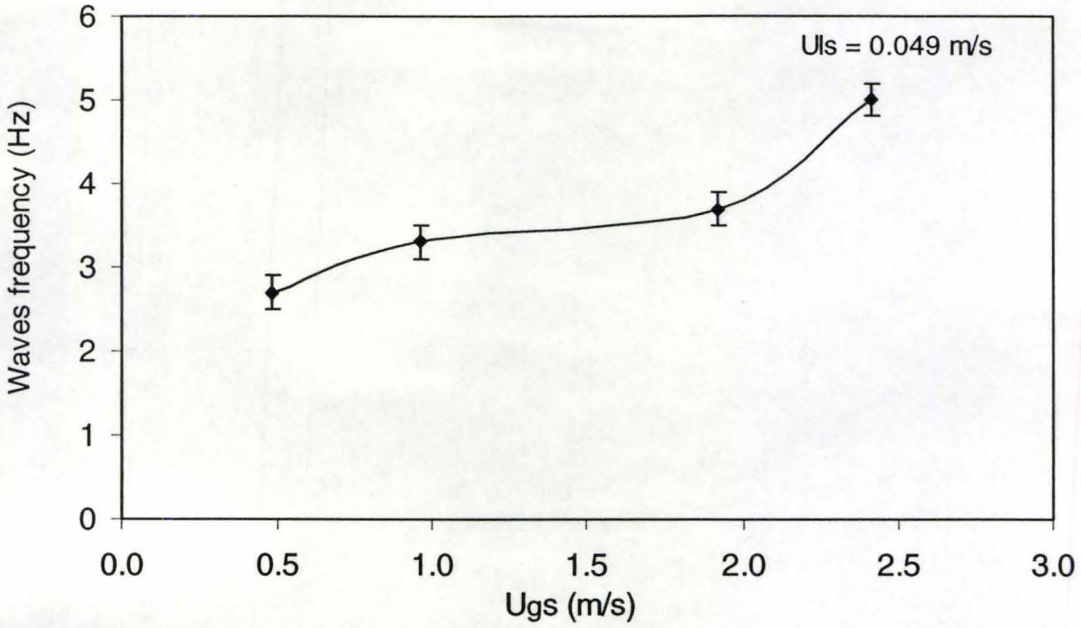

Figure 5-24: *Wave frequency as a function of gas superficial velocity in stratified wavy flow for U_{ls}=0.049m/s.*

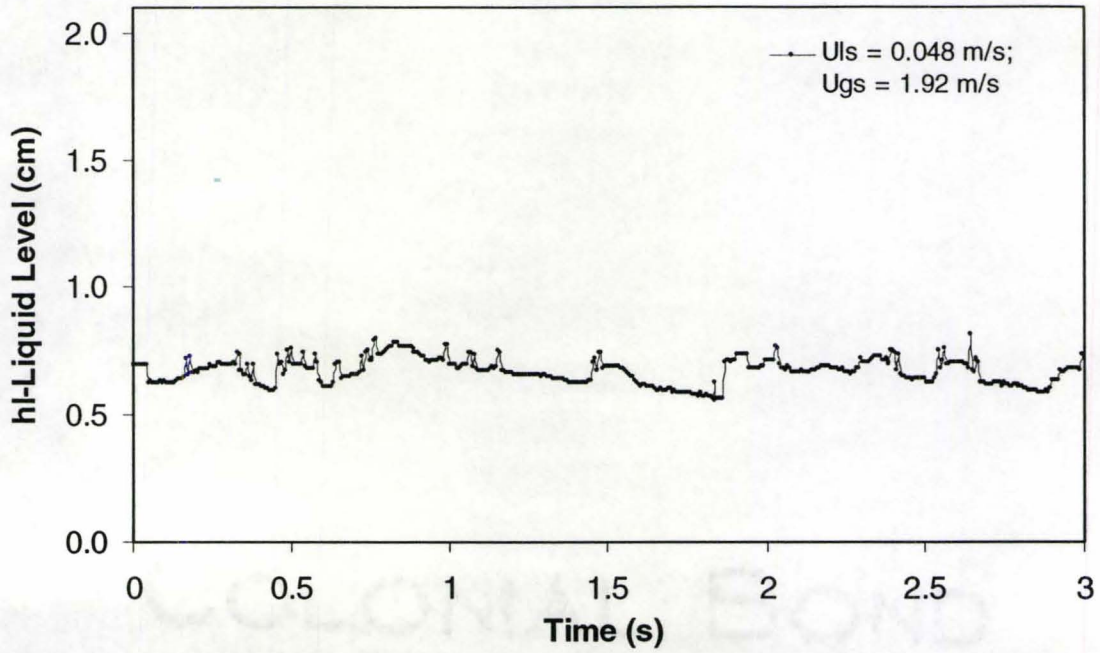

(a)

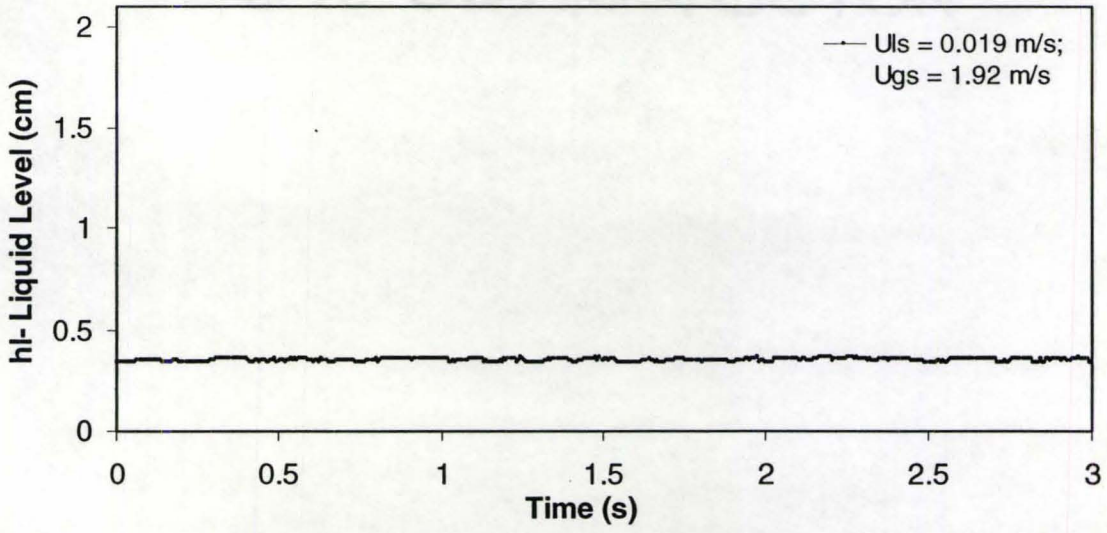

(b)

Figure 5-25: *Comparison of the liquid level evolution in time for different liquid superficial velocities U_{ls}=0.049 m/s (a) and U_{ls}=0.019 m/s (b), at constant gas superficial velocity, U_{ls} = 1.92 m/s.*

5.5.2 Plug and Bubble Velocity Measurements

Plug and slug flow velocity measurements can be conducted since the particular shape of the gas/liquid interface can be tracked by using multiple transducers located at different axial positions on the pipe. In the case of plug flow, both the plug and the elongated bubble can be observed by the transducers and their velocities can be determined accurately. Therefore the plug and bubble velocity was determined by tracking one of the edges of the plug obtained by two probes as shown in Figure 5-25a and 5-25b and by using equation (5-17),

$$Uplug = \Delta Z / \Delta t \qquad (5\text{-}17)$$

where ΔZ is the known distance between the two transducers and Δt is the time interval between the moments when the same edge of the plug was detected by the transducers.

The dependency of the bubble velocity on the superficial liquid velocity is presented in Figure 5-26 for two different superficial velocities of gas (U_{gs}=0.48 m/s and U_{gs}=0.96 m/s). The effect of increasing gas superficial velocity is clearly seen, as the bubble velocity is also increasing. At the same time by increasing liquid superficial velocity a slight increase in the bubble velocity is also observed. The present results are compared with the theoretical correlation by Wallis et al. [41] given by the following relation (5-18) for a rising bubble velocity in a vertical pipe:

$$U_B = 1.2(U_{ls} + U_{gs}) + 0.345\sqrt{gD} \qquad (5\text{-}18)$$

where, U_B is the bubble velocity, U_{ls} and U_{gs} are the liquid and gas superficial velocities, g is the gravitational acceleration and D is the diameter of the pipe.

However in the case of horizontal flow the gravitational acceleration *(g)* can be neglected, hence equation (5-19) becomes:

$$U_B = 1.2(U_{ls} + U_{gs}) \qquad (5\text{-}19)$$

Also Suo and Griffith [42] used the following relation for the slug velocity:

$$U_B = 1.19(U_{ls} + U_{gs}) \qquad (5\text{-}20)$$

Figure 5-26 shows a comparison of the present results with the experimental results obtained from equation (5-19). As can be seen from the figure for a lower gas superficial velocity of 0.48m/s the results agree quantitatively and qualitatively, but at a higher gas superficial velocity of 0.96m/s, there is only quantitative agreement between the results. It is shown that increasing liquid superficial velocity the theoretical model gives a lower bubble velocity than the experimental results and this could be due to the fact that the experimental correlation does not take into account the size and the change in shape of the bubble. The same results are obtained for the plug velocity. The only difference that arises for the plug velocity is that the velocity is higher than the bubble velocity and this is expected since the liquid plug acts as a bridge for the gas bubble. Figure 5-27 show a comparison of the present results obtained for the plug velocity with the experimental correlation by Wallis et al. [41]. The same results as for the bubble velocity are obtained but the discrepancies between the experimental correlation and the present results are even higher. Therefore it is clear that the changes in the plug shape and frequency has an impact on the plug velocity which is not considered by Wallis et al. since he used intrusive techniques for the plug and bubble velocity measurements.

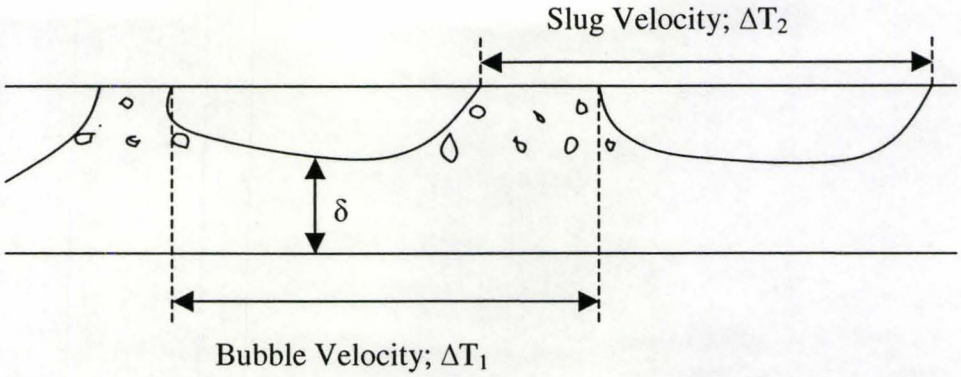

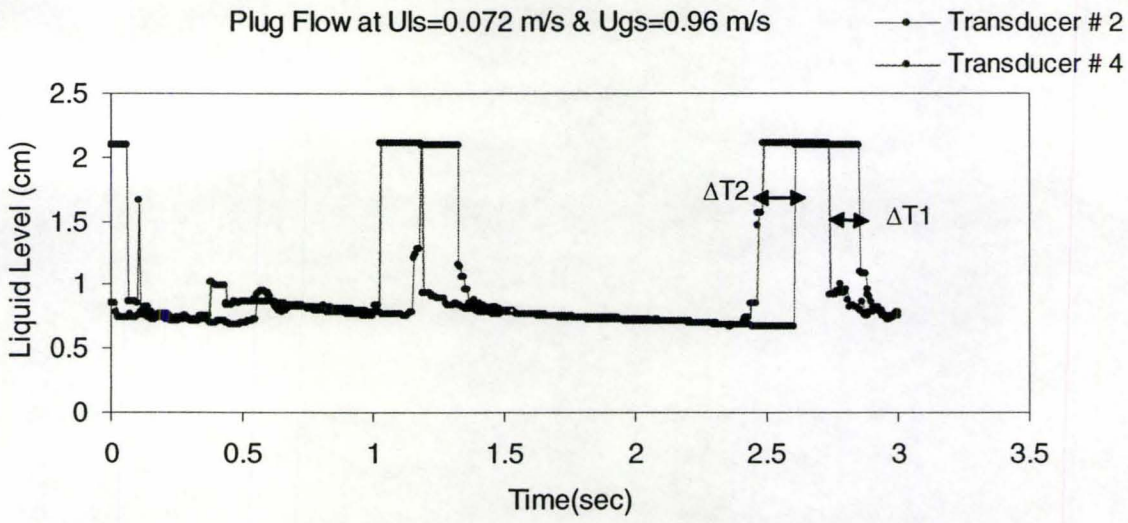

Figure 5-26: *Plug velocity calculation using transducer # 1 and transducer # 3 positioned on the top surface of the pipe with 12cm distance between them for* U_{ls}*=0.072m/s and* U_{gs}*=0.96m/s*

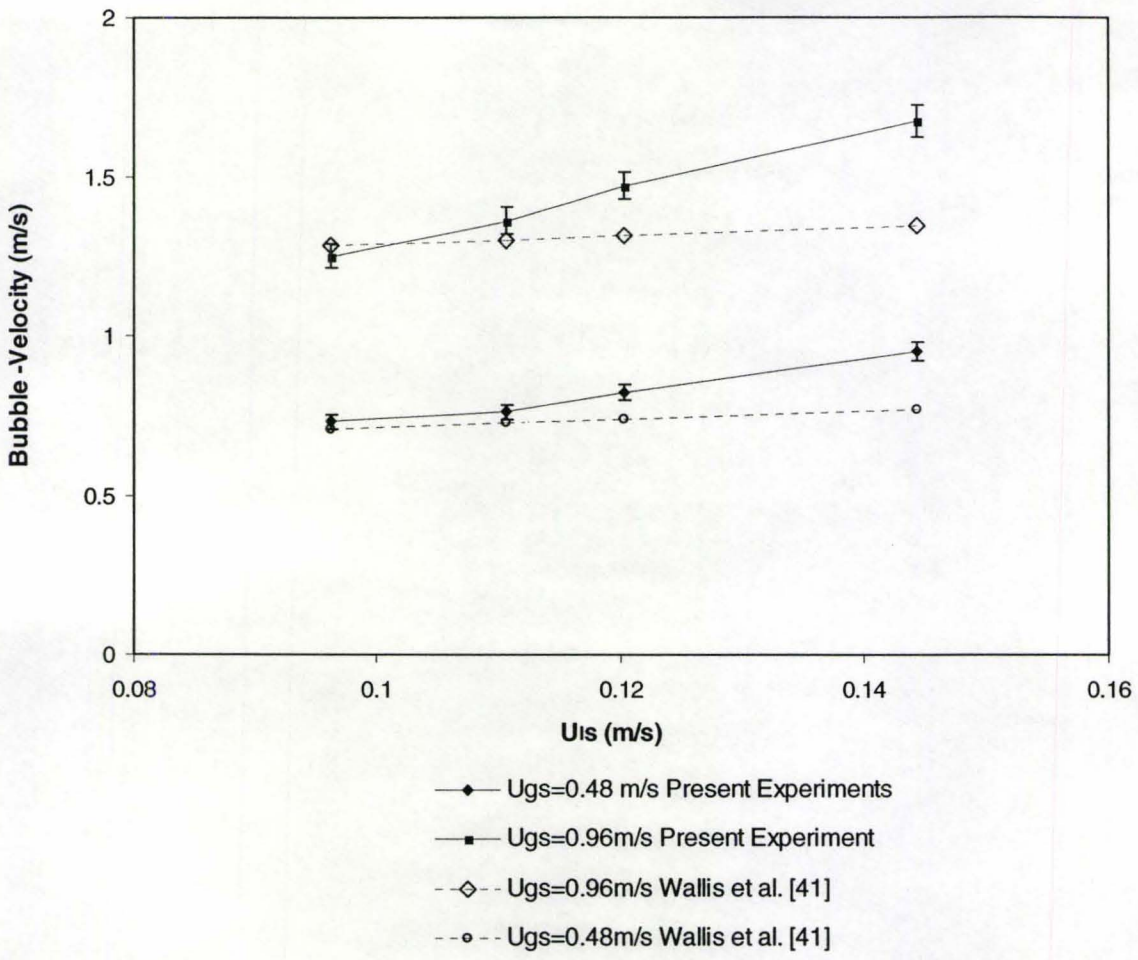

Figure 5-27: *Plug Bubble Velocity as a function of Liquid Superficial Velocity at Ugs =0.48m/s and Ugs =0.96 m/s ; comparison with Wallis et al. correlation [41].*

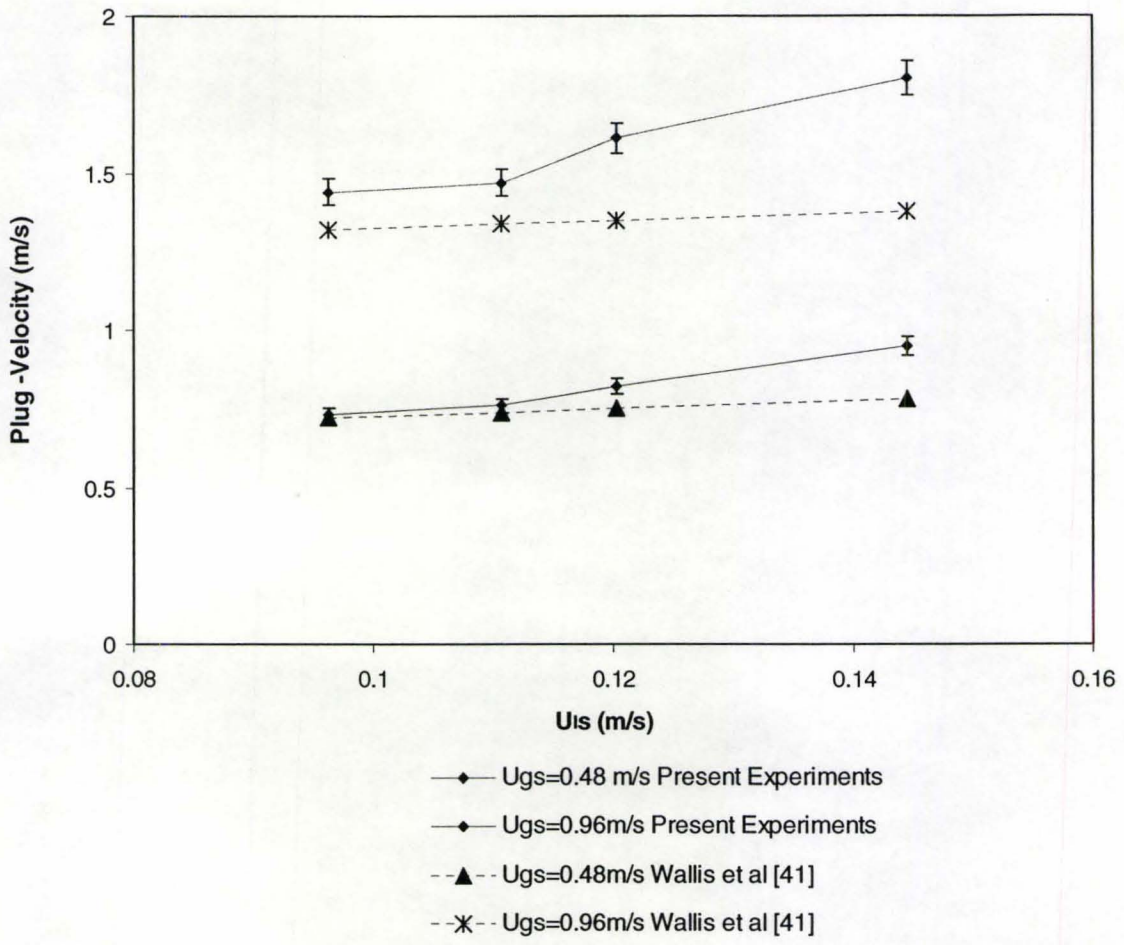

Figure 5-28: *Plug Velocity as a function of Liquid Superficial Velocity at U_{gs} =0.48m/s and U_{gs} =0.96 m/s ; comparison with Wallis et al. correlation [41].*

5.5.3 Slug Flow Velocity Measurement

In the case of slug flow, the slug shape changes during the range of the acquisition time. Furthermore, slug flow is more difficult to investigate because of its more complicated nature, consisting in the formation of many smaller bubbles in the vicinity of the main slug bubble. The results for the slug velocity measurements are represented in Figure 5-28 with an error of 25% in the calculations. The present results are compared

with Suo and Griffith [32] correlation. Suo and Griffith [42] used the following correlation for the slug velocity:

$$U_s = 1.19(U_{ls} + U_{ls}) \tag{5-21}$$

where Us is the slug velocity, U_{ls} - liquid superficial velocity, and U_{gs} - gas superficial velocity. Figure 5-28 shows that the present results agree qualitatively with Suo and Griffith [42] correlation but disagree quantitatively. The slug velocity increases with increasing gas flow velocity but the correlation results show a higher slug velocity than in the present results.

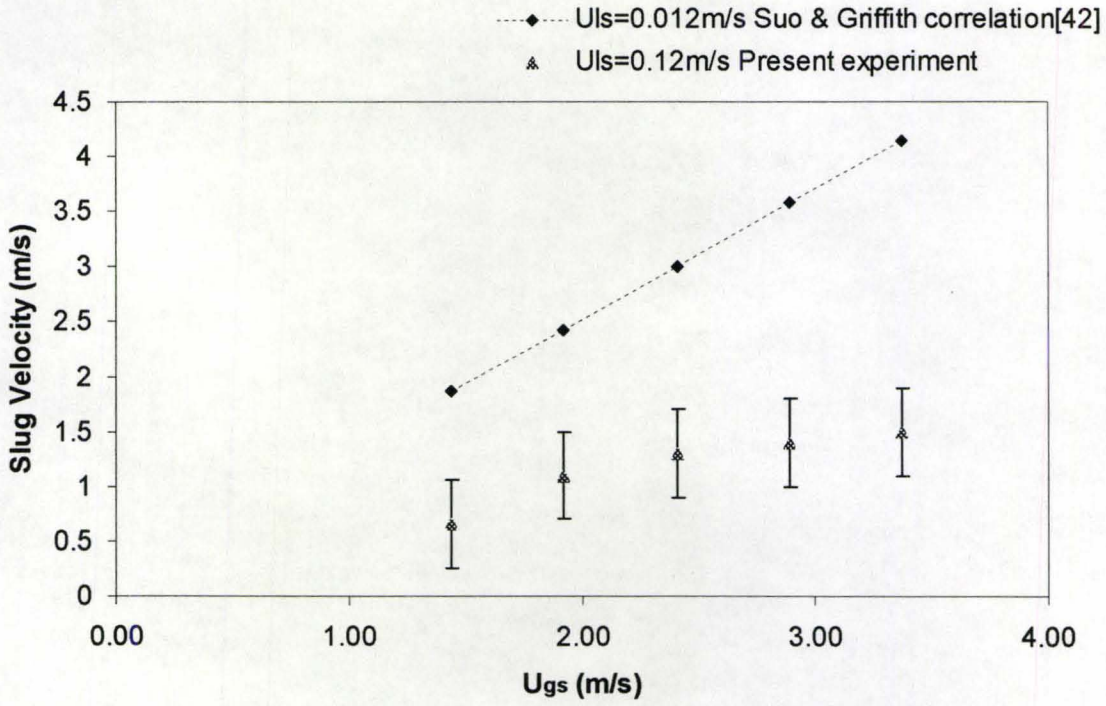

Figure 5-29: *Slug velocity as a function of gas superficial velocity for constant liquid superficial velocity U_{ls}=0.012m/s; comparison with Suo and Griffith correlation [42].*

5.5.4 Annular flow wave amplitude

The interface between the phases in annular two-phase flow is generally not smooth, but covered with a complex pattern of waves, due to the high gas superficial velocity. This characteristic of the annular flow affects a number of important phenomena, like the pressure drop, droplet entrainment, mass and heat transfer within the system.

The ultrasonic system proved capable of measuring small ripples developed at the interface during the annular flow with an error of ±40%, where the error is due to the limitation in the sampling rate (6ms). These small amplitude waves are very common in annular flow and were reported by many authors in literature (Hewitt, [43], Whalley, [44]). The results of the wave amplitude measurements are presented in Figure 5-28. It can be observed that the wave amplitudes decrease with the increasing of liquid superficial velocity which gives the film thickness. This result is confirmed by the work of Mouza et al. [45] who observed the same trend.

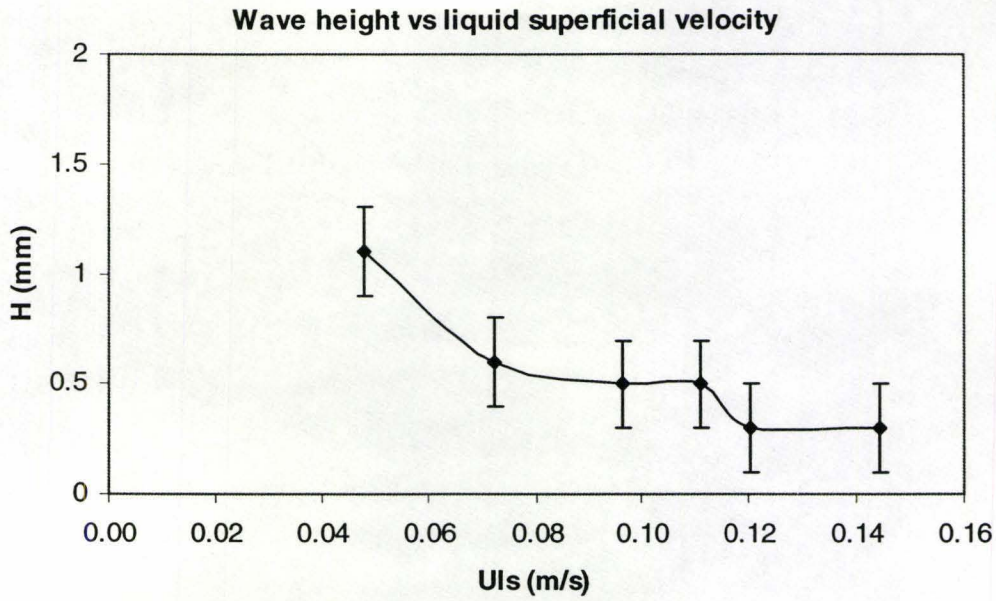

Figure 5-30: *Annular flow; wave height as a function of liquid superficial velocity for a constant gas superficial velocity U_{gs}=4.31m/s.*

CHAPTER 6

Concluding Remarks

In the present study, a new ultrasonic two-phase flow measurement technique has been developed, which uses ultrasonic pulse-echo signals from four transducers to detect the instantaneous location of the gas/liquid interface in a horizontal pipe. The ultrasonic measurement system developed in the present study not only provides the measurement functions required for the identification of horizontal two phase flow pattern, but also allows for real time characterization. It is straight-forward to identify the various horizontal two phase flow patterns such as stratified smooth, stratified wavy, plug flow, slug flow and annular flow from the measurement results. In addition to the identification of flow patterns, quantitative information for each flow pattern can be obtained, which include time averaged void fraction, plug velocity, slug velocity, wave amplitude and frequency and film thickness. With appropriate data acquisition, the length of the plug or slug bubble can also be obtained.

The system has been developed with the capability to acquire the data in high speed 170 frames/s (A-scans/s) using multiple transducers without reducing the acquisition time. The transducers to be used for a given experimental run are chosen in software, allowing consecutive runs to use the multi-transducer capability and the high-speed single transducer capability without hardware changes. All data are displayed on-

screen in real time (6 msec) with a sampling rate of 2μ in the form of a C-scan or numerical readout and liquid level versus time strip chart for each transducer. Additionally, time stamped data is saved to a text file readable by a spreadsheet program allowing for post-analysis.

Specific advantages for the High Speed Ultrasonic Pulse-Echo System are the ability to measure two-phase flow phenomena non-intrusively, through metallic and transparent pipes. Non-intrusive measurement is important as this allows for detailed knowledge of the two-phase flow parameters without disturbing the flow. With proper transducers, two phase flow parameters under high temperature conditions can be measured.

The following conclusions are obtained from the studies performed in this work:

- The High Speed Ultrasonic Pulse-Echo System performed well in the interpretation of the flow regimes and accurate flow regime maps can be established using this system. The flow regime map established in the present work is in satisfactory agreement with Lightstone et al. 1-D Model [38] and Mandhane experimental map [3].
- The High Speed Ultrasonic Pulse-Echo System also proved to give accurate results within ±1.5% in the determination of the liquid level measurements. Time averaged liquid level measurements performed in the present work agree well within ±10% with Taitel and Dukler [4] theoretical model.
- Time averaged void fraction measurements for a stratified smooth flow, stratified wavy, plug flow and annular flow qualitatively agree with Lightstone et al. [38] theoretical model. In the case of slug flow regime, the High Speed Ultrasonic Pulse-Echo

System gave less accurate results for the gas/liquid interface since there is high entrainment of gas bubbles. In addition, due to the angle between gas/liquid interfaces with ultrasonic waves, the scattered signal in some cases will not return to the transducer and some bubbles may block the signal scattered from the actual liquid/gas interface. Therefore in the case of slug flow regime, the void fraction is more difficult to determine accurately because of the high entrainment of gas bubbles in the slug body.

- Liquid plug and bubble velocity measurements for lower gas superficial velocities than 0.48m/s qualitatively and quantitatively agree with Wallis et al. [41] correlations, but for higher gas superficial velocities there is only qualitative agreement between the results. The discrepancies is likely due to the accuracy of the correlation to predict the plug and bubble velocities since the correlations do not take into account any change in the plug or bubble shape. For slug velocity, there is only qualitative agreement with Suo and Griffith's [42] correlation. Again, the discrepancy is due to inaccuracy in the correlation predictions because of the slug shape effects.

- Finally, wave height and frequency for a stratified wavy flow were determined and there was a clear indication that as the gas superficial velocity was increasing, the height of the wave and frequency was also increasing.

CHAPTER 7

Recommendations for Future Work

Although horizontal pipe flow has been extensively studied in this work, there are some remaining analyses that can be used to improve the performance of the High Speed Ultrasonic Pulse-Echo system. Therefore in this chapter the aspects regarding improvements of the present work such as plug shape in cross section and longitudinal section, interfacial plug velocity measurements, wave frequency in a stratified wavy regime will be discussed.

In the case of plug flow measurements more experiments should be conducted to verify the assumptions that were made regarding the shape of the plug, which would directly affect the results for void fraction and interfacial area in this particular case. In the present work, the cross-sectional shape of the plug was considered to be elliptical. Experiments could be performed for the determination of the plug shape by using four transducers or even eight in special configurations. One of them involves placing the transducers circumferentially and operating in pulse-echo mode. Then each transducer can provide information about the liquid level or gas/liquid interface. Therefore data collected from all the transducers will give the cross-sectional shape of the plug. This shape can then be reconstructed by using an interpolation algorithm. It should be noted that the accuracy in reproducing the plug shape is given by the number of transducers

used, which also can be limited by the pipe diameter and the interpolation method. Also the plug flow measurements should be conducted at various conditions that may affect the plug cross-sectional shape, like gas and liquid superficial velocities, the pipe diameter, different pipe materials or even pipe roughness that may affect the superficial tension that is responsible for the plug cross-sectional shape.

A second configuration that can be used, which is intended to provide information about the axial profile of the plug flow is to use the same configuration that was employed in the present work. This means two of the transducers placed on the top surface of the pipe and the other two on the bottom surface of the pipe. The axial distance between the transducers should be increased to about 15cm, and the acquisition time for the system should be also increased to 10s. In this way, more information can be obtained regarding the length of the gas bubble and plug interfacial velocity.

In the case of stratified wavy flow regime, although the ultrasonic system offers the capability to count the waves in stratified wavy flow, the frequency of the waves could not be determined accurately, in part because the acquisition time of 3 seconds was too short to allow for an accurate estimation of the wave frequency. Yet, the waves can be counted over a certain time interval to accurately calculate an average frequency of the waves. Therefore it is recommended that this measurement should be done in the future for an acquisition interval of at least 10 seconds for an accurate estimation of the wave frequency.

REFERENCES

[1] Govier, G. W. and Aziz, K. "The Flow of Complex Mixtures in Pipes" Van Nostrand Reinhold Company, New York, NY, 1972.

[2] Rouhani, S.Z. and Sohal, M.S., "Two-phase flow patterns: Review of Research Results", Progress in Nuclear Energy, Vol. 11 No. 3, pp 219-259, 1983.

[3] Mandhane, J. M., Gregory, G. A. and Aziz, K. "A flow pattern map for gas-liquid flow in horizontal pipes" Int. J. Multiphase Flow, Vol. 1, pp 537-553, 1974.

[4] Taitel, Y and Dulker, A. E., "A model for predicting flow regime transitions in horizontal and near horizontal gas-liquid flow", AIChE J. Vol. 22, pp. 47-55, 1976.

[5] Harvel, G.D. and Chang J.S., "Handbook of Electrostatic Processes", J.S. Chang, Arnold J. Kelly, Joseph M. Crowley, New York, Marcel Dekker, Inc., Chapter 13, 1995

[6] Andreussi P., Di Donfrancesco A., and Messia M., "An impedance method for the measurement of liquid hold-up in two-phase flow", Int. J. Multiphase Flow, Vol. 14. pp 777-785, 1988

[7] Mi, Y., Ishii, M., Tsoukalas, L.H., "Investigation of vertical slug flow with advanced two-phase flow instrumentation", Nuclear Engineering and Design Vol. 204, pp 69-85, 2001

[8] Le Corre, J. M., Hervieu, E., Ishii, M., Delhaye, J-M., "Benchmarking and improvements of measurement techniques for local-time-averaged two-phase flow parameters", Experiments in Fluids Vol. 35, pp 448-458, 2003

[9] Chang J.S., Myint T.A., Donevsky B., Berezin A.A., Irons G.A., and Lu W.K. "Determination of the interfacial parameters in gas-solid two-phase pipe flow by capacitance transducers", Particulate and Multiphase Processes- Colloidal and Interfacial Phenomena, Hemisphere Publishing Corporation – Springer- Verlog, pp 173-187, 1985

[10] Elkow, K.J., Rezkallar, K.S., "Void fraction measurements in gas-liquid flows using capacitance sensor", Measure. Sci. Technol. Vol. 7, 1153–1163, 1996.

[11] Albouelwafa M.S.A. and Kendall E.J.M., "Analysis and design of helical capacitance sensors for volume fraction determination", Rev.Sci. Instrume. Vol.

50, 872, 1979

[12] Chang J. S and Girard R. "Reflux condensation phenomena in single vertical tubes", Int. J. Heat and Mass Transfer, Vol. 35, pp 2203-2218, 1992

[13] Jalava, J.-P., Taavitsainen, V.-M., Haario, H. and Lamberg, L., "Determination of particle and crystal size distribution from turbidity spectrum of TiO2 pigments by means of T-Matrix", J. Quant. Spectrosc. Radiat. Transfer, Vol. 60, no. 3, 399–4098, 1998.

[14] De-Lasa, H., Lee, S. L. P. and Bergougnou, M. A., "Bubble measurement in three phase fluidized beds using U-shaped optical fiber", Can. J. Chem. Eng., Vol. 62, pp. 165–169, 1984.

[15] Andreussi, P., Bendiksen, K. H. and Nydal, O. J., "Void distribution in slug flow," Int. J. Multiphase Flow, Vol. 19, No. 5, pp. 817–828, 1993

[16] Lindken, R., Merzkirch, W., "A novel PIV technique for measurements in multiphase flows and its application to two-phase bubbly flows", Experiments in Fluids, Vol 33. pp 814-825, 2002

[17] Friebolin H. "Basic one- and two-dimensional NMR spectroscopy", 3rd Revised Edition, December 1998.

[18] Hoyle, B.S., "Process tomography using ultrasonic sensors", Meas. Science Technology Vol. 7, pp 272-280, 1996.

[19] Ashrafi, M. E. H. and Tuzun, U., "A tomographic study of voidage profiles in axially symmetric granular flows", Chem. Eng. Sci., Vol. 25, no. 3, pp. 373–380, 1993.

[20] Herman, G. T., "Image Reconstructions From Projections — The Fundamentals of Computerized Tomography", Academic Press, 1980.

[21] Harvel, G. D., Hori, K., Kawanishi, K. and Chang, J. S., "Cross-sectional void fraction distribution measurements in a vertical annulus two-phase flow by high speed X-Ray computed tomography and real-time neutron radiography techniques", Flow Measurement and Instrumentation, Vol. 10, no. 4, pp. 259–266, 1999.

[22] Swift, W. L., Dolan, F. X. and Runstadler, P. R., "A scanning gamma ray attenuation system for void fraction measurements in two-phase flow," in Measurements in Polyphase Flows, Proc. of the Winter Annual Meeting of ASME, (San Fransisco, USA), pp. 25–35, 1978.

[23] Chang, J.S., Morala, E.C., "Determination of two-phase interfacial areas by an ultrasonic technique", Nuclear Engineering and Design vol. 122, pp. 143-156, 1990.

[24] Morriss, S.L. and Hill, A.D., "Ultrasonic imaging and velocimetry in two-phase pipe flow", Transaction of the ASME, Vol 115, pp 108-116, 1993.

[25] Chang, J.S., Ichikawa, Y., Irons, G.A., Morala, E.C. and Wan, P.T., "Void fraction measurement by an ultrasonic transmission technique in bubbly gas-liquid two-phase flow", Measuring Techniques in Gas-Liquid Two-phase Flow, eds. J.M. Delhaye and G. Cognet (Springer, Berlin, 1984) pp. 319-335.

[26] Gai, H., Beck, M.S. and Flemons, R.S., "An integral ultrasound transducer/pipe structure for flow imaging", IEEE Ultrasonic Symposium, Montreal, Canada, 1989, pp. 42C1-42C5.

[27] Serizawa, A., Nagane, K., Ebsiu, T., Kamei, T., Kawara, Z. and Torikoshi, K., "Dynamic measurement of liquid film thickness in stratified flow by using ultrasonic pulse echo technique", The 4th International Topical Meeting on Nuclear Thermal Hydraulics, Operation and Safety; April 6-8, Taipei, Taiwan, 1994.

[28] Xu, L.-J. and Xu, L.-A., "Ultrasound tomography system used for monitoring bubbly gas/liquid two-phase flow", IEEE Transactions on Ultrasonic, Ferroelectrics and Frequency Control, Vol. 44, No 1, pp 67-76, January 1997

[29] Xu, L.-J., Han, Y., Xu, L.-A. and Yang, J., "Application of ultrasonic tomography to monitoring gas-liquid flow", Chemical Engineering Science, Vol. 52, No 13, pp 2171-2183, 1997.

[30] Yang, M., Schlaberg, I., Hoyle, B.S., Meck, M.S., Lenn, C., "Real-time ultrasound process tomography for two-phase flow imaging using a reduced number of transducers", IEEE Transactions on Ultrasonic, Ferroelectrics, and Frequency Control, Vol 46. No. 3, May 1999

[31] Utomo, M.B., Warsito, W., Sakai, T., Uchida, S., "Analysis of distribution of gas and TiO2 particles in slurry bubble column using ultrasonic computed tomography", Chemical Engineering Science Vol. 56, pp 6073-6079, 2002.

[32] Warsito, W., Ohkawa, M., Kawata, N., Uchida, S., "Cross-sectional distributions of gas and solid holdups in slurry bubble column investigated by ultrasonic computed tomography", Chemical Engineering Science Vol.54, pp 4711-4728, 1999

[33] Weigand, F. and Hoyle, B.S., "Simulations for parallel processing of ultrasound reflection-mode tomography with applications to two-phase flow measurement", IEEE Transaction on Ultrasonic, Ferroelectric, and Frequency Control, Vol. 36, No.6, pp 652-660, 1989.

[34] Li, T.-Q., "Velocity Measurements of fiber suspensions in pipe flow by the nuclear magnetic resonance imaging method", Tappi J.,Vol. 77(3), March 1994.

[35] Filipczynski, L., Pawlowski, Z., and Wehr, J., "Ultrasonic methods of testing materials", Butterworth, London, 1966.

[36] UTEX Scientific Instruments , "Winspect Reference Guide- Version 6" pp 1-132, 2004

[37] Lubbers J. and Graaff R. "A simple and accurate formula for the sound velocity in water", Ultrasound Med Biol. Vol. 24, pp-1065-1080, 1998.

[38] Lightstone L. "Two-phase flow in dividing and non-dividing horizontal tubes". Master Theses, Dep. of Engineering Physics, McMaster University 1984

[39] Lightstone L., and J. Chang S.I. "Gas-liquid two-phase flow in symmetrically dividing horizontal tubes"AICHE Journal, Vol 37, No.1. pp.111-122, 1991.

[40] Whalley, P.B., "Boiling, condensation, and gas-liquid flow", Clarendon Press, Oxford, 1987

[42] Suo M. and Griffith P. "Two-phase flow in capillary tubes" , ASME paper, 63-WA-96, March 1963.

[41] Wallis G.B. "General correlations for the rise velocity of cylindrical bubbles in vertical tubes", Rept. Vol. 62. GL. 130, General Electric Co., 1962.

[43] Hewitt, G.F., Hall-Taylor, N.S., "Annular two-phase flow", Pergamon Press, Oxford, 1970

[44] Laurinat J.E. and Hanratty T.J. "Pressure drop and film thickness measurements for annular gas-liquid flow", Int. Journal of Multiphase Flow Vol. 10, No 3. 1984, pp. 341-356

[45] Mouza, A.A., Paras, S.V., Karabelas, A.J., "The influence of small tube diameter on falling film and flooding phenomena", International Journal on Multiphase Flow Vol. 28, pp 1311-1331, May 2002.

[46] Matikainen L., Irons G.A., Morala E.C. and Chang J.S. "Ultrasonic system for detection of transient liquid-gas interfaces using the pulse-echo technique". Rev. Sci. Instruments, Vol. 57, pp. 1661-1666, 1986.

NOMENCLATURE

A-cross-sectional area of the pipe

A_g-cross-sectional area occupied by the gas

A_l-cross-sectional area occupied by the liquid

AN-annular flow

c-sound velocity

DB-dispersed bubbles

f-frequency

g- gravitational acceleration

h_l-liquid level

PL-plug flow

Q_g-volumetric gas flow rate

Q_l-volumetric liquid flow rate

SL-slug flow

SS-strtaified smooth

SW-stratified wavy

t_s-time of flight

U_g-gas average velocity

U_{gs}- gas superficial velocity

U_l-liquid average velocity

U_{ls} – liquid superficial velocity

V_l- volume of liquid

V_{total}-total volume

X-Martinelly parameter

α_g-gas volume fraction

α_l-liquid volume fraction

α-void fraction

δ-film thickness

λ-wavelength

ν_g-kinematic viscosity of gas 1.5*10exp(-5) m^2/s

ν_l-kinematic viscosity of liquid 10exp(-6) m^2/s

ρ_g-gas density

ρ_l-liquid density

Z-acoustic impedance

U_{plug}-plug velocity

U_s-slug velocity

U_B-Bubble velocity

Δt –time interval

ΔZ-interval distance

L-length

SNR – Signal to Noise Ratio

PC – Personal Computer

RAM – Random Access Memory

A/D – Analog-to-Digital converter

P/R – Pulser-Receiver

CS12100 – CompuScope12100

IRQ – Interrupt Request

DMC 1800- Galil Motion Controller

1, 2, 3, 4 – Ultrasonic Panametrics Transducers

FIFO – First-In-First-Out data flow in the buffer

SMB – System Management Bus

APPENDIX 1 - Peak Detection Algorithm Logic Diagram

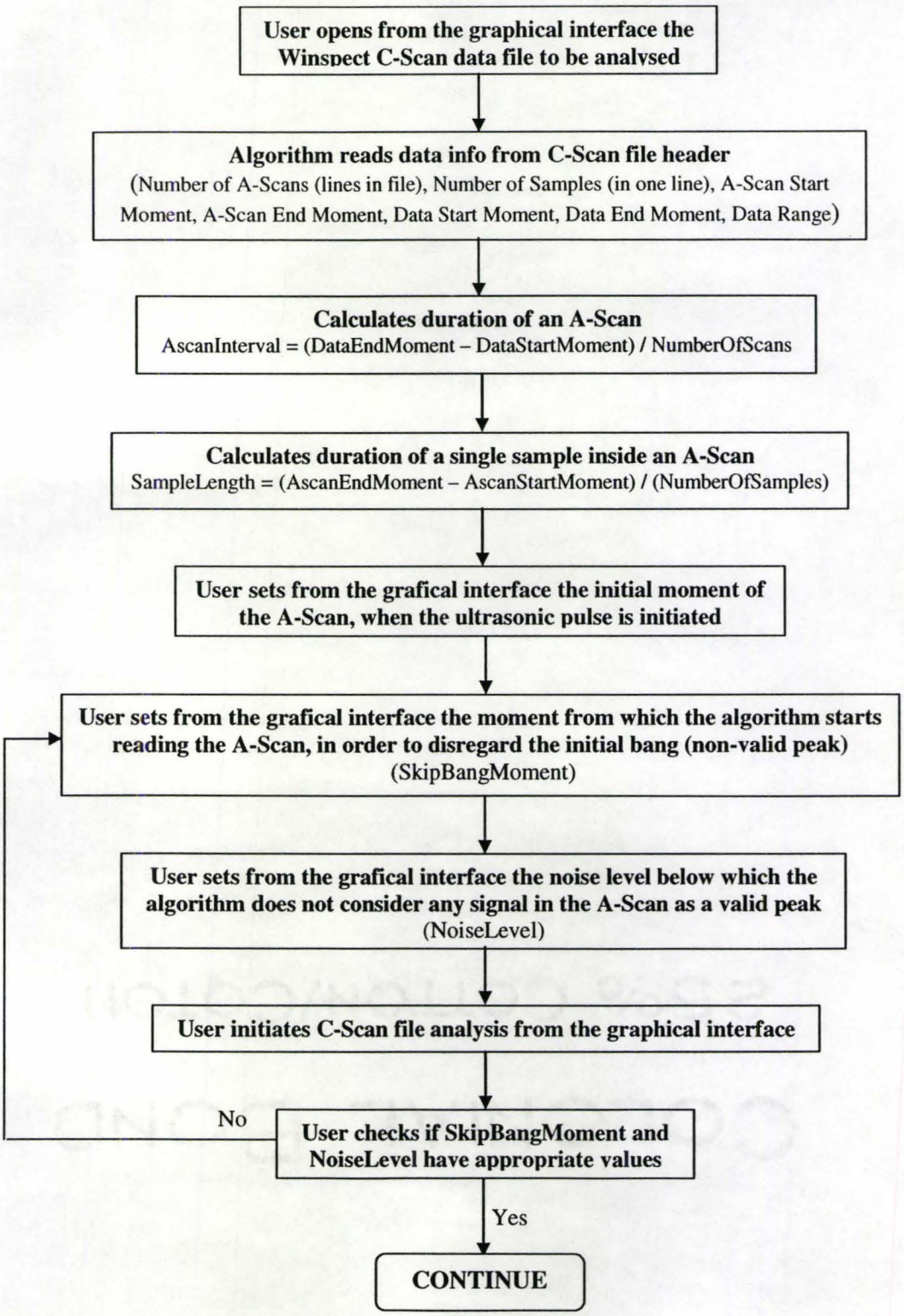

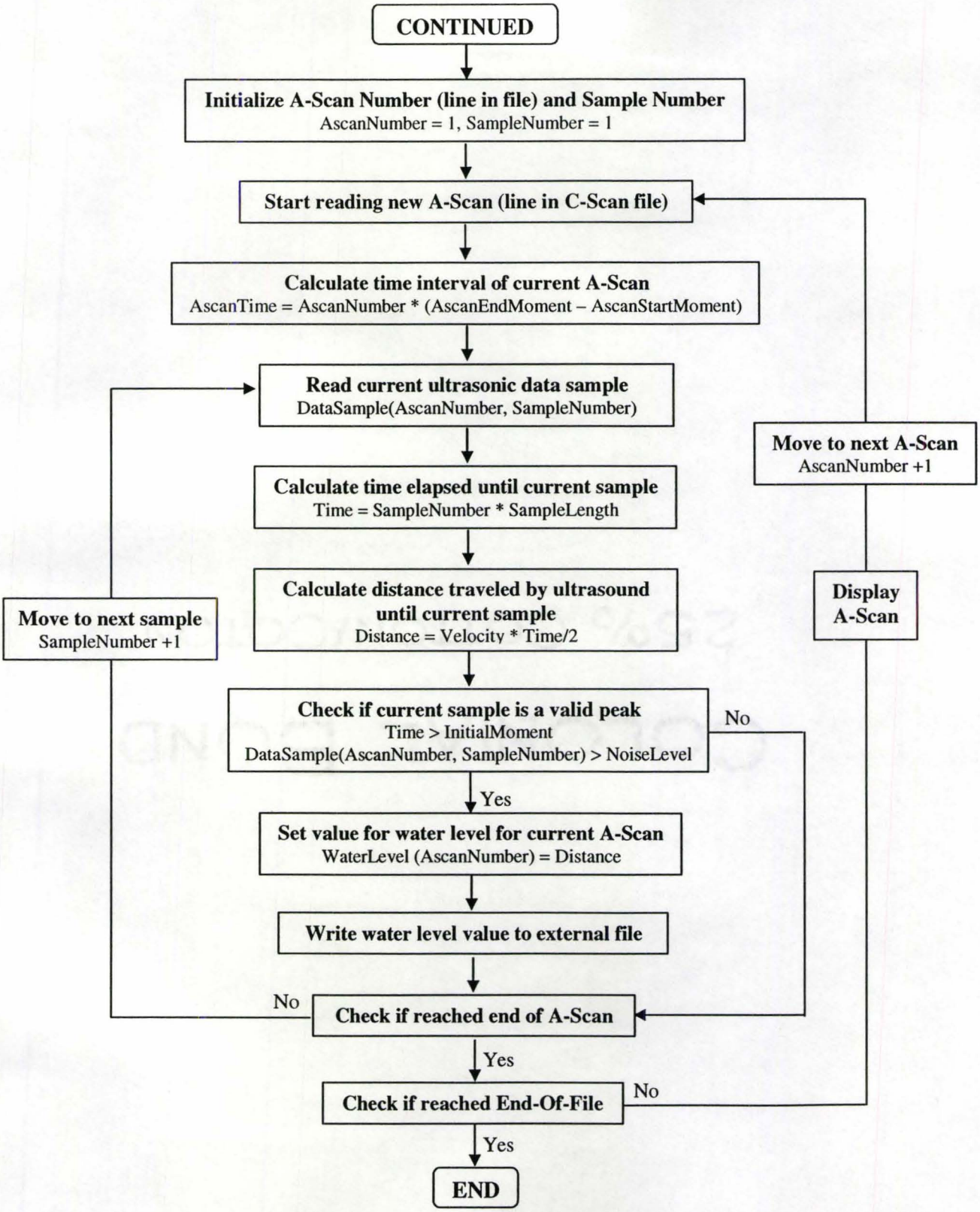
CONTINUED
Initialize A-Scan Number (line in file) and Sample Number
AscanNumber = 1, SampleNumber = 1
Start reading new A-Scan (line in C-Scan file)
Calculate time interval of current A-Scan
AscanTime = AscanNumber * (AscanEndMoment – AscanStartMoment)
Read current ultrasonic data sample
DataSample(AscanNumber, SampleNumber)
Calculate time elapsed until current sample
Time = SampleNumber * SampleLength
Calculate distance traveled by ultrasound until current sample
Distance = Velocity * Time/2
Check if current sample is a valid peak
Time > InitialMoment
DataSample(AscanNumber, SampleNumber) > NoiseLevel
No
Yes
Set value for water level for current A-Scan
WaterLevel (AscanNumber) = Distance
Write water level value to external file
Move to next sample
SampleNumber +1
No
Check if reached end of A-Scan
Yes
Check if reached End-Of-File
No
Yes
END
Move to next A-Scan
AscanNumber +1
Display A-Scan

APPENDIX 2 - Peak Detection Algorithm (Visual Basic Source Code)

```
"Declaring variables module"

Const ForReading = 1, ForWriting = 2, ForAppending = 3

Dim NoOfSamples As Integer 'Samples in one Ascan'

Dim NoOfAscans As Integer

Dim AscanStart As Single, AscanEnd As Single 'Time interval for the
Ascans (for each pulse, or line in file)

Dim SampleLength As Single 'Length of a sample

Dim DataStart As Single, DataEnd As Single 'Time interval for all data
in the file'

Dim DataRangeMin As Single, DataRangeMax As Single

Dim cale As String, cale2 As String 'cale is for the data file read,
and cale2 is for the water level file written out


Dim Cursor As Integer

Dim fs, f, f2    'f is for opening the input data file, while f2 is for
creating and writing on output water level data file'

Dim str As String

Dim sel As Byte

Dim Data(1000, 3000)    'Values for all samples in an A-Scan are stored
in this variable'

Dim SampleNo As Integer  'Index for samples in an A-Scan

Dim AscanNo As Integer      'Index for A-Scans

Dim NumberLength As Byte      'Number of digits of a number used to
identify numbers in file

Dim NumberStart As Integer

Dim NoiseLevel As Single

Dim WaterLevel(1000) As Single   'The water level calculated for each
Ascan'

Dim InitialMoment As Single 'The initial moment used for looking for a
reflection'

Dim UnitX As Single, UnitY As Single

Dim OriginX As Single, OriginY As Single

Dim viteza As Single
```

```
Dim timp As Single  'Time inside an A-Scan'
Dim distanta As Single

Dim AscanTime As Single 'Time when each A-Scan starts (AscanNo 8
(AscanEnd - AscanStart)'

Dim FirstSignal As Boolean 'This refers to the signals received by the
transducer in an A-Scan. This is used when looking for the reflection
on water surface, considered when FirstSignal = True)

Dim TubeDiameter As Single

Dim Pause As Boolean
Dim ShowAscan As Boolean
Dim SkipSamples As Integer 'Number of samples skipped in an A-Scan
during reading data'
Dim SkipAscan As Integer 'Number of A-Scans (lines) skipped during
reading file'
Dim SelectedFile As String


Private Sub Command1_Click()
Frame3.Visible = False

SampleNo = 0
cale = SelectedFile

Set fs = CreateObject("Scripting.FileSystemObject")
'Open file for transducer 1. Do the same thing for the other
transducers. If they are in the same file, include a for...next loop to
repeat the operation for each transducer'
Set f = fs.OpenTextFile(cale, ForReading)
GoTo 40
30
MsgBox "The path entered in the box was not found. Please try again."
Exit Sub

40
```

```
'Read the file info from the file header (first 9 lines of the file)
For i = 1 To 9 + AscanNo    'Read each line in the header
    Cursor = 0
    NumberLength = 0
    Cursor = 0
    If i = 1 Or i = 3 Or i = 5 Or i = 7 Or i = 9 Then
        GoTo 90
    End If

    str = f.ReadLine
    Text2.Text = str

    'If i = 2 Then   'Analyze second line
        NumberStart = 0
        Do  'Read the first number in line
        Text2.SelStart = Cursor
            Text2.SelLength = 1
            If Text2.SelText = " " Or Text2.SelText = Chr(9) Then
'End of the number in current line
                Text2.SelStart = NumberStart
                Text2.SelLength = NumberLength
                If i = 2 Then
                    NoOfSamples = Text2.SelText
                ElseIf i = 4 Then
                    AscanStart = Text2.SelText
                ElseIf i = 6 Then
                    DataStart = Text2.SelText * 10 ^ 4
                ElseIf i = 8 Then
                    DataRangeMin = Text2.SelText
                End If
                GoTo 60
            Else
                NumberLength = NumberLength + 1
            End If
            Cursor = Cursor + 1
        Loop
```

```
60
        Do      'Analyzes the space between the numbers in current line
            Text2.SelStart = Cursor
            Text2.SelLength = 1
            If Text2.SelText = " " Or Text2.SelText = Chr(9) Then
                Cursor = Cursor + 1
            Else
                GoTo 70
            End If
        Loop
70
        NumberStart = Cursor
        NumberLength = 0
        Do  'Read the second number in line
            Text2.SelStart = Cursor
            Text2.SelLength = 1
            If Text2.SelText = Chr(10) Or Text2.SelText = Chr(13) Or
Text2.SelText = " " Or Text2.SelText = Chr(9) Or Text2.SelText = ""
Then      'End of the current line
                Text2.SelStart = NumberStart
                Text2.SelLength = NumberLength
                If i = 2 Then
                    NoOfAscans = Text2.SelText
                ElseIf i = 4 Then
                    AscanEnd = Text2.SelText
                    SampleLength    =    (AscanEnd    -    AscanStart)    /
NoOfSamples
                ElseIf i = 6 Then
                    DataEnd = Text2.SelText * 10 ^ 4
               ElseIf i = 8 Then
                    DataRangeMax = Text2.SelText
                End If
                GoTo 80
            Else
                NumberLength = NumberLength + 1
            End If
```

```
            Cursor = Cursor + 1
        Loop
80
        Do      'Analyzes the space between the numbers in current line
            Text2.SelStart = Cursor
            Text2.SelLength = 1
            If Text2.SelText = Chr(10) Or Text2.SelText = Chr(13) Or
Text2.SelText = " " Or Text2.SelText = Chr(9) Then        'End of the
current line
                GoTo 100
            ElseIf Text2.SelText = "" Then
                GoTo 100
            End If
        Loop
90

    f.skipline
100
Next i

Text12.Text = NoOfSamples
Text3.Text = NoOfAscans
Text4.Text = SampleLength
Text11.Text = AscanEnd - AscanStart
Text6.Text = (DataEnd - DataStart) / 1000

SampleLength = (AscanEnd - AscanStart) / NoOfSamples     'Duration of a
single sample inside an A-Scan
UnitY = Picture1.Height / (DataRangeMax - DataRangeMin)
UnitX = Picture1.Width / (AscanEnd - AscanStart)
'Opens text file for writing level data
cale2 = App.Path & "\" & Text10.Text & ".txt"
Set f2 = fs.OpenTextFile(cale2, ForWriting, True)
f2.writeline "ID" & Chr(9) & "Time (ms)" & Chr(9) & "Level (cm)"
```

```
AscanNo = 0
End Sub
Private Sub Command2_Click()
Frame3.Left = Form1.Width / 2 - Frame3.Width / 2
Frame3.Top = Form1.Height / 2 - Frame3.Height / 2
Frame3.Visible = True
End Sub
Private Sub Command3_Click()
Command3.Enabled = False
InitialMoment = Text9.Text
NoiseLevel = Text8.Text
5
If SkipAscan > 1 Then
    For i = 2 To SkipAscan
        f.skipline
    Next i
End If
FirstSignal = True
If Pause = True Then Exit Sub
AscanTime = AscanNo * (AscanEnd - AscanStart)
Cursor = 0
SampleNo = 0    'Int(InitialMoment / SampleLength)
Picture1.Cls
X1 = InitialMoment * UnitX + OriginX
Picture1.Line (X1 - 10, 100)-(X1 - 10, Picture1.Height - 100),
QBColor(12)
str = f.ReadLine
Text2.Text = str
DoEvents

Do      'Read the current A-Scan (file line)
    SampleNo = SampleNo + 1
    Text2.SelStart = Cursor
    Text2.SelLength = 1
    If Text2.SelText = "-" Then
        sel = 6
```

```
    Else
        sel = 5
    End If
    Text2.SelLength = sel     'Current sample value
    If Text2.SelText = "" Then GoTo 10    'End of A-Scan (line)
    Cursor = Cursor + sel + 2
    Data(AscanNo, SampleNo) = Text2.SelText
    timp = SampleNo * SampleLength
    distanta = viteza * timp / 2
    oldx = x
    oldy = y
    x = timp * UnitX + OriginX
    y = Data(AscanNo, SampleNo) * UnitY + OriginY
    X2 = AscanTime * Picture2.Width / (DataEnd - DataStart)       'X
coordinate for Picture2 graph - time when the current A-Scan initiated
    If timp > InitialMoment And Data(AscanNo, SampleNo) > NoiseLevel
And FirstSignal = True Then
        FirstSignal = False
        WaterLevel(AscanNo) = Format(distanta, "###0.000")
        f2.writeline AscanNo & Chr(9) & Format(AscanTime / 1000,
"###0.00") & Chr(9) & Chr(9) & WaterLevel(AscanNo)
        Picture2.Line (X2, -olddistanta * Picture2.Height /
TubeDiameter + Picture2.Height)-(oldx2, -distanta * Picture2.Height /
TubeDiameter + Picture2.Height)
        Picture1.Line (x, 100)-(x, Picture1.Height - 100), QBColor(10)
        oldx2 = X2
        olddistanta = distanta
    End If
    On Error Resume Next
    If ShowAscan = True And SampleNo > 1 Then
        Picture1.Line (x, -y + Picture1.Height)-(oldx, -oldy +
Picture1.Height)
    End If
Loop
Exit Sub    'If the code gets to this point, all the file data has been
stored in variable Data( , )
10
AscanNo = AscanNo + SkipAscan
```

```
Text7.Text = AscanNo
GoTo 5
20
MsgBox "End of File. " & AscanNo & " columns have been written."
f.Close
f2.Close
End Sub
Private Sub Command4_Click()
If Pause = True Then
    Pause = False
ElseIf Pause = False Then
    Pause = True
End If

If Pause = False Then Call Command3_Click

End Sub


Private Sub Command5_Click()
If ShowAscan = True Then
    ShowAscan = False
ElseIf ShowAscan = False Then
    ShowAscan = True
End If
End Sub
Private Sub Command6_Click()
Open SelectedFile For Random Access Write As #1
Get #1, 10, Data(10, 10)  ' Read third record.
Close #1   ' Close file.
MsgBox WaterLevel(1)

End Sub
Private Sub Dir1_Change()
File1.Path = Dir1.Path
```

```
End Sub
Private Sub Drive1_Change()
Dir1.Path = Drive1.Drive
End Sub
Private Sub File1_Click()
SelectedFile = File1.Path & "\" & File1.FileName
Text1.Text = File1.FileName
End Sub
Private Sub File1_DblClick()
Call Command1_Click
End Sub
Private Sub Form_Load()
Combo1.AddItem ("Initial and First")
Combo1.AddItem ("Initial and Second")
Combo1.AddItem ("First and Second")
Form1.Width = 12000
Form1.Height = 10000
Line1.Y1 = Picture1.Height / 2
Line1.Y2 = Picture1.Height / 2
OriginY = Picture1.Height / 2
OriginX = Line1.X1
TubeDiameter = 5
FirstSignal = True
ShowAscan = True
Command4.ZOrder 1
Command5.ZOrder 1
On Error GoTo 200
SkipAscan = Text13.Text
Exit Sub
200
MsgBox "Enter valid number"
End Sub
Private Sub Form_Unload(Cancel As Integer)
f.Close
f2.Close
```

```
End Sub
Private Sub Text13_Change()
On Error GoTo 200
SkipAscan = Text13.Text
Exit Sub
200
MsgBox "Enter valid number"
End Sub
Private Sub Text8_Change()
NoiseLevel = Text8.Text
End Sub
Private Sub Text9_Change()
If Text9.Text = "" Then
    InitialMoment = 0
Else
    InitialMoment = Text9.Text
End If
End Sub
```